POLITEKNIK NEGERI BALI

Journal of Engineering Design and Technology

logic

Vol. 25 No. 1 March 2025

LOGIC

Jurnal Rancang Bangun dan Teknologi

p-ISSN. 1412-114X

e-ISSN. 2580-5649

LOGIC

Jurnal Rancang Bangun dan Teknologi

Journal of Engineering Design and Technology

Gedung P3M, lt.1 Politeknik Negeri Bali, Bukit Jimbaran
PO BOX 1064 Kuta Selatan, Badung, Bali - Indonesia
Telp. (+62)361 701981 Fax. (+62)361 701128
Email: logic@pnb.ac.id

LOGIC JOURNAL TEAM

PREFACE

Logic: Jurnal Rancang Bangun dan Teknologi (Journal of Engineering Design and Technology) is a peer-reviewed research journal aiming at promoting and publishing original high quality research in all disciplines of engineering and applied technology. All research articles submitted to Logic should be original in nature, never previously published in any journal or presented in a conference or undergoing such process across the world. All the submissions will be peer-reviewed by the panel of experts associated with particular field. Submitted papers should meet the internationally accepted criteria and manuscripts should follow the style of the journal for the purpose of both reviewing and editing.

Logic is a journal covering articles in the field of civil and mechanical engineering, design, and technology published 3 times a year in March, July, and November. Language used in this journal is English.

LOGIC. P-ISSN 1412-114X
LOGIC. E-ISSN 2580-5649
Indexing : GOOGLE SCHOLAR, DOAJ, EBSCO OPEN SCIENCE DIRECTORY, SINTA, GARUDA

Best Regard,

LOGIC Editorial Team

TABLE OF CONTENTS

The Effect of Sengon Wood Powder Particle Size and Composite Composition on The Performance of Non-Asbestos Brake Linings	1 – 12
The Effect of Injection Pressure and Injection Temperature in The Compression Moulding Process on Flashing Defects of Shoulder Products	13 – 18
Construction of A Thermoelectric Coolbox System With Ice Pack Modification for Mango Storage Based on The Internet of Things	19 – 26
Analysis of Leakage Test Results on Flange-Gasket Piping System Simulator Device	27 – 34
Lean Ergonomic Approach to Ergonomic Risk Analysis for Workplace Assessment	35 – 44
Determination The Cooling Capacity of The Fan Coil Unit (FCU) in A Hotel Room - Based on Heat Transfer Analysis	45 – 53
Mold Design for Injection Molding Machine Using Recycled Aluminum	54 – 60
The Role of Aluminium Nitride as Reinforcement Material for Phase Change Materials (PCMS)	61 - 71
Application of Anthropometric Data on Redesign of Lightweight Brick-Cutting Tools to Reduce Workers' Musculoskeletal Complaints	72 - 77

LOGIC
Journal of Engineering Design and Technology
Vol. 25 No.1 March 2025 ; p. 1 - 12

p-ISSN : 1412-114X
e-ISSN : 2580-5649
http://ojs2.pnb.ac.id/index.php/LOGIC

THE EFFECT OF SENGON WOOD POWDER PARTICLE SIZE AND COMPOSITE COMPOSITION ON THE PERFORMANCE OF NON-ASBESTOS BRAKE LININGS

Robby Ridwan [1)], Moh. Hartono [1)]

1) Mechanical Engineering Departement, State Polytechnic of Malang, Jl Soekarno-Hatta 9, Malang, Indonesia

Correponding email [1)] : moh.hartono@polinema.ac.id

Abstract.. The purpose of this study was to determine the effect of particle size and composite composition on the mechanical properties of non-asbestos brake linings. This type of research uses quantitative experiments. There are 3 kinds of variables used, namely a) independent variables consisting of particle size and composite composition; b) dependent variables consisting of hardness value and wear rate value; c) controlled variables consisting of shore D durometer method and Wear Rate with 800 rpm, 120 seconds time, and 20 psi pressure. The data analysis technique uses the factorial anova method because it is to determine the effect of the interaction between particle size and composite composition on brake lining. Data analysis was carried out twice, namely hardness test data and wear rate tests. After that, the data obtained was processed using the Minitab application. The results showed that particle size and composite composition affect the hardness and wear of brake lining. Smaller particle size increases hardness, especially in specimens using Fe composition. The use of iron powder resulted in higher hardness. Iron powders with better mechanical properties showed lower wear rates. The interaction effect of particle size and composite composition on brake lining performance is that the interaction of the two independent variables has a significant effect on brake lining performance.

Keywords : brake pads, hardness, non asbestos, wear

1. INTRODUCTION

The braking system is an important component in a vehicle because it functions to slow down or stop the speed of the vehicle. Most vehicles today use disc brakes because they are better at conducting heat than drum brakes [1]. Brake systems that do not function properly can be caused by several factors, one of which is due to wear on the disc and brake lining due to friction. So that the construction of brake linings is made of materials that have good and effective abilities to achieve optimal braking performance [2].

In the last two decades, the use of asbestos materials has been popular for making brake linings due to its strength, heat resistance and fire resistance. However, the impact of asbestos materials has been known to be carcinogenic or a dangerous substance that causes lung cancer and other health problems, so it should not be used as a material for making brake linings [3]. According to a report from the Ministry of Environment and Forestry, deaths from asbestos globally reached 255,000 people per year. Seeing the impact of the use of asbestos which is so dangerous, the government made a regulation regarding the use of asbestos, the regulation is stated in PP No. 18 of 1999 that asbestos is included in the category of B3 (Hazardous and Toxic Material) waste, and stated in PP No. 74 of 2001 that the use of asbestos must be supervised.Therefore, new asbestos-free alternative friction materials as brake pads have been developed. Thus, many studies have been conducted and are still ongoing for the development of not only asbestos-free brakes but also those with less impact on human health and better technical efficiency. Natural fibers that can be utilized in the manufacture of non-asbestos brake linings are bamboo, jute, coconut powder, corn cob, teak wood powder, rice husk ash and many more [4].

Several studies have been conducted in the field of asbestos-free brake pad development. The use of

bagasse [5], glugu wood sawdust waste charcoal [6], banana peel [7] teak wood powder [8] etc. has been investigated. Various studies around the world are focusing on how to utilize industrial or agricultural waste as a source of industrial raw materials. The utilization of this waste is not only economical, but it can also maintain a better nature. One of the agricultural wastes that are widely available in Indonesia is sengon wood waste, sengon wood is a production wood that is widely produced and produces powder that becomes waste, and incidentally in my environment there is a lot of sengon wood waste that has not been utilized properly, so this raises the idea of using the powder as one of the research materials in making brake lining. Zincon wood powder is combined with iron ore or aluminum powder as reinforment to produce brake linings that have good mechanical strength and wear resistance. In this case, for a disc brake system, no single material meets the desired performance-related criteria, such as safety and durability under different braking conditions. Friction materials are required to provide a stable coefficient of friction and low wear rates over a wide range of operating speeds, pressures, temperatures and environmental conditions. In addition, they must also be compatible with the brake rotor or disc material to reduce severe wear, vibration, and noise during braking [4]. Therefore, based on previous studies [7] and [8], the reason for choosing the particle size and composition of its components is the novelty of this study and this is what distinguishes it from previous research specially in material Sengon wood. In addition to considering practical matters for the purpose of ease in the brake pad moulding process. Because with a smaller particle size and the selection of composition using sengon wood will help facilitate the brake pad moulding process.

From the description above that by mixing sengon wood powder, iron ore and aluminum powder with a resin to form a composite is expected to have good mechanical strength. In this study biocomposites from sengon wood powder with variations in particle size and composite composition as an application of brake lining by testing hardness and wear as a non-asbestos brake lining material. Therefore the objectives of this research are: 1) Knowing the effect of variations in particle size and composite composition on the hardness of brake lining; 2) Knowing the effect of variations in particle size and composition of composites used on the wear rate of brake linings; and 3) Knowing the interaction of variations in particle size and composition of composites on performance in non-asbestos brake linings.

2. METHODS

2.1 Material

Since the target of this study is to compare the results of previous similar studies with different materials used in this study, the criteria for selecting particle size and the composition of the mixture are made the same as the previous study. The only difference lies in the use of sengon wood material. The sengon wood material was obtained from around the house because it so happened that the area (Banyuwangi Regency) is one of the producers of sengon wood. The materials used during this work were polyester resin, sengon wood powder, iron powder and aluminum powder as shown in Figure 1 with the material composition shown in Table 1 below.

Figure 1. Ingredients

2.2 Specimen Making Method

The materials were prepared and mixed in the container and the mixing of the materials was done properly so as to achieve a homogeneous state and then transferred into the mold. The mixtures were added according to their respective compositions as shown in Table 1 in terms of specimen weight:

Table 1. Material Composition

Specimen Number	Specimen Code	Unit Composition Presentation (%)				Particle Size (Meh)
		Sengon Wood Powder	iron powder	Aluminum Powder	Polyester Resin	
1	A1	50	0	10	40	40
2	A2	50	0	10	40	60
3	A3	50	0	10	40	80
4	A4	50	0	10	40	100
5	B1	50	10	0	40	40
6	B2	50	10	0	40	60
7	B3	50	10	0	40	80
8	B4	50	10	0	40	100
9	G	(Comparison Sample)				

The specimens are produced using a compression machine with a press molding technique. This stage is called the compaction stage which aims to compact the powder. In this compaction process, marking the hardness of the material also affects the length of time for molding and the amount of pressure applied during the compaction process given in the process of making brake lining. The longer the time required and the greater the compaction pressure applied, the harder the brake lining specimen. In this process, the compressive force applied was 3ton for 5 minutes. Furthermore, the specimen is removed from the mold to carry out the sintering process so that the bond between the materials becomes heavier. Sintering is done at 80°C for 30 minutes. The brake lining was dried at room temperature for 2 hours to ensure the material was dry. The brake disc lining specimens are then glued to the brake lining mounting plate with the application of an adhesive layer, the brake lining mounting plate is made of mild steel, which must be prepared by cleaning the plate behind the brake lining and applying an adhesive layer. The strength of the adhesive bond between the material and the friction and lightness of the steel is very important to avoid debonding during use. The following photos of the resulting brake lining are shown in Figure 2.

Figure 2. Brake lining results

2.3 Specimen Testing

Hardness values of the specimens were obtained using a durometer hardness tester. A 63 mm high sample was used to conduct the test on a wide variety of different material compositions. The test was conducted using a shore D type durometer tester with testing standards according to ASTM D2240.

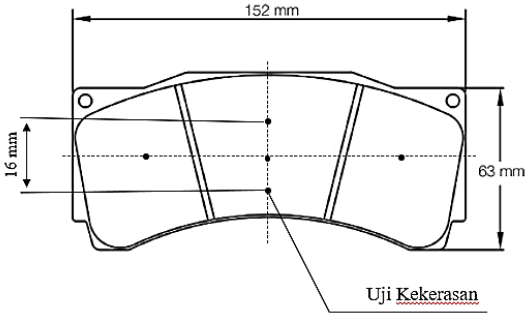

Figure 3. Hardness test equipment

Wear Rate Testing is done with a disc brake simulator. Before the brake lining is installed on the simulator, it needs to be weighed to determine the initial weight of the brake lining. The compressive force acting on the brake lining is generated by the brake lever and the amount of pressure generated is controlled using a pressure gauge and for the rotation speed of the brake disc is measured using a tachometer. After the brake disc stops, the weight of the brake lining is weighed after friction. Before testing, the surface of the specimen is heated at a temperature of 10°C to 35°C to determine the effect of heat treatment of the specimen on the wear rate. During the test, it must be placed on a smooth and flat surface free of oxide scale, foreign objects, and free of lubricants so that no displacement occurs during the test. Wear rate testing is carried out for 60 seconds with a rotation speed of 800 rpm. The weight difference measured before and after the test gives the sample wear. The formula used to convert weight loss into wear rate is:

$$M = \frac{W0-W1}{A.t} \quad (1)$$

M = wear rate (gram/mm^2.second)

W0 = weight before wear rate (gr)

W1 = weight after wear rate(gr)

t =time testing (second)

A = cross sectional area (mm)

3. RESULTS AND DISCUSSION

3.1 Hardness Test Results

In the process of collecting data in this study using a shore D Teclock GS-702 durometer hardness tester at the Mechanical Engineering Material Testing Laboratory of Malang State Polytechnic and obtained the results of research on the hardness of zincon wood powder brake materials, aluminum, iron powder as follows:

Table 2. Hardness test results

Specimen No	Specimen Code	Hardness Value (HD)					Average
		1 st Tes	2 st Tes	3 st Tes	4 st Tes	5 st Tes	
1	A1	64	66	68	67	65	66
2	A2	70	68	69	70	69	69
3	A3	75	76	76	74	75	75
4	A4	78	78	79	78	79	78
5	B1	69	68	67	69	68	68
6	B2	75	76	74	76	75	75
7	B3	76	76	79	78	76	77
8	B4	81	82	80	82	80	81
9	G	74	75	74	75	73	75

Data collection that has been carried out, then processed using statistical software. The following are the results of the analysis that has been carried out. Analysis of Variance (anova) is used to determine the relationship between the dependent variable and the independent variable. In this case the method used is factorial anova.

Table 3. Anova and Model Summary

Analysis of Variance

Source	DF	Adj SS	Adj MS	F-Value	P-Value
Model	7	1002,58	143,225	133,23	0,000
Linear	4	974,70	243,675	226,67	0,000
Uk Partikel (Mesh)	3	875,48	291,825	271,47	0,000
Kom Komposit (1=Al ; 2=Fe)	1	99,23	99,225	92,30	0,000
2-Way Interactions	3	27,88	9,292	8,64	0,000
Uk Partikel (Mesh)*Kom Komposit (1=Al ; 2=Fe)	3	27,88	9,292	8,64	0,000
Error	32	34,40	1,075		
Total	39	1036,98			

Model Summary

S	R-sq	R-sq(adj)	R-sq(pred)
1,03682	96,68%	95,96%	94,82%

This study uses alpha (α) of 5% or 0.05. From the table above, it is known that the particle size and composite composition variables have a significant effect on the hardness value (response) because the P-value is less than the specified alpha (α) (p-value < alpha (α), so the null hypothesis (H0) is rejected and the alternative hypothesis (H1) is accepted. And the interaction of the two variables has a significant effect because the P-value is less than the specified alpha (α) (p-value < alpha (α), so the null hypothesis (H0) is rejected and the alternative hypothesis (H1) is accepted. From (R-square) of 96.68%, the remaining 3.32% is an error caused by other variables not in the study.

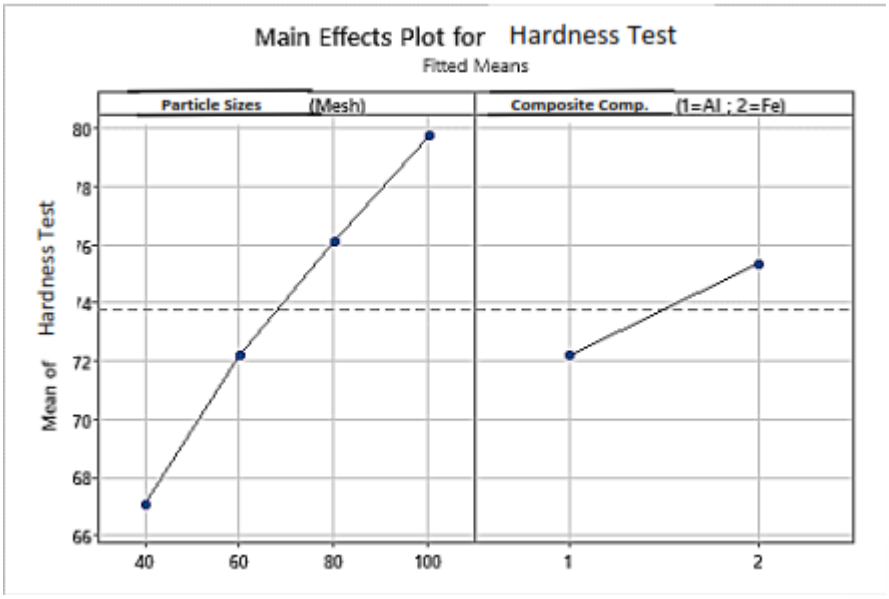

Figure 4. Factorial Plot

Based on Figure 4. there are two main lines, namely horizontal which shows the independent variable and vertical which shows the dependent variable. The graph shows that the smaller the particle size or the larger the mesh size used during testing causes the higher or increase in the resulting hardness value. The composite composition graph shows that the use of iron powder material produces a better hardness value than aluminum powder.

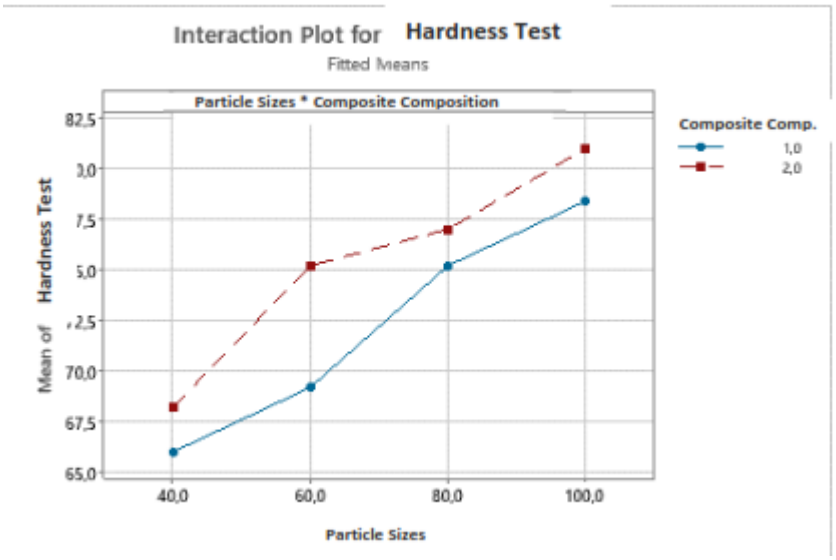

Figure 5 . Factorial interaction plots

Figure 5. is an interaction graph between particle size and composite composition which aims to determine the effect of interaction between independent variables on the dependent variable, where in this study describes the relationship between particle size and composite composition on hardness value. In graph 2 the line shows the independent variable composite composition with different colors according to the material used from the specimen, namely blue shows the specimen with aluminum material while orange shows the specimen with iron powder material. In the graph, it can be seen that the level of hardness of the specimen is getting bigger along with the use of smaller particle sizes or the larger the mesh size used, while in the composite composition the use of iron powder has a higher hardness than the use of aluminum powder in the specimen.

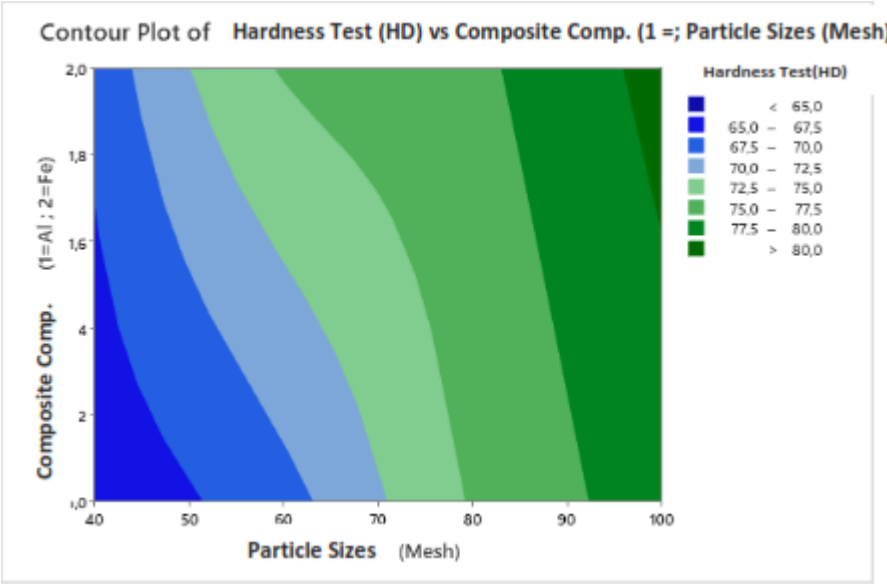

Figure 6. Countour plot graph

Figure 6 is a contour plot graph of the effect of particle size and composite composition on the hardness value of the specimen, showing that the horizontal line on the graph is the variation of particle size and the vertical line on the graph is the composite composition. The dark green color number 2 from the right shows the hardness level area of 77.5 - 80 HD, with a particle size of 100 mesh in composite composition number 1 and 2. The light green color shows the hardness level area of 75 - 77.5 HD with a particle size of 80 mesh in composite composition number 1 and 2, and at a particle size of 60 mesh in composite composition number 2. Tosca green color or the middle part which means the hardness level of 72.5 - 75 HD with a particle size of 80 mesh in composite composition number 1, and at a particle size of 60 mesh in composite composition number 2. In sky blue or the middle part which means the hardness level of 70 - 72.5 HD with a particle size of 60 mesh in composite composition number 1, and at a particle size of 50 mesh in composite composition number 2. The light blue color shows the hardness level area of

67.5 - 70 HD with a size of 60 mesh in composite composition number 1, and at a particle size of 40 mesh in composite composition number 2. While the azure blue color or the leftmost part of the graph shows the hardness level area of 65 - 67.5 HD with a particle size of 40 mesh in composite composition number 1. And the sapphire blue color shows the hardness level less than < 65HD in composite composition number 1.

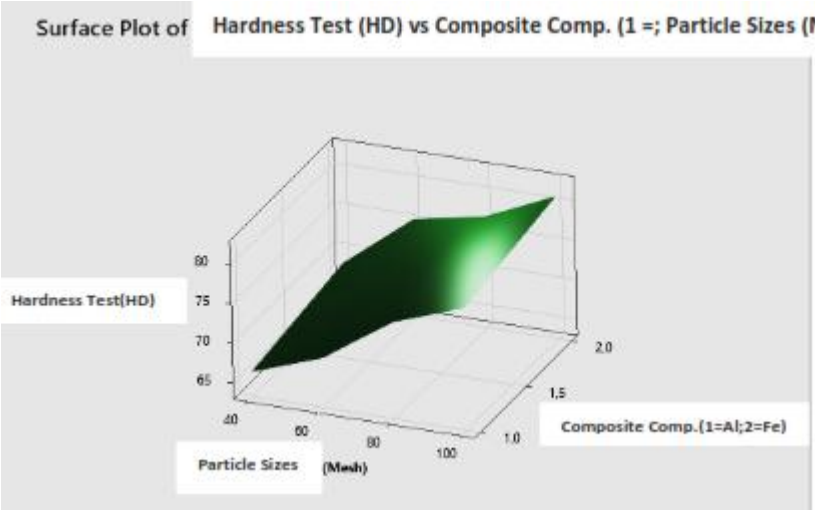

Figure 7. Surface plot graph

Figure 7 is a surface plot graph of the results of the study of the effect of particle size and composite composition on specimen hardness. In the graph, the x-axis shows the particle size, the y-axis shows the composite composition, and the z-axis shows the hardness level. From the graph it can be concluded that, the effect of particle size on hardness is the smaller the particle size or the larger the mesh size, the greater the level of hardness produced. In the effect of composite composition on the level of hardness, it can be concluded that the use of composition number 2 or iron powder has better hardness than the use of composition number 1 or aluminum powder.

3.2 Wear Test Results

In the process of taking data in this study using formula 1.1 the results of the wear test are as follows:

Table 4. Wear Test Results

No	Kode	Wear Rate (gram/ mm^2 .sec)					Average
		1 st Tes	2 st Tes	3 st Tes	4 st Tes	5 st Tes	
1	A1	0,000000336	0,000000318	0,000000309	0,000000315	0,000000326	0,000000321
2	A2	0,000000316	0,000000328	0,000000323	0,000000316	0,000000324	0,000000321
3	A3	0,000000272	0,000000265	0,000000257	0,000000280	0,000000272	0,000000269
4	A4	0,000000252	0,000000253	0,000000249	0,000000253	0,000000246	0,000000251
5	B1	0,000000319	0,000000330	0,000000335	0,000000325	0,000000327	0,000000327
6	B2	0,000000272	0,000000268	0,000000277	0,000000265	0,000000268	0,000000270
7	B3	0,000000258	0,000000261	0,000000241	0,000000246	0,000000249	0,000000251
8	B4	0,000000234	0,000000242	0,000000251	0,000000241	0,000000258	0,000000245
9	G	0,000000354	0,000000360	0,000000327	0,000000309	0,000000363	0,000000343

Analysis of Variance (anova) is used to determine the relationship between the dependent variable and the independent variable. In this case the method used is factorial anova..:

Table 5 Anova dan model summary

Analysis of Variance

Source	DF	Adj SS	Adj MS	F-Value	P-Value
Model	7	0,000000	0,000000	114,31	0,000
Linear	4	0,000000	0,000000	178,60	0,000
U Partikel(Mesh)	3	0,000000	0,000000	220,12	0,000
Kom Komposit(1=Al ; 2=Fe)	1	0,000000	0,000000	54,04	0,000
2-Way Interactions	3	0,000000	0,000000	28,58	0,000
U Partikel(Mesh)*Kom Komposit(1=Al ; 2=Fe)	3	0,000000	0,000000	28,58	0,000
Error	32	0,000000	0,000000		
Total	39	0,000000			

Model Summary

S	R-sq	R-sq(adj)	R-sq(pred)
0,0000000	96,15%	95,31%	93,99%

This study uses alpha (α) of 5% or 0.05. From the table above, it is known that the particle size and composite composition variables have a significant effect on the wear value (response) because the P-value is less than the specified alpha (α) (p-value < alpha (α), so the null hypothesis (H0) is rejected and the alternative hypothesis (H1) is accepted. And the interaction of the two variables has a significant effect because the P-value is less than the specified alpha (α) (p-value < alpha (α) then the null hypothesis (H0) is rejected and the alternative hypothesis (H1) is accepted. From (R-square) of 96.15%, the remaining 3.85% is an error caused by other variables not in the study.

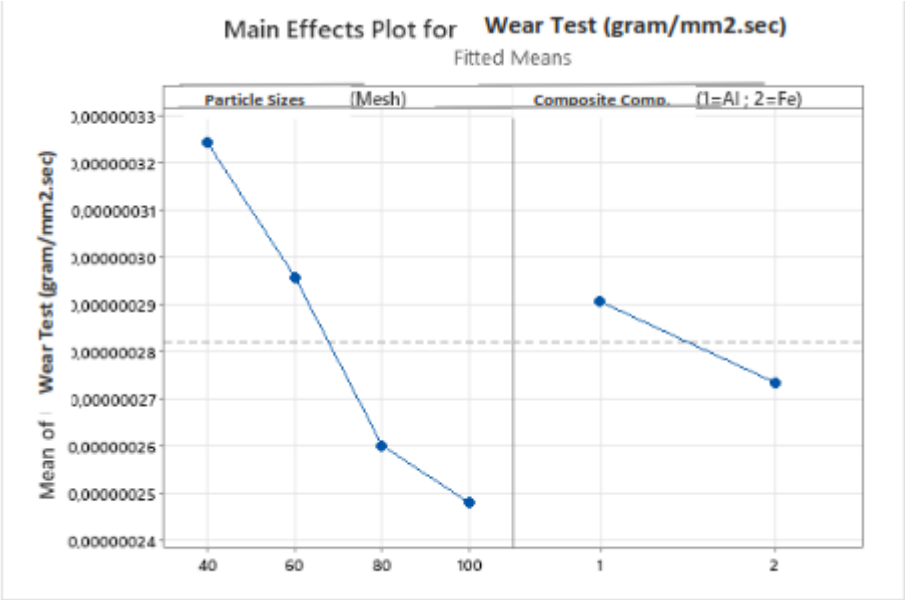

Figure 8 Factorial Plot

Based on Figure 8. there are 2 main lines, namely horizontal which shows the independent variable and vertical which shows the dependent variable. The graph shows that the smaller the particle size or the larger the mesh size, the lower or lower the wear rate produced. In the composite composition shows the use of iron powder material the wear rate is lower or decreases than aluminum powder.

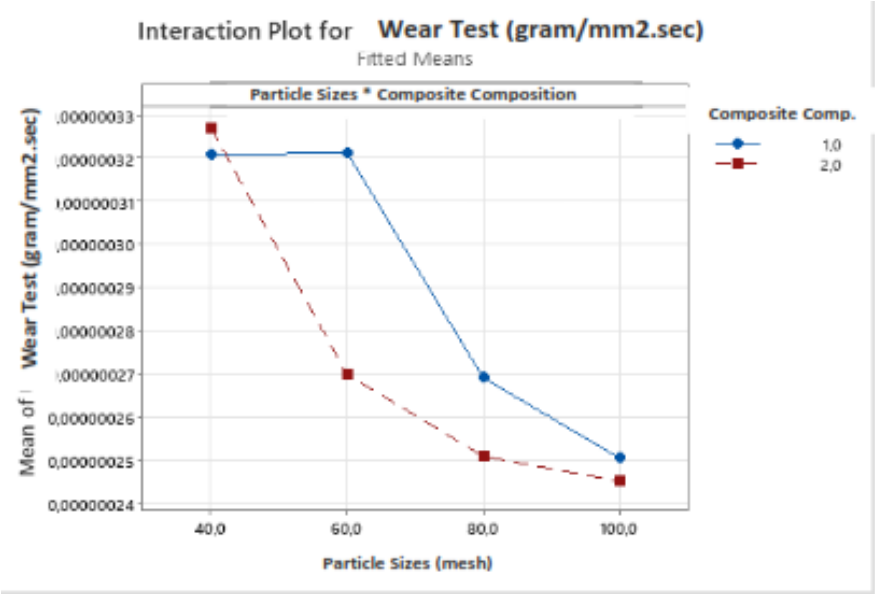

Figure 9. Factorial interaction plots

Figure 9. is a graph of the interaction between particle size and composite composition which aims to determine the effect of the interaction between the independent variable on the dependent variable, where in this study describes the relationship between particle size and composite composition on wear rate. In the graph there are 2 lines showing the independent variable composite composition with different colors according to the material used from the specimen, namely blue and orange. In the graph, it can be seen that the wear rate of the specimen is getting smaller along with the smaller the particle size or the larger the mesh size used, while in the composite composition the use of iron powder has a smaller wear rate than the use of aluminum powder in the specimen.

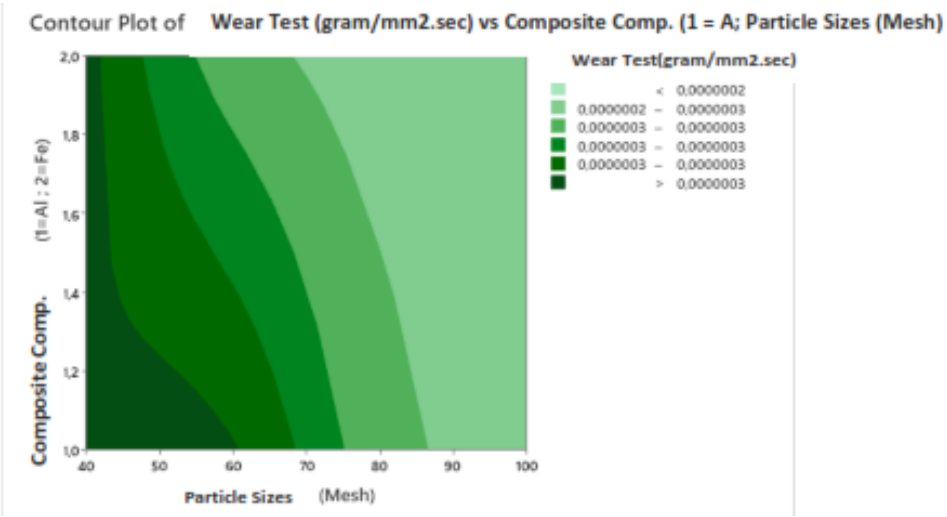

Figure 10. Countour plot graph

In Figure 10. above is a contour plot graph of the effect of particle size and composite composition on the wear rate value of the specimen, showing that the horizontal line on the graph is the variation of particle size and the vertical line on the graph is the composite composition. In the figure above, the tosca green color or the rightmost part of the graph shows the smallest wear rate area of 0.0000002 g/mm^2.second with a particle size of 90 - 100 mesh in composite compositions 1 and 2 and at a particle size of 80 mesh in composite composition number 2. The jade green color or the right part shows the wear rate area of 0.0000002 - 0.0000003 g/mm^2. seconds with a particle size of 80 mesh in composite composition number 1, at a particle size of 60 mesh in composite composition number 2. In the middle part of the figure above shows Emerald green color shows the wear rate area of 0.0000003 g/mm^2.seconds with a particle size of 80 mesh in composite composition number 1, and at a particle size of 60 mesh in composite composition number 2. The dark green color shows the wear rate area of 0.0000003 g/mm^2.second with a particle size of 60 mesh in composite composition number 1, and at a particle size of 50 mesh in composite composition number 2. The dark green color or the leftmost part of the graph shows the area of the

greatest wear rate of >0.0000003 g/mm^2.second with a particle size of 60 mesh in composite composition number 1 and at a particle size of 40 mesh with composite compositions number 1 and 2.

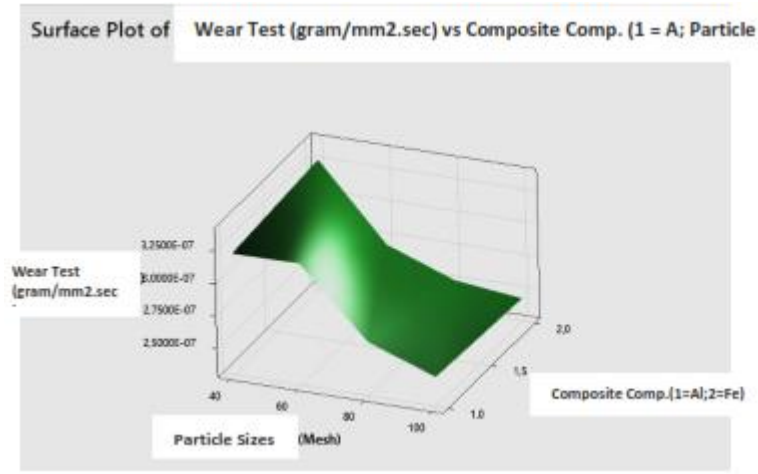

Figure 11. Surface plot graph

Figure 11 is a surface plot graph of the results of the study of the effect of particle size and composite composition on specimen wear. In the graph, the x-axis shows the particle size, the y-axis shows the composite composition, and the z-axis shows the wear rate. From the graph it can be concluded that, the effect of particle size on wear is the larger the mesh size or the smaller the particle size, the smaller the wear rate produced will be. This can be caused by the level of hardness which also increases against the particle size as the previous research variables did. The greater the level of hardness, the smaller the wear rate produced. On the effect of composite composition on wear rate, it can be concluded that the use of composition number 2 or iron powder has a relatively lower wear rate compared to the use of composition number 1 or aluminum powder.

3.3 Discussion

Effect of Particle Size and Composite Composition on Hardness Level

Based on the processing of hardness test data above is a significant effect. The hardness level of the particle size is known to be higher at a larger mesh size, this is because the small particle size has smaller pores so that more material bonds will create a smaller space, with small pores, the performance of the brake lining will be good. While the hardness value of the composite composition using iron powder has increased the hardness value, because iron powder has a higher density value of 7.87 gr/cm^3 while the density value of aluminum powder is 2.7 gr/cm^3. The highest hardness value is found in specimen B4 with an average of 81 HD using a mesh of 100 and a composite composition of iron powder, from this study it was found that specimens A4, B3, B4 have an average hardness value that is higher than the comparison sample on the market. Particle size variations produce good hardness values supported by research conducted by Purboputro (2020) entitled "Making Brake Pads Using Variations of Grain Mesh Aluminum Silicon (Al-Si) 50, 60, 100 With Teak Wood Powder Against Hardness Level Values, Wear and Coefficient of Friction" states that the value of the finished wood powder brake lining with Mesh 100 variation is 81.60 HD and the lowest is at Mesh 50 variation which is 75.45 HD, so it is concluded that the smaller the grain of Aluminum Silicon can affect the increase in hardness value on the natural-based brake lining teak wood powder.

While in the composition of the material it can be concluded that the higher the density value of a material, this will cause the hardness value to increase. This is in accordance with previous research entitled "Experimental Study of the Effect of Bamboo Powder Particle Size on Composite Mechanical Properties for Motorcycle Brake Pad Applications" which states that the higher the mark density value of a material can cause the mark hardness to increase as well.

Effect of Particle Size and Composite Composition on Wear Rate

In the wear test, it is known that there is a significant effect of the particle size of the non-asbestos brake lining composite. The use of smaller particle sizes or larger mesh sizes results in smaller wear rates of brake lining specimens. This indicates that the wear rate of brake lining with a mesh size of 100 is better than that of mesh sizes 40, 60, and 80. This is due to the extent of particle-matrix interface interactions at smaller particle sizes allowing small particles on the surface of the brake lining to be difficult to escape, and vice versa.

Meanwhile, the effect of composite composition on wear. Composite compositions that use iron powder materials have higher hardness compared to aluminum. This is because the mechanical characteristics of the two

materials are different. From this study it can be seen that specimens with codes A1, A2, A3, A4, B1, B2, B3, B4 have a wear rate that is close to the comparison sample.

Interaction Effect of Particle Size and Composite Composition on Hardness and Wear

The interaction of the two independent variables has a significant effect on hardness and wear. This is because composite composition and particle size are closely interconnected in determining the properties and performance of brake linings. Composite composition affects the basic characteristics of the material, while particle size affects the mechanical properties of the brake lining, smaller particle size, higher strength and stiffness due to better load distribution. So the interaction of the two results in high hardness and low wear.

Knowledge gap and contribution of this study

From the results of this study, information was obtained regarding the current knowledge gap related to brake pads made of non-asbestos fibers and natural fibers used from Sengon wood. This is an innovative idea to expand the alternative use of natural fibers other than the widely used natural fibers such as bamboo, teak wood, and coconut shells. In addition, it turns out that Sengon wood also has a significant impact on the performance of non-asbestos brake pads. East Java Province is a Sengon wood producing area so it will be useful in utilizing the potential of natural resources.

4. CONCLUSION

The following conclusions can be obtained from the research on the effect of particle size and composite composition on the performance of non-asbestos brake linings:

1. The effect of particle size and composite composition on the hardness level of non-asbestos brake linings can be concluded that:
   a. Particle size affects the hardness value received. The larger the mesh size used, the higher the hardness value obtained, namely in specimen B4 with an average of 81 HD using mesh 100 and iron powder composite composition.
   b. The composite composition affects the hardness value of non-asbestos brake linings, namely with different types of materials used, the characteristics of these materials are also different. In this study, the highest hardness value was obtained in specimens using iron powder.
2. Effect of Particle Size and Composite Composition on Wear Rate
   a. Particle size variation has an influence on the wear rate, namely the larger the mesh size, the smaller the wear rate value will be obtained. This is because the particle-matrix interface interaction at a smaller particle size allows small particles on the surface of the brake lining to be difficult to escape
   b. Composite composition has an effect on the effect on canvas wear rate because the higher the mechanical properties of the type of material produced, the more the material produced is also good.
3. The interaction of the two independent variables has a significant effect on hardness and wear. This is because composite composition and particle size are closely interconnected in determining the properties and performance of brake linings. Composite composition affects the basic characteristics of the material, while particle size affects the mechanical properties of the brake lining, smaller particle size, higher strength and stiffness due to better load distribution. So, the interaction of the two results in high hardness and low wear.

5. ACKNOWLEDGMENT

The author would like to express gratitude to family members and colleagues for their support in completing this research.

6. REFERENCES

[1] P. Blau and J. McLaughlin, “Effect of water films and sliding speed on the frictional behavior of truck disc brake materials,” Wear, vol. 36, no. 10, pp. 709–715, 2003.
[2] L. Mulyani, F. Setiawan, and E. Sofyan, “Analisis karakteristik keausan material dengan matriks resin menggunakan filler serat bambu dan pasir besi untuk aplikasi kampas rem,” Teknika STTKD: J. Tek. Elektron. Eng., vol. 8, no. 1, pp. 103–111, 2022, doi: 10.56521/teknika.v8i1.549.
[3] S. Kumar and S. K. Ghosh, “Particle emission of organic brake pad material: A review,” Proc. Inst. Mech. Eng. D J. Automob. Eng., vol. 234, no. 5, pp. 1213–1223, 2020, doi: 10.1177/0954407019879839.
[4] Suhardiman and M. Syaputra, “Wear analysis of non-asbestos brake linings made from polymer composites of rice dust and coconut shells,” Inovtek Polbeng, pp. 210–214, 2017.
[5] N. A. Ademoh and A. I. J. D. Olabisi, “Development and evaluation of maize husks (asbestos-free) based brake pad,” J. Dev., vol. 5, no. 2, pp. 67–80, 2015.
[6] I. Puja, “Studi sifat impak ketahanan aus dan koefisien gesek bahan komposit arang limbah serbuk gergaji kayu glugu dengan matrik epoxy,” J. Energi Manuf., vol. 4, no. 2, pp. 2–6, 2010.

[7] Rina, “Experimental study of the effect of bamboo powder particle size on the mechanical properties of composites for motorcycle brake lining applications,” Unpublished manuscript, 2016.
[8] M. L. I. Sholihin, “Pengaruh komposisi dan temperatur material biokomposit terhadap kinerja kampas rem non-asbestos,” J. Energi Teknol. Manuf., vol. 5, no. 1, pp. 29–34, 2022, doi: 10.33795/jetm.v5i01.117.

LOGIC
Journal of Engineering Design and Technology
Vol. 25 No.1 March 2025 ; p. 13 - 18

p-ISSN : 1412-114X
e-ISSN : 2580-5649
http://ojs2.pnb.ac.id/index.php/LOGIC

THE EFFECT OF INJECTION PRESSURE AND INJECTION TEMPERATURE IN THE COMPRESSION MOULDING PROCESS ON FLASHING DEFECTS OF SHOULDER PRODUCTS

Moh. Hartono [1)], Febrian Akbar Pratama [1)]

1) Mechanical Engineering Departement, State Polytechnic of Malang, Jl Soekarno-Hatta 9, Malang, Indonesia

Correponding email [1)] : moh.hartono@polinema.ac.id

Abstract. Plastic objects are everywhere: toys, household utensils, playthings, and cosmetic containers. One of the processes used was the plastic production process in the compression molding process to make a cover (shoulder) on the tube. Flashing defects are one of the biggest defects that can cause a product to fail in the assembly of shoulder extrusion tube products in PT. XYZ. This research was to determine the effect of injection pressure and injection temperature parameters on flashing defects in shoulder extrusion tube products. This research uses quantitative research and experimental research methods to collect data. Varying parameter settings carry out this method with an injection pressure of 4 bar, 5 bar, and 6 bar as well as injection temperatures of 250°C, 260°C, and 270°C. The results of the study show that both parameters have significant effects on the flashing defects in shoulder extrusion tube products. The combination of injection pressure of 4 bar and injection temperature of 250°C resulting in flashing defects of 0 mm or no defects.

Keywords : compression moulding, flashing defects, injection pressure, injection temperature, shoulder.

1. INTRODUCTION

Plastic objects are almost everywhere from food wrappers, to household utensils, toys, and cosmetic containers. Plastic is a material that is easy to shape, light, anti-corrosive, and cheap [1]. Plastic products can be produced through certain processes according to their needs. Based on the properties of plastic, the plastic product can gradually replace other materials. Therefore, improving the quality of plastic products is an important factor in getting good quality plastic products. The plastic molding process can be broadly classified as injection, extrusion, blow molding, calendering, and compression. The molding process is an effective and efficient forming process in the industry [2].

The shoulder manufacturing process uses a compression molding process. The compression molding process is where the plastic pellets are heated so that the phase changes from solid to melt and passes into the mold (matrix). The mandrel (punch) with the sleeve (extrusion process) applied pressure to the matrix, allowing it to freeze and cool for a while, where a shoulder will form and connect to the tube.

Machine parameters, material properties, mold shape, and machine capacity used during the production process influence the plastic molding process [3]. Parameters that influence the compression molding process which contributes to product defects include injection time, injection pressure, holding pressure, and injection temperature. These defects can be eliminated or reduced by designing process parameters appropriately and correctly [4]. Many things must be considered in the product production process so that the product has a quality that meets the specified standards. Injection pressure and injection temperature are important parameters that must be considered in the production process for shoulder extrusion tube products.

The production process of making shoulder extrusion tubes cannot be separated from product defects. One of the product defects that often occurs is unmolded shoulders, folded shoulders, and flashing. The flashing defect is one of the most common defects in the shoulder tube manufacturing process. To eliminate flashing on the product, a finishing process is needed on the product. Flashing is a defect where there is excessive material on the product [5]. Flashing defects can cause the product to fail to be assembled, so this causes big losses for the company because a lot of material is wasted and customers experience delays in product delivery.

2. METHODS

The type of research used is quantitative with experimental methods. This method is used to find out what factors can affect the result of the research. Data analysis was carried out to test the research hypothesis with the ANOVA method. The tools used in this research include compression molding machines with screw diameters of 34 mm and can produce tubes with diameters ranging from 13.5 to 63.5 mm. The material used in making shoulder extrusion tubes is a mixture of HD 80% + LD 20% (PE). The injection time is 0.25 s with a holding pressure of 2.5 bar. The height gauge used measures the flashing defect deviation of the shoulder extrusion tube.

3. RESULTS AND DISCUSSION

3.1 Result

The result of product identification and height measurement obtained from the data collection process was 90 shoulder extrusion tube products. Products with flashing defect height of more than 13.6 ± 0.1 mm, as shown in Table 1.

Table 1. Measurement flashing defect

Injection Pressure (bar)	Injection Temperature (°C)	Flashing Defect (mm)										Average (mm)
		1	2	3	4	5	6	7	8	9	10	
4 bar	250°C	0	0	0	0	0	0	0	0	0	0	0.00
	260°C	0.05	0.07	0.08	0.07	0.06	0.07	0.09	0.07	0.11	0.12	0.08
	270°C	0.09	0.1	0.16	0.24	0.22	0.1	0.1	0.15	0.23	0.23	0.16
5 bar	250°C	0	0	0	0	0.04	0.05	0.06	0.11	0.07	0.06	0.04
	260°C	0.14	0.07	0.06	0.15	0.07	0.09	0.21	0.07	0.14	0.15	0.12
	270°C	0.56	0.57	0.55	0.53	0.58	0.59	0.58	0.52	0.51	0.5	0.55
6 bar	250°C	0	0	0.11	0.06	0.09	0.12	0.07	0.14	0.12	0.08	0.08
	260°C	0.08	0.15	0.18	0.2	0.22	0.2	0.15	0.09	0.1	0.22	0.16
	270°C	0.95	0.98	0.92	0.95	1,02	1	0.99	0.98	0.99	1,01	0.98

The data collection that has been carried out, then processing is then continued using statistical software. Figure 1 shows the results of the analysis that has been carried out.

The normal probability plot graph shows that the residual points are formed close to the red straight line. A significant value is indicated (P-Value > 0.05). If the significant value is > 0.05 the data is normally distributed. The result of the residual normality test can be said to mean that the data follows a normal distribution. It is assumed that the regression model that has been created can be used.

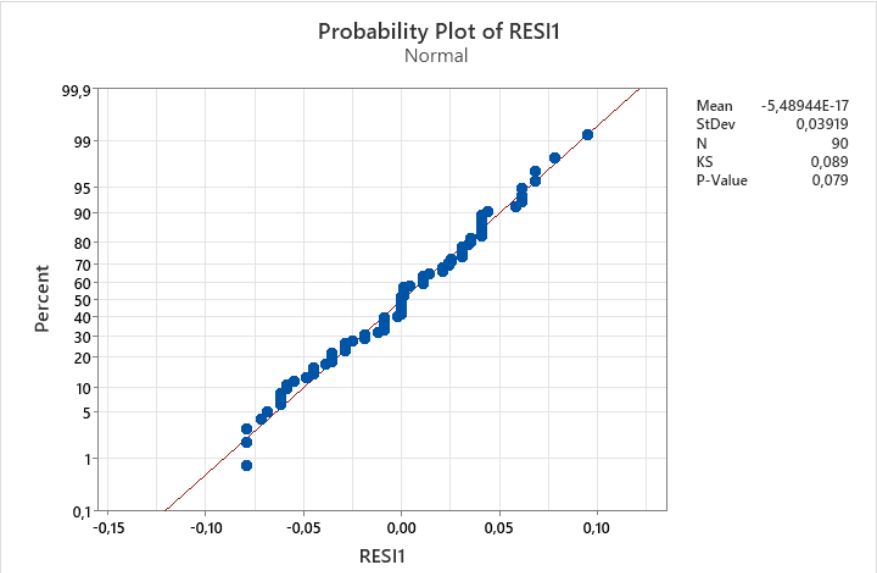

Figure 1. Graphic normal probability plot

Table 3. Analysis of Variance

Analysis of Variance

Source	DF	Adj SS	Adj MS	F-Value	P-Value
Model	8	8,2093	1,02616	608,04	0.000
Linear	4	6,3949	1,59872	947,30	0.000
Inject Pressure (bar)	2	1,5895	0.79475	470.92	0.000
Inject Temperature (°C)	2	4,8054	2,40269	1423,68	0.000
2-Way Interactions	4	1,8144	0.45361	268,78	0.000
Inject Pressure (bar)*Inject Temperature (°C)	4	1,8144	0.45361	268,78	0.000
Error	81	0.1367	0.00169		
Total	89	8,3460			

The ANOVA shows that injection pressure and injection temperature have a p-value of 0.000 so based on the hypothesis in this study the decision is to reject the initial hypothesis because the p-value is less than the alpha (α) tolerance level of 5% or 0.05 which is has been determined (p-value < alpha (α)). So the null hypothesis is rejected and the alternative hypothesis is accepted and the conclusion is that injection pressure and injection temperature have a significant effect on flashing defects in shoulder extrusion tube products.

Model Summary

S	R-sq	R-sq(adj)	R-sq(pred)
0,0410811	98,36%	98,20%	97,98%

Figure 3. Model Summary

The coefficient of determination (R-square) value aims to predict or see how much influence the independent variable contributes to the dependent variable. Based on the model summary above, it is known that the coefficient of determination value is 98,36%, this figure shows that the injection pressure and injection temperature for flashing defects in shoulder extrusion tube products is 98,36% and the remaining 1,64% is an error caused by other variables not studied.

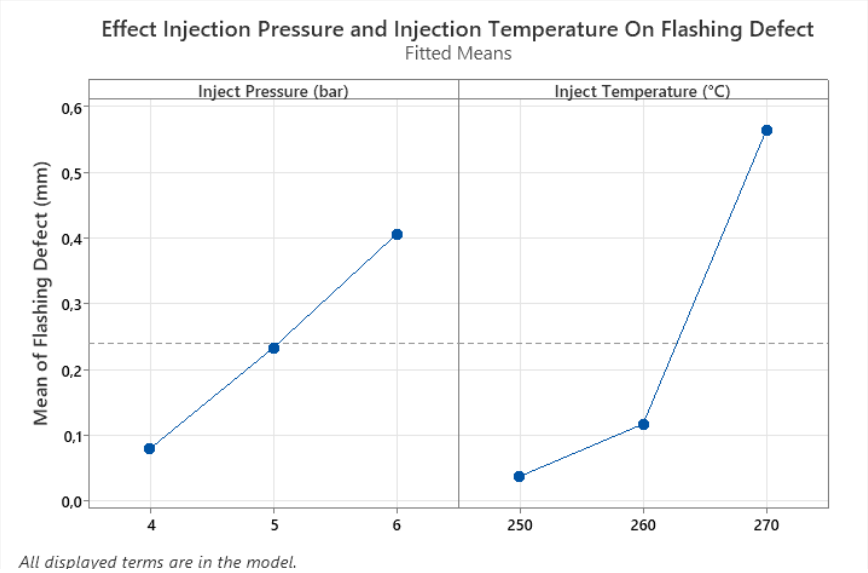

Figure 4. Effect of Injection Pressure and Injection Temperature on Flashing Defects

The main effect plot above is that the higher the level of injection pressure and injection temperature caused the flashing defects in the product to become larger, this is because increasing injection pressure facilitated the flow of plastic melt into the mold causing excess material so that flashing defect in the products increase. Meanwhile, higher injection temperature decreases the viscosity of the plastic material and makes it easier for the material to flow into the mold so that flashing defects in the product increase.

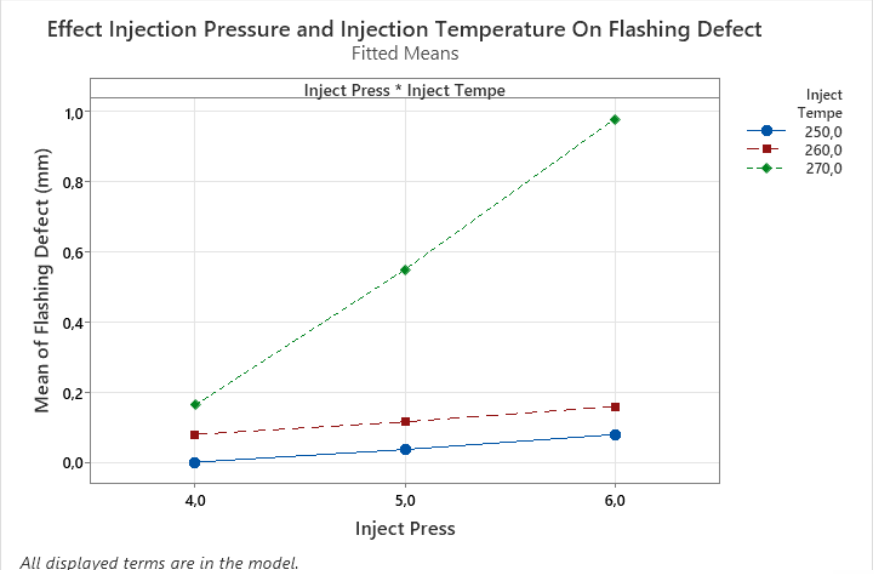

Figure 5. Effect of Injection Pressure and Injection Temperature on Flashing Defects

In figure 5 shows the interaction between injection pressure and injection temperature, there are different colored lines representing the independent variable injection temperature, namely blue, red, and green. The green line shows the injection temperature level of 270°C. The red line shows the injection temperature level of 260°C and the blue line shows the injection temperature level of 250°C. The horizontal line shows the level of the independent variable injection pressure which has levels of 4 bar, 5 bar, and 6 bar. The vertical line shows the dependent variable, the namely flashing defect. The interaction graph shows the result on the blue line for an injection temperature of 250°C with an injection pressure of 4 bar the possible defect value is 0. which means there are no flashing defects, and injection pressure of 5 bar the possible value of flashing defect value is 0.036 mm and injection pressure 6 bar, the possible value of flashing defect value is 0.079 mm. In the red line for an injection temperature of 260°C with an injection pressure of 4 bar, the possible flashing defect value is 0.079 mm. and the flashing defect value continues to increase injection pressure of 5 bar and injection pressure of 6 bar, amounting to 0.115 mm and 0.159 mm. In the green line for injection temperature of 270°C with injection pressure of 4 bar,

the possible flashing defect value is 0.162 mm, and the flashing defect value continues to increase at injection pressure 5 bar and injection pressure 6 bar, amounting to 0.549 mm and 0.979 mm.

3.2 Discussion

Effect of Injection Pressure on Flashing Defect

The use of injection pressure parameters in this research shows that the greater injection pressure will produce large product flashing defects, while the smaller injection pressure parameter will produce small product flashing defects. This is because the greater the injection pressure, the easier it is for the melted plastic to flow into the mold, causing excess material. Using injection pressure will cause the material to have difficulty flowing when filling the liquid plastic into the mold cavity. This is by previous research entitled "The Effect of Inject Pressure and Clamping Force on Flashing Defects in the Pot Cover Injection Molding Process" This research explains that the injection pressure parameter influences flashing defects. The higher the injection pressure, the greater the possibility of flashing defects occurring [6].

Effect of Injection Temperature on Flashing Defect

The use of the injection temperature parameter in this research shows that the greater injection temperature will produce large product flashing defects, while the smaller injection temperature parameter will produce flashing defects. This is because the higher the material temperature, the smaller the viscosity of the plastic material fluid so that the easier it is for the material to flow onto the mold, the fluid temperature is inversely proportional to the viscosity value. Using a low temperature will cause the material not to melt completely so that the material cannot directly enter the mold. This is by previous research entitled "Analysis of the Effect of Injection Molding Temperature and Pressure on Product Defects" The higher the injection pressure and injection temperature will cause too much material supply and too runny material to the mold cavity [7].

Interaction between Injection Pressure and Injection Temperatur on Flashing Defect

The interaction of the two independent variables, namely injection pressure and injection temperature on flashing defect in shoulder extrusion tube product, can be concluded that if the injection pressure and injection temperature are high, the resulting flashing defect will be larger. However, if the injection pressure is low and the injection temperature is low, it will produce a small product flashing defect. Based on this research and the two previous studies, the results were the same, namely producing products with small flashing defect values, which were achieved by using injection pressure and injection temperature parameters with the lowest values for each level.

4. CONCLUSION

The research effect injection pressure and injection temperature in the compression molding process on flashing defect of shoulder extrusion tube product, then the conclusions obtained are:

1. The influence of injection pressure on flashing defect of shoulder extrusion tube product. It can concluded that the influence of injection pressure has a significant effect on the flashing defect in the product. The research average flashing defect was 0.080 mm at an injection pressure level of 4 bar. The injection pressure increased and the highest average flashing defect was obtained at an injection pressure level of 6 bar with an average flashing defect of 0.405 mm.
2. The influence of injection temperature on flashing defect of shoulder extrusion tube product. It can concluded that the influence of injection temperature has a significant effect on the flashing defect in the product. The research average flashing defect was 0.038 mm at an injection pressure level of 250°C. The injection temperature increased and the highest average flashing defect was obtained at an injection temperature level of 6 bar with an average of flashing defect of 0.563 mm.
3. The result to determine the interaction of the two independent variables, namely injection pressure and injection temperature on flashing defect of shoulder extrusion tube product, can be concluded that the optimal combination of the two parameters for shoulder extrusion tube product is obtained at a combination of injection pressure of 4 bar and injection temperature of 250°C with a flashing defect value of 0 mm or no defect.

5. REFERENCES

[1] B. Pradika, S. Supriyadi, and A. Burhanudin, "Analysis of the Effect of Temperature on Result of Micro Injection Molding Product in Making Sauce Cups Made from Polypropylene (PP)" SENS vol 5 772-780. 2020.
[2] M. Hartono, "Improving the Quality of Plastic Product Using the Taguchi Method" Jurnal Industrial Engineering, vol 13, No.1, 93-100
[3] P. T. Devalia and T.M. Arief, "Analysis and Optimization of Multi Cavity Plastic Injection Process Parameters to Minimize Short Mold Defect" Ind. Res. Work National. Seminar., vol. 10. No.1, pp.553-560. 2019.

[4] E. Sunarto, and E. Prayogi, “Effect of the Cooling Process on Shrinkage and Dimensions of TS Plug Made from PVC in Injection Molding” Aplikasi Teknologi Industri 235-241, 2018.
[5] H. Permana, Topan, and S. Anwar, ”Production Process of Flip Flop Plastic Components Using a Hydraulic Type Injection Molding Machine” J. Baut and Manufactur, vol. 03, no. 02, pp. 2686-5351, 2021.
[6] S. Qomariah and A. Dani, “The Effect Inject Pressure and Clamping Force on Flashing Defects in the Pot Cover Injection Molding Process” JETM, 2023
[7] H. Yanto, I. Saputra and S. Wiratno, “Analysis of the Effect of Injection Molding Temperature and Pressure on Product Deffects” Jurnal Integrasi (Vol.10. Issue 1), 2018

LOGIC
Journal of Engineering Design and Technology
Vol. 25 No. 1 March 2025; p. 19 - 26

p-ISSN : 1412-114X
e-ISSN : 2580-5649
http://ojs2.pnb.ac.id/index.php/LOGIC

CONSTRUCTION OF A THERMOELECTRIC COOLBOX SYSTEM WITH ICE PACK MODIFICATION FOR MANGO STORAGE BASED ON THE INTERNET OF THINGS

Fauzan Amri [1)], Ardiansyah Rahma Putra [2)], Moh. Abdul Gofur [2)], Doli Bonardo [3)]

1) Instrumentation and Control Engineering Technology, Politeknik Negeri Indramayu, Jawa Barat, Indonesia.
2) Refrigeration Engineering and Air Conditioning, Politeknik Negeri Indramayu, Jawa Barat, Indonesia.
3) Department of Electrical Engineering, Faculty of Maritime Engineering and Technology, Universitas Maritim Raja Ali Haji, Tanjungpinang, Indonesia

Correponding email [1)] : fauzanamri@polindra.ac.id

Abstract. This study aims to design a thermoelectric system for a coolbox utilizing additional ice pack components for mango storage by leveraging a TEC1-12706 Peltier element based on IoT technology. Thermoelectric is an energy conversion technology that directly converts thermal energy into electrical energy and vice versa through thermoelectric materials. The system operates based on the Peltier effect, which generates a temperature difference between two sides of the material when an electric current is applied. Based on the test results, the developed thermoelectric system achieved a cabin temperature of up to 12.6 ºC within 60 minutes, according to the ideal storage temperature requirements for mangoes (12–15 ºC). The addition of an ice pack plays a significant role in accelerating the temperature reduction inside the cabin. The cold sink and heatsink components function effectively in absorbing and releasing heat to the environment. This system achieved a COP of 0.60 with an efficiency of 60%. The thermoelectric system has also been successfully integrated with IoT technology through the Blynk application, enabling users to monitor temperature and humidity in real-time via an internet-connected smartphone, thereby facilitating the control of mango storage conditions.

Keywords: thermoelectric coolbox system, ice pack, mangoes, IoT

1. INTRODUCTION

Mangoes are one of the important horticultural commodities in Indonesia. The abundant production of mangoes in Indramayu [1] often encounters post-harvest challenges, particularly in storage and maintaining fruit quality [2]. Mangoes are climacteric fruits that continue to ripen after being harvested, making them prone to damage and spoilage if not properly handled. Post-harvest losses can lead to significant economic losses for farmers and traders [3], [4]. The ideal storage temperature for mangoes generally ranges between 12–15 °C, with relative humidity of 85–90% [5], [6]. Conventional storage methods, such as using ice blocks or open-air storage, are often less effective in maintaining mango quality over an extended period. Ice blocks have limitations in maintaining stable temperatures, while open-air storage is highly dependent on environmental conditions. Therefore, a more effective and controlled storage solution is required to extend the shelf life and preserve the quality of mangoes [7].

Thermoelectric technology offers an environmentally friendly and efficient cooling solution. Thermoelectric systems operate based on the Peltier effect, which generates a temperature difference between two sides of a material when an electric current is applied. Thermoelectric cooling systems have several advantages, including compact size, the absence of refrigerants, and precise control capabilities [8], [9]. Permana et al. successfully designed a thermoelectric refrigeration system utilizing solar energy for banana storage, achieving a minimum cold-side temperature of 12.7 °C after 180 minutes of operation [10]. Aziz et al. developed a temperature control system for fruit and vegetable storage applications using TEC1-12706 thermoelectric coolers, demonstrating cabin temperature stability at 15 °C, which is considered suitable for storing fruits and vegetables [11]. Another thermoelectric system developed by Tuapetel et al. managed to cool 1.2 liters of water to 14.9 °C

[12]. Despite extensive development of thermoelectric systems, their efficiency remains relatively low [13], [14], necessitating modifications to thermoelectric materials and module designs to improve performance.

One modification that can be implemented is the addition of ice packs. Ice packs act as supplementary cold storage, prolonging cooling time and reducing temperature fluctuations inside the coolbox [15]. Furthermore, thermoelectric systems can be integrated with Internet of Things (IoT) technology, enabling real-time and remote monitoring and control of temperature, humidity, and other parameters, thereby improving system efficiency. IoT also facilitates damage prediction and preventive actions, providing significant benefits in system maintenance in terms of convenience, accuracy, and efficiency. Based on the above considerations, this study focuses on constructing a modified thermoelectric coolbox system with ice packs, integrated with IoT via the Blynk application, to optimize mango storage. This system is expected to maintain the quality and extend the shelf life of mangoes efficiently and economically.

2. METHODS

2.1 Tools and Materials

The tools and materials used in this study include Krisbow screwdrivers, Tekiro measurement tape, Wipro saw, Krisbow hammer, magnetic spirit level, TEC1-12706 thermoelectric cooler, heatsink, cold sink, power supply, wooden blocks, plywood, stainless steel plates, polyurethane polymer, aluminum foil, DC fan, 2 kg of mangoes, Monotaro Group terminal block, Eterna cables, ESP32 Series Wemos D1 R32, switches, 2-channel relays, DHT11 sensor, and a 16 x 2 I2C Liquid Crystal Display (LCD). All these tools and materials were prepared to design the construction of an IoT-based thermoelectric coolbox system.

2.2 Construction of the Thermoelectric Coolbox System

The construction of the thermoelectric system consists of two parts: a trainer table and a coolbox cabin, as shown in Figure 1(a). The trainer table is made of 3 x 3 cm² wooden blocks and 65 x 50 cm² plywood. Meanwhile, the coolbox cabin is constructed using a combination of stainless steel, polyurethane polymer, and aluminum foil to maximize cooling efficiency and thermal insulation. In detail, the layout of each component in this thermoelectric cooler box system is also presented in Figure 1(a).

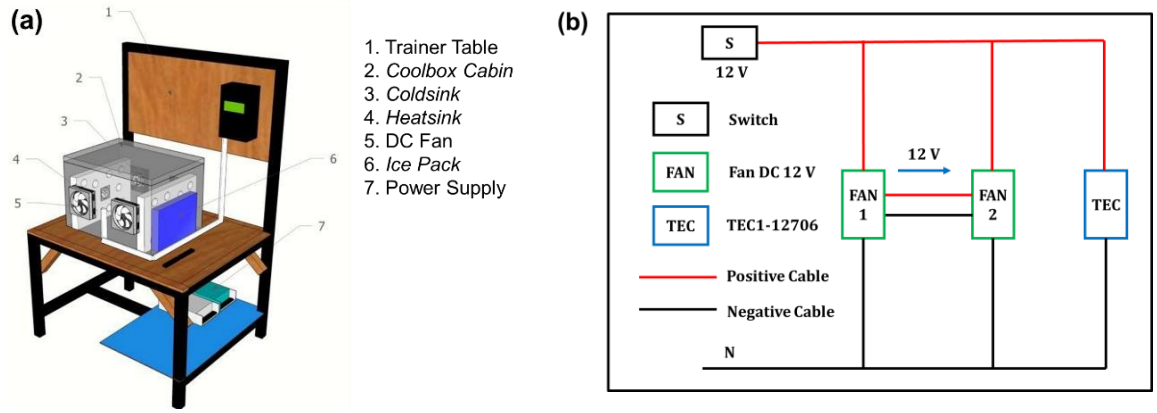

Figure 1. (a) Construction of the thermoelectric coolbox system and (b) electrical wiring diagram for the thermoelectric system

Figure 1(b) presents the electrical wiring diagram of the thermoelectric system in the coolbox, which maps the connections between the load, control devices, safety devices, and measurement instruments. To prevent short circuits, the positive and negative wires are placed at a distance from each other [10]. A 12-volt DC unidirectional current from the power supply flows through the cooling fan on the heatsink and coldsink, as well as the Peltier element.

2.3 IoT-Based System Design

The IoT-based system is designed using ESP32, DHT11 sensor, relay, power supply, fan, and LCD. All of these components are assembled according to the wiring diagram shown in Figure 2(a). Based on this diagram (Figure 2a), the DHT11 sensor is connected to the ESP32 with the Vcc pin to 3V3, GND to GND, and Data to GPIO19. Next, the GND, Vcc, SDA, and SCL pins on the LCD are connected to the GND, Vin, GPIO21, and GPIO22 pins of the ESP32, respectively. The Vin pin of the ESP32 is then connected to a 3.3-volt power supply to activate and operate the system [16]. A summary of the steps for reading sensor data, processing it, displaying it on the LCD, and sending it to the IoT platform can be seen in Figure 2(b). After all the component pins are installed according to the diagram in Figure 2(a), the system is programmed using the Arduino IDE software.

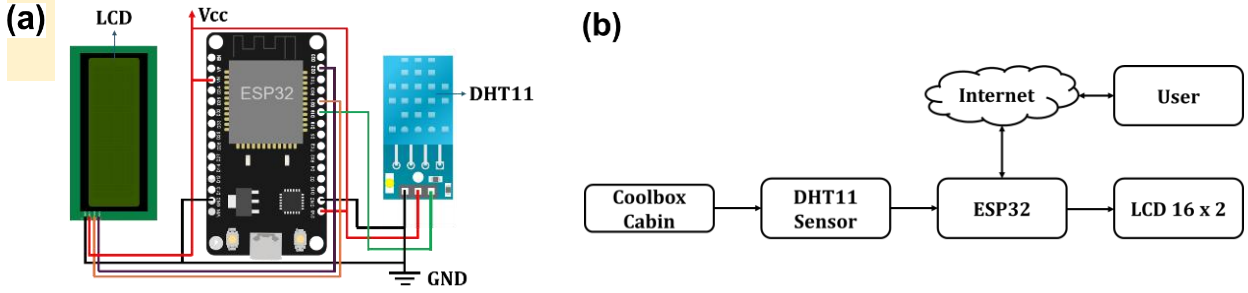

Figure 2. IoT-based system design. (a) wiring diagram and (b) block diagram

2.4 System Operating Principle

This mango storage system works by utilizing the thermoelectric Peltier effect to generate cooling. To enhance cooling efficiency, the system is equipped with an ice pack as a secondary cooler and a heat transfer system consisting of a DC fan, cold sink, and heatsink mounted on the coolbox. The operation of the system begins with applying DC current to the thermoelectric component (Peltier), which creates a temperature difference between the two sides: one side becomes cold, and the other becomes hot. The cold side is further cooled by the cold sink and circulated into the coolbox with the help of the fan. The ice pack helps maintain the temperature inside the coolbox. Meanwhile, the heat from the hot side of the Peltier is dissipated into the environment through the heatsink and fan. On the other hand, the DHT11 sensor detects the temperature and humidity in the coolbox cabin, and then sends this data to the ESP32. The ESP32 then sends the data to the LCD and the Blynk application for display. Users can easily monitor the temperature and humidity data in real time through the Blynk application.

3. RESULTS AND DISCUSSION

3.1 Design Data

Before the data collection process, calculations were performed for the design of the thermoelectric coolbox system. These calculations serve as guidelines for testing and data collection on the system. The transmission load can be calculated using Eqs. (1) and (2) as follows:

$$Q_T = U \,.\, A \,.\, (T_{ambient} - T_{cabin}) \tag{1}$$

$$U = \frac{1}{\frac{1}{f_{in}} + \frac{x_1}{k_1} + \frac{x_2}{k_2} + \frac{x_3}{k_3} + \frac{1}{f_{out}}} \tag{2}$$

where Q_T is the transmission load (W); U is the heat transfer coefficient (W/m^{2}K); A is the surface area of the outer wall (m^2); $T_{ambient}$ is the ambient temperature (K); T_{cabin} is the cabin temperature (K); f_{in} dan f_{out} is the heat transfer coefficients for the inner and outer surfaces of the cabin wall (W/m^{2}K), respectively; x is the thickness of each layer of wall material (m); and k is the thermal conductivity of each wall material layer (W/mK). By employing the system specifications in Table 1, the calculated heat transfer coefficient *(U)* and transmission load *(Q)* are 1.24 W/m²K and 15.8 W, respectively.

Table 1. Specification of The Thermoelectric Coolbox System

Parameter	Specification
Coolbox dimensions	0.4 x 0.34 x 0.27 m^3
Wall material	
1. stainless steel plate (k_1)	1. thickness 0.3 mm, thermal conductivity 15.1 W/mK [17]
2. polyurethane (k_2)	2. thickness 20 mm, thermal conductivity 0.03 W/mK [17]
3. aluminum foil (k_3)	3. thickness 4 mm, thermal conductivity 0.033 W/mK [17]
4. still air (f_{in})	4. convection coefficient 9.37 W/m^{2}K [17]
5. moving air (f_{in})	5. convection coefficient 22.7 W/m^{2}K [17]
Ambient temperature	$T_{ambient}$ = 32 ºC = 305.15 K
Cabin temperature	T_{kabin} = 13 ºC = 286.15 K

The product load for mangoes can be calculated using Eq. (6) as follows:

$$Q_1 = m \times c_a \times (T_{ambient} - T_{kabin}) \quad (3)$$

$$Q_2 = m \times L_f \quad (4)$$

$$Q_3 = m \times c_b \times (T_{ambient} - T_{kabin}) \quad (5)$$

$$Q_P = \frac{Q_1 + Q_2 + Q_3}{n} \quad (6)$$

where Q_1, Q_2, and Q_3 are sensible heat above freezing, latent heat, and sensible heat below freezing (W), respectively; m is the mango mass (kg); c_a is the specific heat of mango above freezing (kJ/kgK); L_f is the latent heat of mango (kJ/kg), c_b is the specific heat of mango below freezing (kJ/kgK), Q_P is the product load (W), and n is the cooling duration (s). By employing the design data shown in Table 2, the calculated product load is 211.72 W.

Table 2. Thermal Data and Cooling Time of Mango Fruit

Parameter	Value
Mass of mango product, m	2 kg
Specific heat of mango above freezing point, c_a	3.74 kJ/kgK [6]
Specific heat of mango below freezing point, c_b	1.95 kJ/kgK [6]
Latent heat of mango, L_f	273 kJ/kg [6]
Cooling time, n	3600 s
Setpoint temperature of the cabin, T	13 ºC = 286.15 K

By using Equation (7), the total load of the system is calculated to be 227.52 W.

$$Q_{Total} = Q_T + Q_P \quad (7)$$

The performance of the thermoelectric system is influenced by several interrelated factors, including the Seebeck coefficient (α), electrical resistance (R), thermal conductivity (K), heat absorbed by the cold side (Q_c), heat absorbed by the hot side (Q_h), power consumption (P), coefficient of performance (COP), and efficiency (η). These parameters are calculated using Eqs. (8)–(15).

$$\alpha = \frac{V}{\Delta T} \quad (8)$$

$$R = \frac{V}{I} \times \frac{(T_h - \Delta T)}{T_h} \quad (9)$$

$$K = \frac{V \times I \times (T_h - \Delta T)}{2 \times T_h \times \Delta T} \quad (10)$$

$$Q_c = \alpha \times T_c \times I - \frac{1}{2}(I^2 \times R) - K(T_h - T_c) \quad (11)$$

$$Q_h = \alpha \times T_h \times I - \frac{1}{2}(I^2 \times R) - K(T_h - T_c) \quad (12)$$

$$P = W_{te} + W_{fa} + W_{hs} \quad (13)$$

$$COP_{total} = \frac{Q_c}{W} \quad (14)$$

$$\eta = COP_{total} \times 100\% \quad (15)$$

To determine the values of the above quantities, thermoelectric design data as shown in Table 3 were used.

Table 3. Design Data for the Thermoelectric System

Parameter	Measured Result
Heatsink temperature, T_h	39 °C = 312.15 K
Coldsink temperature, T_c	10 °C = 283.15 K
Voltage, V	12.3 V
Current, I	6 A

Based on the calculation results, the performance parameters of the thermoelectric system were obtained as presented in Table 4.

Table 4. Performance of the Designed Thermoelectric System

Parameter	Calculation Results
Seebeck coefficient, α	0.42 V/K
Electrical resistance, R	1.86 Ω
Thermal conductivity, K	1.15 W/K
Heat on cold side, Q_c	653.62 W
Heat on cold side, Q_h	727.42 W
Power consumption, P	1106 W
COP	0.59
Efficiency, η	59 %

3.2. Testing Data

The thermoelectric system was operated for one hour to cool 2 kg of mangoes. Figure 3 compares the measured temperatures inside the coolbox/cabin and the mango product. Data was collected every five minutes up to the 60th minute. The measured cabin temperature was consistently lower than the product temperature, as the cooling system actively maintained a low cabin temperature. Over time, thermal equilibrium was achieved, with the cabin and product temperatures equalizing at the 60th minute [18]. The cabin temperature decreased by 1°C every five minutes, stabilizing at 12.6 °C, which aligns with the recommended setpoint of 13 °C (see Table 2). This temperature indicates that the system meets the ideal storage temperature requirements for mangoes [5], [6].

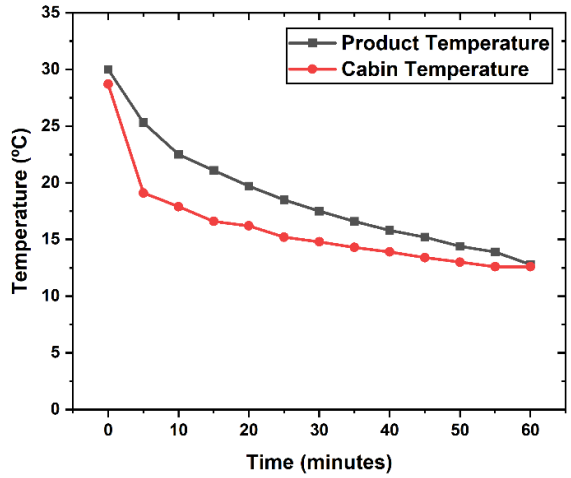

Figure 3. Cabin and product temperatures in the thermoelectric system

Figure 4 presents the temperature measurement results for the cabin, coldsink, and heatsink with and without the mango product. At the beginning of the measurement (minute 0), a significant temperature drop is observed across all components, especially the cold sink (COTSP and COTWP) and the cabin (CTSP and CTWP). This indicates that the cooling system is operating effectively during the initial phase. A comparison between the graphs with the product (CTWP, COTWP, and HTWP) and without the product (CTSP, COTSP, HTSP) shows the effect of the product's presence on the temperature. The cabin temperature with the product (CTWP) tends to be higher than the cabin temperature without the product (CTSP), although the difference is not significant. This phenomenon suggests that the product slightly slows the temperature drop in the cabin. The temperature difference between the cold sink with and without the product (COTWP and COTSP) is relatively small. The heatsink with the product (HTWP) also shows a slightly higher temperature compared to the heatsink without the product (HTSP).

After the initial drop, the temperatures of all components tend to stabilize after approximately 15-30 minutes, although there is still some ongoing slight reduction in temperature for a few components. This indicates

that the cooling system reaches a steady-state condition after the initial cooling period. The cold sink (COTSP and COTWP) reaches a lower temperature compared to the cabin, while the heatsink (HTSP and HTWP) maintains a higher temperature than the cold sink. These conditions are consistent with the roles of the cold sink and heatsink as heat absorbers and heat emitters, respectively.

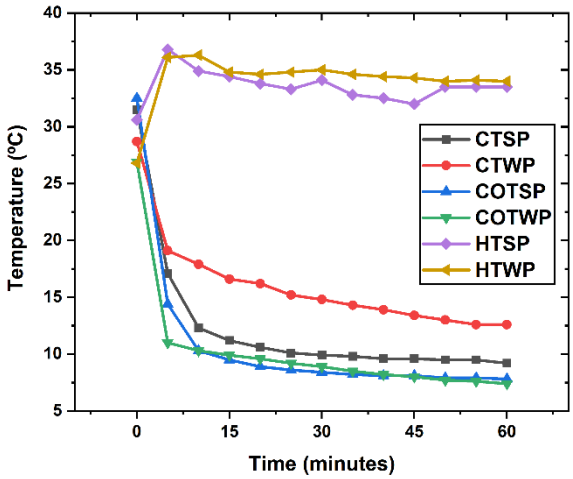

Figure 4. Temperatures of the cabin, coldsink, and heatsink with and sans the product. CTSP (cabin temperature sans product, black); CTWP (cabin temperature with the product, red); COTSP (coldsink temperature sans product, blue); COTWP (coldsink temperature with the product, green); HTSP (heatsink temperature sans product, purple); and HTWP (heatsink temperature with the product, brown).

To evaluate cooling effectiveness, the system's performance was assessed using measurement data from TEC1-12706, as presented in Table 5.

Table 5. Measurement Data of TEC1-12706

Parameter	Measured Result
Heatsink temperature, T_h	34 °C = 307,15 K
Coldsink temperature, T_c	7,4 °C = 280,55 K
Voltage, V	12,3 V
Current, I	6 A

The performance parameters of the thermoelectric system were obtained from the tests, using Eqs. (8) – (15), were compared with the design data previously obtained (see Table 6).

Table 6. Comparison of Thermoelectric System Performance between Design Data and Test Results

Parameter	Design Data	Test Results
Seebeck coefficient, α	0.42 V/K	0.46 V/K
Electrical resistance, R	1.86 Ω	1.87 Ω
Thermal conductivity, K	1.15 W/K	1.27 W/K
Heat on cold side, Q_c	653.62 W	707.92 W
Heat on cold side, Q_h	727.42 W	781.72 W
Power consumption, P	1106 W	1179.86 W
COP	0.59	0.60
Efficiency, η	59 %	60 %

Based on Table 6, the test results show that the system's performance data is not significantly different from the design data. This indicates that the developed thermoelectric system is consistent with the initial design. To assist users in monitoring mango temperature and humidity inside the coolbox, the thermoelectric system was integrated with IoT technology via the Blynk application, as shown in Figure 5. The system utilizes temperature and humidity sensors placed inside the coolbox. Data captured by the sensors is sent to an ESP32 microcontroller connected to the internet via WiFi. The Blynk application serves as a dashboard displaying the data in real time through graphs and numerical values. Users can access this information anytime and anywhere, provided they have internet access.

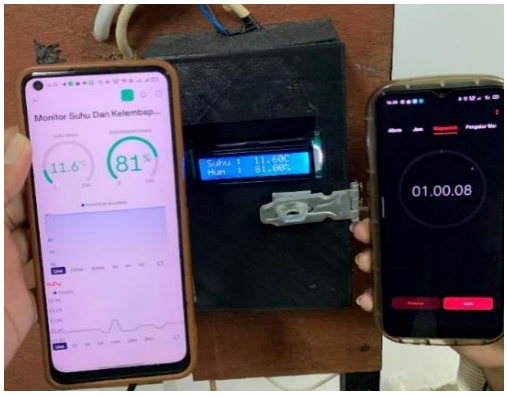

Figure 5. Data transmission to the Blynk application

4. CONCLUSION

The thermoelectric coolbox system modified with ice packs for storing 2 kg of mangoes successfully reached a cabin temperature of 12.6 ºC within 60 minutes. This result demonstrates that the system meets the ideal temperature requirements for mango storage. The addition of ice packs played a crucial role in accelerating the temperature drop inside the cabin. The cold sink and heatsink components functioned effectively in absorbing and releasing heat to the environment. Based on the tests, the thermoelectric coolbox achieved a COP of 0.60 with an efficiency of 60%.

The thermoelectric system has also been successfully integrated with IoT technology via the Blynk application, facilitating users in monitoring the temperature and humidity data of mangoes stored in the coolbox. Users can access this data through their smartphones anytime and anywhere, as long as the device is connected to the internet.

5. REFERENCES

[1] H. Baihaqi, "Indramayu Dominasi Produksi Mangga di Jawa Barat," Bisnis.com. Accessed: Jan. 13, 2025. [Online]. Available: https://bandung.bisnis.com/read/20240205/550/1738350/indramayu-dominasi-produksi-mangga-di-jawa-barat

[2] A. Dirpan, A. Nurfaidah Rahman, M. T. Sapsal, M. M. Tahir, and S. Dewitara, "Perubahan Warna dan Organoleptik Buah Mangga Golek (Mangifera indica L.) Pada Metode Penyimpanan Zero Energy Cool Chamber (Zecc) Dengan Kombinasi Pengemasan," *J. Agritechno*, vol. 14, no. 02, pp. 66–75, 2021.

[3] A. Setiawan, W. Wardika, and M. Imam, "Analisis Pengaruh Variasi Putaran Extra Fan Evaporator terhadap Kinerja Cold Storage Menggunakan Mesin Outdoor AC Split untuk Penyimpanan Puree Mangga," *J. Rekayasa Energi*, vol. 02, no. 02, pp. 1–10, 2023.

[4] W. Wardika, Y. Kurniawan, A. Setiawan, and M. Z. A. Naja, "Analysis of The Effect Evaporator Fan Rotation Variations on Air Blast Freezer Performance For Freezing Mango Puree," *Log. J. Eng. Des. Technol.*, vol. 24, no. 3, pp. 150–159, 2024.

[5] W. Broto, P. Nova, L. H. Sule, K. Yusri, K. Oemi, and P. Purwati, *Budi Daya dan Pascapanen Mangga*. Pusat Perpustakaan Pertanian dan Komunikasi Penelitian, Badan Penelitian dan Pengembangan Penelitian, 1994.

[6] D. P. Yuill, *ASHRAE Handbook Refrigeration*, SI Edition. Atlanta, 2018.

[7] Y. T. Suci, "Perubahan Mutu Buah Mangga Arumanis Selama Penyimpanan Dingin," *AgriHumanis J. Agric. Hum. Resour. Dev. Stud.*, vol. 1, no. 2, pp. 99–106, 2020.

[8] A. A. Adeyanju and K. Manohar, "Design and Analysis of a Thermoelectric Air-Conditioning System," *J. Sci. Res. Reports*, vol. 26, no. 4, pp. 1–11, 2020.

[9] Y. Patel, A. R. M. Siddique, M. R. Mohaghegh, S. H. Tasnim, and S. Mahmud, "Experimental Investigation of the Cooling Effect Generated by a Heat Sink Integrated Thermoelectric-Based U-Shaped Air-Conditioning System," *Appl. Sci.*, vol. 11, no. 21, pp. 1–23, 2021.

[10] I. P. A. A. Permana, K. Bange, and I. W. Temaja, "Rancang Bangun Sistem Refrigerasi Termoelektrik dengan Memanfaatkan Panel Surya," Politeknik Negeri Bali, 2022.

[11] R. Aziz, M. T. Afkar, S. Sunanto, and K. Karsid, "Sistem Kontrol Suhu Penyimpan Buah-Sayur Pada Mesin Pendingin Termoelektrik," *JTT (Jurnal Teknol. Ter.*, vol. 3, no. 2, pp. 32–36, 2017.

[12] J. V. Tuapetel, M. K. Rasyid, and Y. Suryono, "Prototype Sistem Pendingin Ramah Lingkungan Berbasis Sistem Termoelektrik," Tangerang Selatan, 2021.

[13] W. Fikri, "Rancang Bangun Pendingin Buah dan Sayur Berbasis Peltier TEC1-12706," Universitas Islam Negeri Maulana Malik Ibrahim, 2022.

[14] M. Helmy, "Rancang Bangun dan Analisa Termal Showcase Mini Sebagai Alat Pendingin Minuman

Menggunakan Modul Termoelektrik," Universitas Islam Riau, 2020.
[15] H. Wafi, "Rancang Bangun Sistem Kombinasi RSW-CSW Menggunakan Portable Coolbox," Institut Teknologi Sepuluh November, 2021.
[16] F. Amri, I. Fitriyanto, T. Haryanti, I. Fatwasauri, and J. Maknunah, "Perancangan Instrumen Alat Ukur Wattmeter Digital Berbasis Arduino Nano dan Sensor Pzem-004T," *JTT (Jurnal Teknol. Ter.*, vol. 9, no. 1, pp. 44–51, 2023.
[17] D. J. Wessel, *ASHRAE Fundamental Handbook*. Atlanta: Communications and Publications Publisher, 2001.
[18] R. Nopriantoko, *Rekayasa Sistem Termal dan Energi*. Sukabumi: CV Jejak, 2024.

LOGIC
Journal of Engineering Design and Technology
Vol. 25 No.1 March 2025; p. 27-34

p-ISSN : 1412-114X
e-ISSN : 2580-5649
http://ojs2.pnb.ac.id/index.php/LOGIC

ANALYSIS OF LEAKAGE TEST RESULTS ON FLANGE-GASKET PIPING SYSTEM SIMULATOR DEVICE

Muhammad Naufal Abiyyi Hutagalung[1)], Syamsul Hadi [1*)], Bayu Pranoto[1)], Firman Dwiyanto[1)], Dadang Kurniawan[1)]

1) Mechanical Engineering Department, State Polytechnic of Malang, Jl. Soekarno-Hatta 9, Malang 65141, Indonesia

Correponding email: syamsul.hadi@polinema.ac.id

Abstract. Fluid leaks in piping installations often occur in the industrial sector which is detrimental due to the selection of gasket materials, flanges, and improper tightening torque of flange bolts. The fluids that are flowed can be clean water, palm oil with a fatty acid content at an acidity level (pH) of around 4, oil, solutions with a certain pH or fuel. The purpose of the simulator device analysis is to obtain data on the level of tightening torque of bolts-nuts on 1 inch pipe flanges-gaskets and the volume of leakage. The analysis method includes setting the working pressure of the fluid on the globe valve at 1 Bar, 1.3 Bar, and 1.5 Bar on the flange-gasket piping system simulator device, measuring the lowest tightening torque at which the fluid starts to leak to the highest at a condition where there is no leak at all, and two-way Anova analysis on the distribution data. The results of the study showed that the lowest bolt-nut tightening torque at 2 Nm for three M8 bolts-nuts as flange-gasket pair locks resulted in an average fluid droplet leakage of 120 ml/hour and at a torque of 4 Nm the leakage level was about a quarter of that, namely 36 ml/hour and finally at a torque of 5 Nm there was no leakage at all. Implications in industries that use fluid flow with sufficient tightening torque of nuts-bolts on flanges-gaskets can reduce-stop losses due to leakage that occurs in their piping systems.

Keywords: Fluid leaks, centrifugal pumps, fluid pressure, and bolt-nut tightening torque.

1. INTRODUCTION

Hydrolysis in the industrial process of crude palm oil into fatty acids and glycerol is carried out at a temperature of 250 $^{\circ}$C and a pressure of 50 Bar for 2 hours to achieve conversion results between 96% and 99% [1]. Innovation in the simulator device in the form of a piping network device assembled on a wheeled frame table consisting of a reservoir, pipeline, circulation pump, manometer, flowmeter, glove valve to regulate working pressure, valves, fluid filler funnel, a pair of flanges, gaskets, 3 pairs of bolts and nuts equipped with torque wrenches, measuring cups and stopwatches. The purpose of the leak test analysis is to obtain data on the level of tightening torque of bolts and nuts on the 1-inch pipe flange-gasket in the piping system and data on the volume of leakage at the lowest and highest levels of tightening torque of bolts and nuts on the flange-gasket.

A piping system is a combination of interconnected pipes and is used to convey fluids, both liquid and gas, from one piping system to another piping system. Several important components in the distribution of a fluid flow from the results of a process in a piping system so that a fluid distribution process can operate include components used including pumps, manometers, flowmeters, various valves, branch connections, bend connections, and cross-section changes [2]. The operation of fluids can involve components including pumps, manometers, flowmeters, flanges and gaskets, various valves so that the flow can be monitored and controlled, including anticipating leaks.

Pumps are often found in large, medium and small-scale industries. Pumps are generally classified into 2 parts, namely positive displacement pumps and non-positive displacement pumps [3]. Centrifugal pumps are a type of pump where potential energy is converted into speed energy which comes from changing static energy into dynamic energy [4]. The liquid inside rotates due to the push of the blades, giving rise to centrifugal force which

causes the liquid to flow from the center of the impeller out through the channel between the blades and leaves the impeller at high speed [5]. Generally in piping systems, pumps are used as a distribution medium to various destinations.

When the system is running, the gasket experiences stress-strain from changes in fluid flow pressure in the system, which over a long period of time will change the mechanical properties of the gasket. There are many factors that need to be considered to avoid leaks at the flange connections in the piping system. There are several factors or parameters that can cause leaks in connections including tightening torque, fluid working pressure, gasket material, gasket thickness, and flange geometry [6]. Apart from this, the number of bolt holes and bolt size as well as the flatness and smoothness of the contact between the flange-gasket influence whether or not leaks occur easily.

Flange performance is seen in the strength of the connection and evaluation of the connection needs to be carried out in a system [7]. The flanges used use stainless steel because this material is corrosion resistant and heat resistant. Stainless steel is the name given to a family of corrosion-resistant and heat-resistant steels containing a minimum of 10.5% chromium [8]. According to Smith [8], Stainless steel is used for its corrosion resistance properties or for temperatures below zero Celsius containing a minimum of 12% chromium alloy elements. This means that stainless steel flanges are resistant to corrosion with chromium levels that are higher than nickel levels, making stainless steel suitable for use in environments containing low pH or corrosive acids, and are also capable of operating at relatively high temperatures compared to brass flanges. composite, plastic, or cast iron.

Fluid leaks are very detrimental because they can reduce production efficiency in industry and are very dangerous if the fluid distributed is in the form of chemicals or gases that are categorized as dangerous or flammable if they leak into the atmosphere, especially when applied to gaskets. Leakage in gaskets depends on the torque provided by connecting or tightening the bolts and nuts which is carried out with greater gasket or tightening tension to prevent leaks [9], but this is not the case in field applications, because most tighten the bolts and nuts with a torque that is larger than normal to stop leaks, this can result in gaskets being destroyed, flange pairs not being on the same axis or bolts being damaged [10]. Fluid leaks can be detrimental and dangerous when flammable or corrosive fluids are flowed and the application of excessive torque can damage the construction. Therefore, a piping system can be simplified by means of a simulation in the form of a leak test device on a sealing clamp flange on a laboratory scale which is approached with variable values of fluid working pressure and bolt-nut tightening torque on the flange-gasket which is presented in the relationship between fluid pressure and tightening torque. on the bolt-nut on the flange-gasket.

The tightness and strength of flange connections is influenced by several factors including: gasket design and force on the bolt-nut, creep during bolt relaxation, cracks in the flange, axial force of the flange connection on rotation and deformation of the flange connection components, and uniformity of bolt tightening [11]. Several factors have been observed to influence the relationship between flange connection tightness and leakage.

Finite element analysis has been used for detailed leakage evolution [5], modeling and calculation of asymmetric nonlinear multi-bolt connections treated as a system [12], analysis of the strength and sealing performance of pipe joints [13], studying the strength of the flange-bolts mounted on gaskets. pipe joints under different bolting strategies in industry and under a combination of internal pressure and axial loading [14], evaluation of two different flange sizes of ANSI B16.5 900 pressure class [15], studying leakage evolution in detail [16], analysis of rules and regulations related to bolted flange connections on gaskets refers to ASME VIII DIV 1 requirements [17], and the leakage pressure model is in good agreement with the numerical prediction and also with experimental results [18]. The approach to proving the leakage phenomenon has been demonstrated with numerical analysis results.

2. METHODS

The research used in experimental form to obtain the relationship between fluid working pressure and bolt-nut tightening torque on flange-gaskets against fluid leakage is shown in the flow diagram in Figure 1. The simulator device is made according to the design and assembled carefully on a wheeled table, filled with fluid into the reservoir, the pump is operated, the working pressure of the circulating fluid is set, then the tightening torque on the bolts and nuts is set with a torque wrench and the fluid leaks are collected, the working pressure data of the fluid and the fluid leaks are recorded, an analysis is carried out to obtain the tightening torque limit for the nuts in conditions of fluid leaking and fluid without any leaks at all.

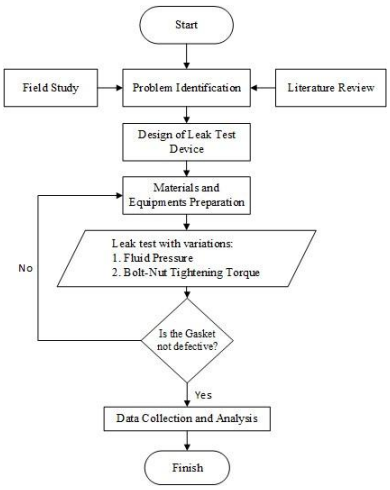

Figure 1. Flow diagram of research on the relationship between fluid pressure and bolt-nut tightening torque on flanges-gaskets against fluid leaks

Research was conducted from January to April 2024 at the Reverse Engineering Laboratory, 3rd Floor, Mechanical Engineering Building, Malang State Polytechnic, Jl. Soekarno-Hatta No. 9, Malang City, East Java. The leak test device has received a Granted Certificate from the Ministry of Law and Human Rights of the Republic of Indonesia with Number IDS000007730 entitled FLUID LEAK TEST DEVICE ON FLANGE-GASKET CLAMPING with Simple Patent protection valid until 05 October 2033 is shown in Figure 2.

Figure 2. Leak Test Device: (a) Top Left View and (b) Top Front View

Before testing, preparations are made to check whether there are leaks, including at bend connections, branch connections, pipe connections to flanges or vice versa, pipe connections to pumps, pipe connections to manometers, pipe connections to flowmeters, and pipe connections to valves. After ensuring that there are no leaks in the piping system connections, testing and data on leak levels can then be carried out. Leak detection is shown in Figure 3.

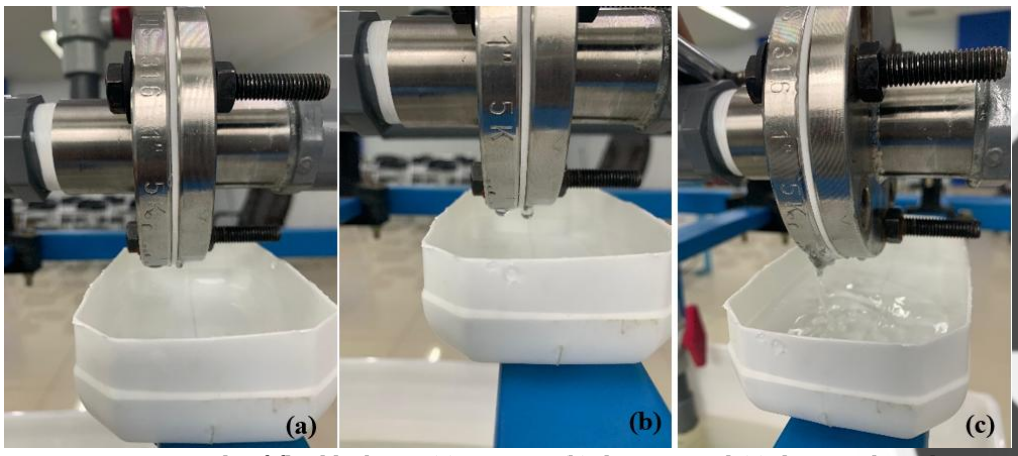

Figure 3. Levels of fluid leakage: (a) seeping, (b) dripping and (c) dripping heavily

A leak test device that has been created to determine the phenomenon of leaks that often occur in piping systems, especially in flange connections and gaskets. The fluid leak in the research carried out occurred at the flange-gasket connection where the fluid leak was collected using a container under the rectangular flange and the resulting fluid leak was transferred and poured into a measuring cup as a measuring tool to determine how much fluid had leaked from the system. The variables used in the research are fluid pressure and bolt-nut tightening torque on the flange which is shown in Figure 4. In the experiment carried out using two flanges with a hole diameter of 34.5 mm, an outer diameter of 95 mm, made of 316L stainless steel, and gaskets of the same size. with a flange, namely a hole diameter of 34.5 mm, an outer diameter of 95 mm made from PTFE (Polytetrafluoroethylene). In the two flange plates that clamp a gasket on the three plates, three bolt holes with a diameter of 10 mm are made at an angle of 120° to each other with a radius of 37.5 mm.

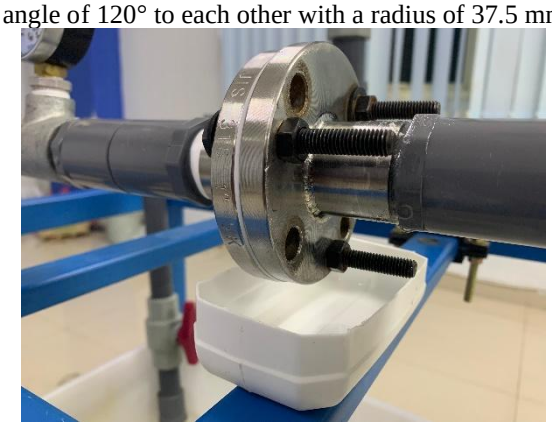

Figure 4. Flanges, gaskets and containers for collecting leaks before pouring them into a measuring cup

In connection with the limited torque wrench available in the trade of at least 5 Nm, it was created by measuring the torque using homemade equipment with a welded lever with a connector on the wrench socket with a weight of sand that had been added according to the load that should be given for sizes smaller than the 5 Nm torque is shown in Figure 5.

Figure 5. Creation of torque measurements smaller than 5 Nm which are not available in the trade

3. RESULTS AND DISCUSSION

If a fluid leak occurs, if the working pressure is low, it only takes the form of seepage, droplets and continues into a flow without becoming a spray in the radial direction of the gasket if the fluid pressure increases, so there is no need for special equipment to contain it in all radial directions of the flange, but rather it is enough to contain it in a suitable container just below it. The results of fluid leakage collected using a measuring cup are shown in Figure 6.

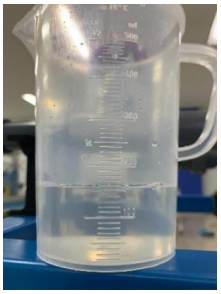

Figure 6. Leak results measured with a measuring cup

Leak test equipment experiments were carried out on flange connections where the fluid pressure was varied by 1 Bar, 1.3 Bar and 1.5 Bar, and the bolt-nut tightening torque was varied by 2 Nm, 3 Nm and 4 Nm with a test duration of 1 hour. The leak data obtained is shown in Table 1. The leakage level test was carried out with 3 replications at a working pressure of 1 Bar with a bolt-nut tightening torque of 2 Nm, 3 Nm, and 4 Nm. Likewise, at a pressure that was increased to 1.3 Bar and 1.5 Bar at a bolt-nut tightening torque of 2 Nm, 3 Nm, and 4 Nm, so that the values in Table 1 were obtained with an average of all at a bolt-nut tightening torque of 2 Nm, a value of 120 ml/hour was obtained and at a bolt-nut tightening torque of 4 Nm, a value of 36 ml/hour was obtained. The data in Table 1 can be processed and displayed into Figure 7 with the relationship between the average leakage and the bolt-nut tightening torque.

Table 1. Clean water Leak Rates

Fluid pressure (Bar)	Bolt-Nut Tightening Torque (Nm)			The average of the mean values (ml)
	2	3	4	
	Average Leakage (ml/hour)			
	95	70	10	
1	135	110	20	77.78
	125	100	35	
Average	118.33	93.33	21.67	
	90	45	60	
1.3	105	70	20	66.67
	80	75	55	
Average	91.67	63.33	45.00	
	160	110	25	
1.5	155	60	40	90.00
	135	70	55	
Average	150.00	80.00	40.00	
Grand Average	120		36	

The data in Table 1 can be displayed graphically as shown in Figure 7.

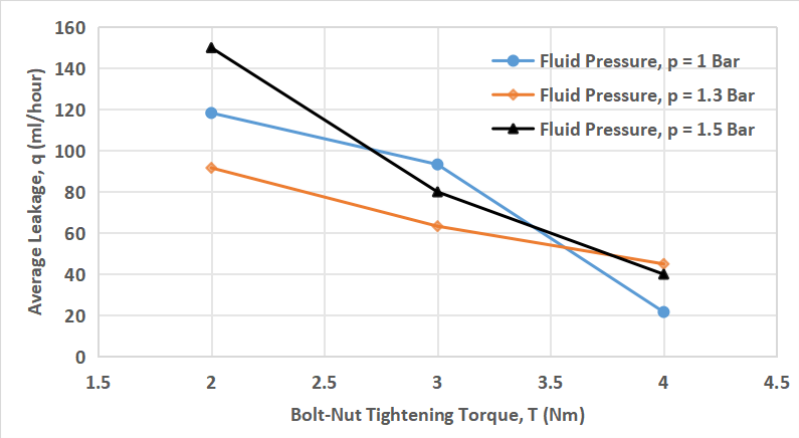

Figure 7. Fluid leak rate due to variations in fluid pressure and bolt-nut tightening torque

The fluid leakage rate decreases with increasing bolt-nut tightening torque on the flange, but it was found that for the bolt-nut tightening torque at 2 Nm, the lowest leakage rate occurred at a pressure of 1.3 Bar, which is possible because the stiffness factor of the new gasket has not provided good contact adjustment at the beginning, possibly the number of bolts is only 3 pieces, the thickness of the gasket and the number of gaskets, still do not provide perfect contact flatness, so the pattern is not consistent. At a bolt-nut tightening torque of 3 Nm, the leakage pattern at a fluid pressure of 1.5 Bar is between the working fluid pressure between 1 Bar and 1.3 Bar which shows an inconsistent pattern, and at a bolt-nut tightening torque of 4 Nm, the leakage pattern is also not consistent, but from the three differences in the increasing bolt-nut tightening torque shows that the distance of the difference is getting closer which finally at a bolt-nut tightening torque of 5 Nm, there is no more leakage. The occurrence of fluctuations and non-linearity in the leakage level can be suggested by increasing the number of bolts, increasing the thickness of the gasket, increasing the number of gaskets, and selecting a less rigid gasket material, so that it is more capable of adjusting to the clamping conditions of a pair of flanges towards perfect contact.

The capability of the leak test simulation device is limited to a reservoir capacity of 50 liters of fluid that can be circulated, a maximum pump working pressure of 1.5 Bar, and a 1-inch diameter installation pipe made of PVC material that can be used for water fluids, water with an acidity level (pH) of 4, coconut/palm oil, and a working temperature of around 50°C.

The potential long-term effects of over-tightening can cause material deformation or faster gasket wear, the torque should be given at a sufficient level and periodically due to vibrations, and the influence of the working fluid temperature-environment requires monitoring and increased torque to provide increased service life under conditions where there are no leaks.

Data processing of leak results carried out using two-way ANOVA analysis is shown in Table 2. The independent variables in the experiment are the working fluid pressure in Bar units and the bolt-nut tightening torque in Nm units, and the dependent variable is the fluid leakage rate in ml units. The controlled variables are the constant pump motor rotation speed at 1400 rpm, the fluid is clean water, and the temperature of the test room is constant at 30 °C. If the results of the F-value for the working fluid pressure show a value greater than F-table at an error level of 5% is greater, it means that the fluid pressure hypothesis (H_{01}) is rejected and the logical consequence is that the alternative hypothesis (H_{11}) is accepted which shows that fluid pressure affects the fluid leakage value. With the same analogy, if the result of F-value for bolt-nut tightening torque (H_{02}) shows a value greater than F-table, then the hypothesis of bolt-nut tightening torque (H_{02}) is rejected and the logical consequence is that the alternative hypothesis (H_{12}) is accepted which can be interpreted that the bolt-nut tightening torque affects the fluid leakage value and also if the result of F-value for the interaction between fluid pressure and bolt-nut tightening torque shows a value greater than F-table, then the hypothesis of interaction between fluid pressure and bolt-nut tightening torque (H_{03}) is rejected and the logical consequence is that the alternative hypothesis (H_{13}) is accepted which can be interpreted that the interaction between fluid pressure and bolt-nut tightening torque affects the fluid leakage value.

Table 2. Results of two ways Annova leak test analysis

Source	DF	Adj SS	Adj MS	F-Value	P-Value
Fluid Pressure (Bar)	2	2452	1225.9	3.66	0.046
Bolt-Nut Tightening Torque (Nm)	2	32096	16048.1	47.88	0.000
Interaction between Fluid Pressure and Bolt-Nut Tightening Torque	4	4926	1231.5	3.67	0.023
Error	18	6033	335.2		
Total	26	45507			

The hypothesis from the results of fluid leak tests in piping system devices is as follows:

Null Hypothesis:

H_{01}: There is no influence of fluid pressure on the level of fluid leakage;

H_{02}: There is no influence of bolt-nut tightening torque on the level of fluid leakage; and

H_{03}: There is no interaction between influence of fluid pressure and bolt-nut tightening torque on the level of fluid leakage.

Alternative Hypothesis:

H_{11}: There is an influence of fluid pressure on the level of fluid leakage;

H_{12}: There is an influence of bolt-nut tightening torque on the level of fluid leakage; and

H_{13}: There is an interaction between influence of fluid pressure and bolt-nut tightening torque on the level of fluid leakage.

The error value in data analysis was chosen at 5% or 0.05. The analysis compared between the results of the Minitab 19 device, manual calculations, and two ways ANOVA using F-table is shown in Table 3.

Table 3. Comparison between F-value and F-table for Leak Test Variables

Independent Variable	F-value from Minitab	F-value from Manual	F-table	Consideration	Decision
Fluid Pressure	3.66	3.66	3.55	F-value > F-table	H_{01} rejected (H_{11} accepted)
Bolt-Nut Tightening Torque	47.88	47.88	3.55	F-value > F-table	H_{02} rejected (H_{12} accepted)
Interaction between Fluid Pressure and	3.67	3.67	2.93	F-value > F-table	H_{03} rejected (H_{13} accepted)

Independent Variable	F-value from Minitab	F-value from Manual	F-table	Consideration	Decision
Bolt-Nut Tightening Torque					

From Table 3, a comparison between F-value and F-table is obtained, all three of which show that F-value is greater than F-table, so the Null hypotheses (H01, H02, and H03) are all rejected, and as a logical consequence alternative hypotheses (H11, H12, and H13) are all accepted which shows that the independent variable, fluid pressure, has a significant influence on fluid leakage; the independent variable bolt-nut tightening torque has a significant influence on fluid leakage; and the independent variable interaction between fluid pressure and bolt-nut tightening torque also has a significant influence on fluid leakage.

4. CONCLUSION

Conclusions from research on fluid leakage levels in flange-gasket connections include:

1) Fluid pressure has a significant influence on fluid leakage, if the higher the fluid pressure, the higher the fluid leakage as indicated by the average value of fluid leakage at a pressure of 1 Bar, a leak of 77.78 ml/hour, at a pressure of 1.3 Bar a leak of 66.67 ml/hour, and at a pressure of 1.5 Bar there was a leak of 90 ml/hour, with the lowest leakage value at a pressure of 1.3 Bar;
2) The bolt-nut tightening torque has a significant effect on fluid leakage. The higher the tightening torque given, the fluid leakage can be overcome, but if the torque is too small than the limit value, the greater the fluid leakage value, at a torque of 2 Nm, there will be a leak of 120 ml/hour, at a torque of 3 Nm there was a leak of 78.89 ml/hour, and at a torque of 4 Nm there was a leak of 28.33 ml/hour, and at a torque of 5 Nm there was no leakage anymore;
3) The interaction of the two variables shows that the smallest amount of fluid leak is at a fluid pressure of 1 Bar and a bolt tightening torque of 4 Nm with an average fluid leak of 21.67 ml/hour; and
4) Tightening the bolt-nut at the flange-gasket connection of the piping system does not need to use a large tightening torque value, because a torque of 4 Nm is almost able to overcome fluid leaks, so it is hoped that the flange-gasket can last longer because excessive compression does not occur.

5. REFERENCES

[1] I. Noor, M. Hasan, and K. Ramachandran, "Effect of operating variables on the hydrolysis rate of palm oil by lipase," *Process Biochemistry*, 39(1), pp. 13-20, 2003, doi:10.1016/s0032-9592(02)00263-7.
[2] A. A. N. H. Susila, I. N. Piarsa, and P. W. Buana, "Geographic Information System for PDAM Tirta Mangutama Pipe Network Mapping (Sistem Informasi Geografis Pemetaan Jaringan Pipa PDAM Tirta Mangutama)," *Merpati*, vol. 2, no. p2, pp. 262-270, 2014.
[3] R. B. Dwantoro, "Effect of Number of Impeller Blades on Centrifugal Pump Performance/Pengaruh Jumlah Sudu Impeler terhadap Unjuk Kerja Pompa Sentrifugal," *Thesis*, Faculty of Engineering, Pancasakti University, Tegal, pp. 11-19, 2020.
[4] D. Wahyudi, "Comparison of Head and Capacity of Single and Series Centrifugal Pumps/Perbandingan Head dan Kapasitas Pompa Sentrifugal Tunggal dan Seri," *Energy Journal*, vol. 9, no. 1, pp. 7-17, 2019.
[5] S. Hariady, "Damage Analysis of Centrifugal Pump 53-101C WTU Sungai Gerong PT Pertamina RU III Plaju/Analisa Kerusakan Pompa Sentrifugal 53-101C WTU Sungai Gerong PT Pertamina RU III Plaju," *Journal of Technology Dissemination*, vol. 2, no. 1, pp. 29-42, 2014.
[6] H. Estrada, "Analysis of Leakage in Bolted-Flanged Joints Using Contact Finite Element Analysis," *Journal of Mechanics Engineering and Automation*, no. 5, pp. 135-142, 2015, doi: 10.17265/2159-5275/2015.03.001.
[7] M. Rahmi, Suliono, D. Canra, Rachmatullah, Y. N. Rohmat, and D. Suwandi, "Analysis of Flange Valve Strength Due to the Effect of Bolt Torque in Different Pressure and Temperature Conditions Using the Finite Element Analysis Method/Analisis Kekuatan Flange Valve Akibat Pengaruh Bolt Torque pada Kondisi Pressure dan Temperature Berbeda dengan Metode Finite Element Analysis," *Journal of Manufacturing Technology and Engineering*, vol. 2, no. 1, pp. 51-60, 2020, https://doi.org/10.48182/jtrm.v2i1.22.
[8] N. Baddoo, *"*Strutural Stainless Steel Design*,"* Structural Engineer, pp. 1-10, 2013.
[9] P. Smith, "Process Piping Design Handbook Volume One: The Fundamentals of Piping Design." *Elsevier's Science & Technology*, 2013.
[10] M. Abid, and D. H. Nash, "Joint Relaxation Behaviour of Gasketed Bolted Flanged Pipe Joint During Assembly," Proceedings of the 2nd WSEAS Int. Conference on Applied and Theoretical Mechanics, pp. 315-325, 2006.
[11] G. Urse, I. Durbacă, and I. C. Panait, "Some Research Results on the Tightness and Strength of Flange Joints," Journal of Engineering Sciences and Innovation, A. Mechanical Engineering, vol. 3, no. 2, pp. 107-130, 2018.

[12] R. Grzejda, "Modelling Nonlinear Multi-Bolted Systems on the Assembly State," *Procedia Engineering*, 206, pp. 1808-1812, 2017.
[13] M. Abid, D. H. Nash, S. Javed, and H. A. Wajid, "Performance of a Gasketed Joint under Bolt Up and Combined Pressure, Axial and Thermal Loading-FEA Study," International Journal of Pressure Vessels and Piping, vol. 168, pp. 166-173, 2018.
[14] N. B. Khan, M. Abid, M. Jameel, and H. A. Wajid, "Joint Strength of Gasketed Bolted Pipe Flange Joint Under Combined Internal Pressure Plus Axial Load with Different (Industrial and ASME) bolt-Up Strategy," *J Process Mechanical Engineering*, pp. 1-10, 2015.
[15] K. A. Khan, and I. Ahmed, "Combined Loading Performance Analysis of Gasketed bolted Flange Joints with Emphasis on Bolt Scattering," Journal of Mechanical Engineering and Sciences, vol. 17, no. 3, pp. 9564-9575, 2023.
[16] W. B. Patel, P. N. Patil, R. Y. Patil, and P. P. Patil, "Analysis of Leakage in Bolted-Flanged Joints with Gasket and Under Thermal Condition, a Critical Review," International Journal of Engineering and Techniques, vol. 1, no. 6, pp. 87-92, 2015.
[17] R. Walczak, J. Pawlicki, and A. Zagorski, "Tightness and Material Aspects of Bolted Connections with Gaskets of Non-Linear properties Exposed to Variable Loads," Arch. Matall. Mater., vol. 61, no. 3, pp1409-1416, 2016.
[18] L. Bertini, M. Beghini, C. Santus, and G. Mariotti, "Metal to Metal Flanges Leakage Analysis," Proceedings of the ASME 2009 Pressure Vessels and Piping Division Conference, Prague, Czech Republic, July 26-30, 2009.

LOGIC
Journal of Engineering Design and Technology
Vol. 25 No.1 March 2025 ; p. 35-44

p-ISSN : 1412-114X
e-ISSN : 2580-5649
http://ojs2.pnb.ac.id/index.php/LOGIC

LEAN ERGONOMIC APPROACH TO ERGONOMIC RISK ANALYSIS FOR WORKPLACE ASSESSMENT

Isana Arum Primasari [1], Tri Budiyanto [2]

1) Industrial Engineering Department, Ahmad Dahlan Universiy, Jl. Ringroad Selatan, Kragilan, Tamanan, Kec. Banguntapan, Bantul, Yogyakarta, Indonesia
2) Industrial Engineering Department, Ahmad Dahlan Universiy, Jl. Ringroad Selatan, Kragilan, Tamanan, Kec. Banguntapan, Bantul, Yogyakarta, Indonesia

Correponding email [1] : Isana_prisa@ie.uad.ac.id

Abstract. IKM NN Aluminum is a metal foundry that produces woks. Based on observations, it appears that the moulding workstation has the highest workload as the operators work in a standing position for 8 hours a day. In addition, the operator lifts a 35 kg mould. This results in un-ergonomic working postures such as excessive bending, head bending and twisting of the body, resulting in waste that has the potential to cause fatigue, physical injury and health problems. The aim of this study is to identify the factors that can cause motion waste, to assess the posture of workers during frying pan moulding activities and to analyse the health implications of the posture assessment. The approach used in this research is lean ergonomics, which combines the principles of lean manufacturing and ergonomics to identify and reduce waste. The methods used are process flow maps to determine the flow of production activities, REBA to identify non-ergonomic postures, and smartwatches for heart rate monitoring to measure worker fatigue. Based on the results of the study, the factor causing motion waste at the moulding workstation is due to the size of the frying pan moulding tool, whose height does not match human anthropometry. Work activities at the moulding station have a high REBA score of 11, which has the potential to cause occupational musculoskeletal disorders. The Pearson correlation test showed a significant relationship between the REBA score and the fatigue level of the workers as measured by heart rate.

Keywords : Lean Ergonomics, Postur Kerja, REBA (Rapid Entire Body Assesment), Waste of Motion

1. INTRODUCTION

The design of work systems in the manufacturing industry is very useful in creating a comfortable, effective and efficient work system, so it is very influential in increasing the quantity and quality of labour productivity in the industrial world [1]. Within the manufacturing industry, some things that need to be done are how to determine efforts to increase production efficiency, product quality and employee welfare. A job is considered to be done effectively and efficiently if it can be completed in a short time. In the production process, waste often occurs in various work activities. This waste can occur in the use of resources in the form of energy, human resources and time, making the production process ineffective and inefficient. This can lead to a decrease in worker performance. Some factors that contribute to improving performance are working conditions, motivation, work systems, effectiveness and efficiency at work [2].

There are several ergonomic approaches that can be used to minimise waste, one of which is lean ergonomics, which is a branch of science that can combine lean thinking with ergonomic approaches [3]. Lean thinking is achieved through the concept of Toyota Production System (TPS) thinking used by the Toyota company. According to the Toyota Production System (TPS) there are 7 wastes, namely overproduction, waiting, transportation, defects, inventory, overprocessing and motion. The main goal of lean thinking is to maximise productivity [4]. Lean ergonomics is about eliminating activities and improving the system to fit the principles of ergonomics [5]. When the principles of ergonomics are not in accordance with the system or the activities performed, it is called ergonomic waste. In lean ergonomics there are two types of waste, transport waste and movement waste. Ergonomics plays an important role in achieving the goal of minimising waste and errors and improving quality by reducing the number of excessive movements and the frequency of repetition, thus saving time and money [6].

One of the manufacturing companies that needs to apply the concept of lean ergonomics is IKM NN Aluminum. The company is involved in metal casting and produces products in the form of frying pans. From the survey results it is known that the workers work for 8 hours a day, from 07.00 to 15.00 WIB, with a break from 11.30 to 12.30 WIB. Although the company has a high production level, the efficiency and health of the employees must be taken into account. The production process at IKM NN Aluminum consists of seven stages, namely melting raw materials, forming, grinding, turning, smoothing and applying labels. Based on initial observations at all workstations, it was found that the moulding workstation has the highest workload, with operators working in a standing position for 8 hours a day. In addition, the operator lifts 35 kg of mould weight.

Un-ergonomic body movements such as excessive bending, head tilting and twisting were also found in frying pan moulding. This can lead to fatigue, physical injury and ongoing health problems. According to the National Institute for Occupational Safety and Health (NIOSH), the recommended weight considered safe for ideal lifting is 23kg, while for prolonged standing, the body can only tolerate standing for 20 minutes. Beyond this limit, tissue elasticity decreases, muscle strain increases and back discomfort occurs [7]. The results of interviews with several workers at the frying pan moulding workstation showed complaints of fatigue and pain in the arms, shoulders, back and legs with non-ergonomic postures. Therefore, there is a need for further identification of movement waste at IKM NN Aluminum. This research is expected to provide recommendations for improving the comfort of the workplace by applying lean ergonomic concepts to minimise activities and systems that are not in accordance with ergonomic principles. The identification of motion wastage will be carried out in the frying pan moulding process as a basis for analysing the impact of posture assessment on body health. Methods used include the Process Flow Map to determine the flow of frying pan making activities, the Rapid Entire Body Assessment (REBA) method to identify non-ergonomic postures, and smartwach to monitor workers' heart rate during work activities to determine the level of fatigue or physical stress experienced.

2. METHODS

This research was conducted at IKM NN Aluminum, a metal foundry located in Sorosutan Village, Yogyakarta. The research was conducted on workplace conditions, work environment, work posture, and potential ergonomic risks to workers' health. Observations were made at all workplaces and all workers were interviewed without sampling.

2.1. Data Collection Method

Data is collected by direct observation to map the overall process flow, measure the working environment such as temperature, noise, lighting, humidity and dust, and identify potential ergonomic risks. Data was collected using video and observed in slow motion to determine correct posture. Fatigue was measured for all workers using heart rate from a smartwatch. Pulse data from the heart rate can be used to determine whether a person is tired or normal. All workers were also asked to complete the SNQ questionnaire to find out about any complaints about parts of the body while working.

2.2. Research Design

The research was carried out using data collection stages as shown in Figure 1, starting with process flow mapping, measuring the work environment, distributing SNQ (Standard Nordic Questionnaire) questionnaires, videotaping work postures, identifying ergonomic risks, assessing ergonomic risks and making suggestions for workplace improvements. Based on the proposed improvements, efficiency was obtained from improving work posture. Improving work posture can reduce energy use during activities so that it can reduce fatigue levels.

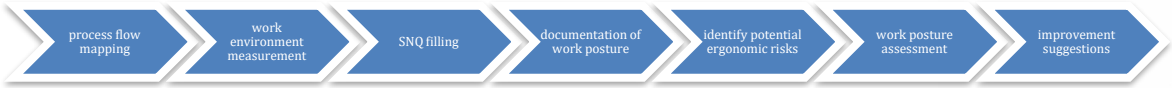

Figure 1. Research Design

2.3. Data Analysis

In this research, data analysis was carried out based on the results of data processing. This included:

a. Analysis of the SNQ (Standard Nordic Questionnaire) questionnaire to find out about complaints about workers' body parts.
b. Workplace analysis, to see how well the work equipment matches the needs of the production process carried out at each workstation.
c. Work environment analysis, to see the work environment conditions such as temperature, noise, vibration, humidity, dust and lighting [8].
d. Work posture analysis, to identify the awkward postures of the workers according to the work carried out using the REBA method [9].

e. Analysis of the results of ergonomic risk identification and assessment as a basis for workplace improvements
f. Te Testing the influence between the REBA score results and the average heart rate. In this study, a Pearson correlation test was conducted, aiming to see the relationship between the independent variables and the dependent variables. Before conducting a correlation test, it is necessary to conduct a classical assumption test, namely the normality test and the linearity test. [10], [11], [12].

3. RESULTS AND DISCUSSION

3.1. Operator and employee demographics

In the frying pan production process there are 10 printing workstations with 1 worker each, with male gender, average worker age 41.20 ± 9.11 years, average worker height 163 ± 5.55 cm, average worker body weight 56.30 ± 9.30 kg. Full demographic data can be found in Appendix 2. During production, workers at the printing station perform work in a static standing position for 7 hours of work, respondent data are presented in Table 1.

Table 1. Employee Demographics

No	Demographic data	N (%)	Mean±Sd	Min	Max
	Gender				
1	Male	10 (100)			
	Female	0 (0)			
2	Age		41,20 ± 9,11	21	55
3	Height		163 ± 5,55		
4	Weight		56,30 ± 9,30		
5	Type of work				
	Moulding wok	10 (100)			

3.2 Working Method

a. Tools/Machines: The production process of making pans at the molding work station uses a mold made of clay and a mold clamp made of wood. To release the mold hook requires strong force because the weight of the wooden hook is 15 kg. Other equipment used to smooth the pans are grinders and lathes.
b. Working environment: In the frying pan production room, the room temperature is 37˚C. The production room consists of several rooms, namely the melting and moulding room, the turning room, the grinding and filing room, the sticker application and quality control room, and the polishing room. At each work station there is a pile of frying pans that will be processed by the next work station.
c. How it works: The frying pan production process at the molding station begins with pouring molten aluminum into the mold, then letting it sit for a few minutes to flatten the mold. After being removed from the mold, the next step is to smooth it using a lathe and grinding machine.

3.3 Heart rate (HR) analysis

During activities at the printing workstation, the average heart rate (HR) for all workers was 128 bpm. The highest heart rate was 130 bpm and the lowest was 123 bpm. Table 2 below shows the overall average heart rate of the workers.

Table 2. Worker Heart Rate Summary

Worker	Age	Heart Rate
		Mean
Worker 1	21	123
Worker 2	43	128
Worker 3	42	127
Worker 4	42	126
Worker 5	55	130
Worker 6	48	129
Worker 7	29	124
Worker 8	35	125
Worker 9	53	129
Worker 10	49	128

From the heart rate results above, it can be seen that according to Astrand & Rodahl, based on existing HR measurement theory on a theoretical basis, the standard mean heart rate of 112-132 bpm is classified as heavy work [13]. This may be due to a number of factors, such as a high room temperature of 37°C and work activities that involve lifting weights, continuous movement and continuous work. This is in line with research conducted by Artayasa which stated that the average pulse rate of coconut transport workers was 126.24 ± 14.10 bpm which is also classified as heavy work [14]. Fatigue will quickly arise due to monotonous work, heavy and long-lasting physical work, poor microclimate, mental and psychological problems, illness, pain at work and lack of energy.

According to the American Heart Association, there are several factors that can influence an increase in heart rate, including the outside temperature and the intensity of the activity being performed. According to the Republic of Indonesia KEPMENKES concerning Health Requirements for Office and Industrial Work Environments, the temperature that meets the requirements for an industrial work environment is in the range of 18-30°C. High temperatures can affect heart rate because the body has to work harder to maintain its internal temperature, increasing the strain on the cardiovascular system.

From the heart rate data above it can be seen that the physical factors influencing the heart rate include the age of the worker. Worker 1, Worker 7 and Worker 8 are workers aged 23-35 years who have a better resistance to physical stress compared to Worker 2, Worker 3, Worker 4, Worker 5, Worker 6, Worker 9 and Worker 10 who are workers aged 42 -55 years. This is because the capacity of the heart and circulatory system decreases with age. This is also in line with research conducted by Akbar showing that nurses over 40 years old have a lower heart capacity, so they tend to have a higher heart rate compared to nurses under 40 years old [15].

3.4 Waste of Movement

Waste of movement data was collected by direct observation at IKM NN Aluminum. Table 3 shows the waste data collected at the wok printing workstation:

Tabel 3. *Waste Of Motion Idenification*

No	Process	Waste	Description	Cause
1	O-3 : opening wood on aluminum mold	Motion	The back and neck are too bent, the posture changes and the legs are not properly supported.	When opening the frying pan mould, the worker has to bend down to reach the handle. When bending down, the posture twists and there is a rapid change in position from the bent position where the legs support the body to maintain balance.
2	O-3 : Opening the aluminium moulding	Motion	Upper arm posture forms a large angle and excessive weight load	This process takes place when the worker opens the frying pan mould, where the worker grabs the 35 kg frying pan mould and crosses his arms to open and lift it.
3	O-4 : Smooth out the sides of the frying pan	Motion	The body posture is too bent and one leg is supporting the body.	During the levelling process, the worker has to bend down to see and level the required parts. This causes the back and neck to be bent too far, and the worker's feet are not properly supported or one leg is lifted to maintain body balance..
4	O-4 : Smooth out the sides of the frying pan	Motion	The upper arm posture forms a large angle	The worker holds the side of the frying pan to be flattened by applying pressure to ensure the surface of the frying pan is flat.
5	T-6 : Moving the pan to another place	Motion	Unergonomic posture of body and legs bent	Workers have to bend and stoop to see the side of the pan and then move it.
6	T-6 : Moving the pan to another place	Motion	A large angle is formed on the upper arm	When moving the pan to another place, the worker's hand is raised to put the pan down, causing the hand position to become tense.
7	T-7: Place the lid on the mould of the frying pan	Motion	Unergonomic body posture	When lifting and placing the 35 kg rying fpan molder, there is a change in posture from a straight back to a hunched back. The worker's neck is bent too far, and the hands are in a tense position, forming too large an angle to ensure the pan lid is properly closed.

No	Process	Waste	Description	Cause
8	0-3, 0-4, T-6, dan T-7	Motion	Potential for musculoskeletal injuries (MSDs)	During the work process which lasts for 8 hours, with the work being done while standing and with a non-ergonomic body posture.

3.5 Work posture assessment using the REBA method

Posture assessment is essential for identifying the risk of musculoskeletal disorders (MSDs) in different work environments. The Rapid Entire Body Assessment (REBA) method is used to identify the whole body posture and provide a risk score to assist in decision making for ergonomic improvements. Figure 2 shows the measurement of the worker's postural angle and Figure 3 shows the assessment score using REBA.

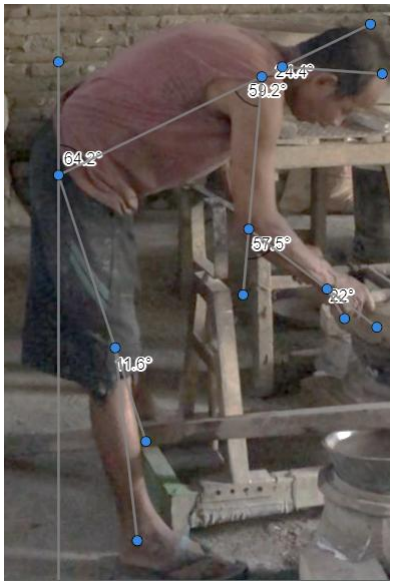

Figure 2. Measurement of Worker Posture

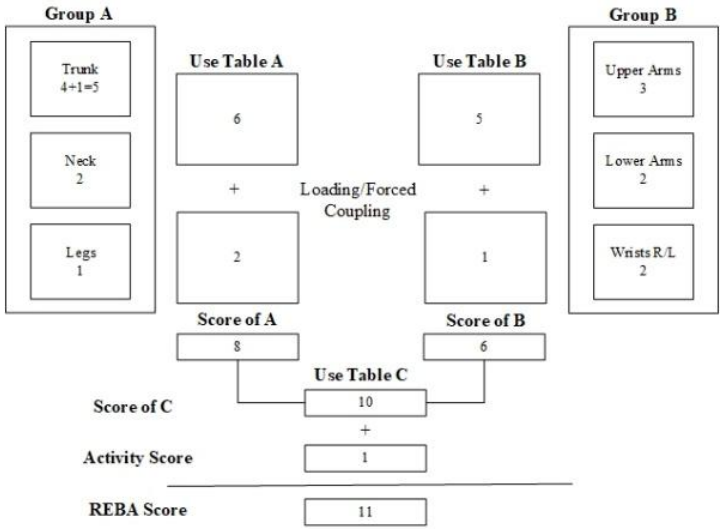

Figure 3. The Calculation of The REBA Score

As shown in Figure 3, the calculation of the REBA score follows the guidelines of the REBA Employee Assessment Worksheet.

a. Grup A
The posture forms an angle of 64.2˚, worth +4 because the flexion is over 60˚, plus +1 because the posture turns sideways while working.

The position of the neck forms an angle of 24.4˚, worth +2 because the flexion is >20˚. The position of the feet forms an angle of 11.6˚, worth +0, and the position of the feet is well supported, worth +1. The force or load the worker is lifting is >22 lbs, worth +2. This gives a Group A score of 8.

b. Grup B
The position of the upper arm forms an angle of 59.2˚, with flexion between 46˚ - 90˚, which is +3. The forearm position forms an angle of 59.2˚, with flexion <60˚, which is +2. The wrist position forms an angle of 22˚, with wrist flexion >15˚, which is +2. If the coupling is in the fair category, the score is +1. The score for group B is therefore 6.

c. Skor C
The result of the calculation of the scores for Group A and Group B was a score of 10.

d. Skor REBA
During work activities, there is a rapid change in posture, so an additional score of +1 is given. The REBA score obtained is therefore 11.

According to the National Institute for Occupational Safety and Health, the classification of semi-direct methods based on the cause of MSDs includes the use of REBA to identify strained postures. Research shows that unergonomic postures can lead to wasted movement and increased risk of injury. Wardhani uses REBA to identify postures in activities that cause wasted motion in the core assembly process. The following is an identification of worker postures using the REBA method [5]. Summary of REBA assessment results can be seen in the Table 4.

Table 4. REBA Score Recapitulation

Worker	Group A Scores	Body Angle	Neck Angle	Leg Angle	Group B Scores	Upper Arm Angle	Lower Arm Angle	Wrist	Group C Scores	Aktivity Score	REBA Score	Risk Level
Worker 1	7	47,4	28,5	14,7	6	48,4	12	22,8	9	1	10	High
Worker 1	7	55,1	23,6	1,2	6	59	75,5	72,8	9	1	8	High
Worker 1	5	52,9	19,8	13,7	3	27,7	87	59	4	1	5	Medium
Worker 1	7	57,5	25,9	6	4	37,3	55	35,3	8	1	9	High
Worker 2	7	54,2	27,7	12	6	57,4	28,2	39,4	9	1	10	High
Worker 2	6	71,1	17,1	20,3	6	20,3	45,2	65,3	8	1	9	High
Worker 2	5	57,2	17,7	5,1	6	80,6	35,9	27,7	7	1	8	High
Worker 2	7	53,6	22	10,7	6	48,7	59,3	40,4	9	1	10	High
Worker 3	8	44,3	26,9	26,9	4	31,8	27,5	22,9	9	1	10	High
Worker 3	7	47	35,1	40	4	41,1	24,5	33,8	10	1	9	High
Worker 3	8	72,3	34,1	23,4	5	51,4	87,5	42,9	10	1	11	Very High
Worker 3	8	66,9	32,4	27,4	6	56,8	42,7	30,8	10	1	11	Very High
Worker 4	7	50,5	32,7	17,4	4	41,2	28,2	23,3	8	1	9	High
Worker 4	7	56,5	26,7	23,7	4	39,1	26,5	44,1	8	1	9	High
Worker 4	7	51,7	32,4	14,3	6	62,7	58,2	33,5	9	1	10	High
Worker 4	7	58,8	30,6	13,5	6	56,8	43,7	27,4	9	1	10	High
Worker 5	9	37,3	23,7	33,2	4	40,7	25,9	25,9	10	1	11	Very High
Worker 5	7	41,5	25,9	11,7	6	50	67,3	23,3	9	1	10	High
Worker 5	7	50,4	23	6,6	4	36,5	58,4	22	8	1	9	High
Worker 5	8	64,2	28,5	11,6	26	59,2	33,7	32,8	10	1	11	Very High
Worker 6	7	25,7	21,6	19,8	3	17,8	12,5	33,5	7	1	8	High
Worker 6	8	65,2	26	17,8	6	78,4	52,5	35,3	10	1	11	Very High
Worker 6	7	46,7	26,4	3,4	4	37,6	54,7	35	8	1	9	High
Worker 6	7	46,6	32,7	5	4	37,3	31,9	31,7	8	1	9	High
Worker 7	8	57,1	31,5	30,8	4	44,1	22,3	29	9	1	10	High
Worker 7	8	62,5	33	29,6	6	82,2	42,2	45,6	10	1	11	Very High
Worker 7	8	42,1	30,5	14	6	58,5	45,7	38	10	1	11	Very High
Worker 7	7	46,1	33,7	19,9	4	52,8	19,5	29,4	9	1	10	High
Worker 8	9	39,9	33,3	50,2	4	35,4	15,5	31,2	10	1	11	Very High
Worker 8	7	65,2	26,7	24,7	4	41,1	31,6	58,2	9	1	9	High
Worker 8	7	52,5	27,2	2,2	3	17,4	93,2	18,7	7	1	8	High
Worker 8	7	45,3	55,2	7,2	4	38,8	33,5	24	8	1	9	High
Worker 9	9	68,3	30,2	19,3	6	77,5	42,3	29,9	10	1	11	Very High

Worker	Group A Scores	Body Angle	Neck Angle	Leg Angle	Group B Scores	Upper Arm Angle	Lower Arm Angle	Wrist	Group C Scores	Aktivity Score	REBA Score	Risk Level
Worker 9	6	79,7	19,9	26,4	6	84,6	51,3	42,7	8	1	9	High
Worker 9	8	61,2	25,2	15,9	3	61,9	84,8	34,3	10	1	11	Very High
Worker 9	8	71,5	22	19,2	6	86,3	51,9	29,2	10	1	11	Very High
Worker 10	7	48,4	33	21	6	49,6	23,3	21,4	9	1	9	High
Worker 10	8	63,7	22,5	14,5	6	58,4	75,8	36,4	10	1	11	Very High
Worker 10	7	48	28,3	14,6	5	61,3	63,1	28,2	9	1	10	High
Worker 10	7	48,9	25,5	9,5	6	52	27	26,7	9	1	10	High

After identifying all the postures reported as wasteful, the next step is to identify the postures of the work activities that cause wasteful postures by calculating the REBA score of 200 work activities performed by 10 workers at the printing workstation. The lowest score obtained was 5, with a moderate risk category requiring action, found in 5 work activities with a percentage of 3%. In addition, scores of 8, 9 and 10, which are in the high risk category and require immediate action, were found in 158 work activities with a percentage of 79%. The highest score was 11, which is in the very high risk category and requires immediate action, found in 37 work activities with a percentage of 19%.

This is in line with the findings of Johanes who stated that after obtaining the score and analysing it using the REBA method, the REBA activity score indicates a high risk in the operator's work posture, which requires immediate corrective action [16]. If left untreated, this will cause pain over a period of time and may lead to WRMDs (work-related musculoskeletal disorders), which is a group of musculoskeletal disorders involving muscles, tendons and nerves caused by material handling work.This needs to be done immediately as there is a fear that workers will experience musculoskeletal disorders.

The parts of the body at risk and showing signs of musculoskeletal disorders are the trunk, neck, legs and upper arms when working at the moulding workstation.

a. Open the frying pan molding
   In the activity of opening the frying pan mould, the most risky back angle is for worker 9 with an angle of 68.3˚. The most risky neck angle is for worker 8 with an angle of 33.3˚. The most risky leg angle is for worker 8 with an angle of 50.2˚ and the most risky upper arm angle is for worker 9 with an angle of 87.4˚.
b. Smooth out the sides of the frying pan
   In the activity of levelling the frying pan, the most risky back angle is found for worker 9 with an angle of 82.5˚. The most risky neck angle is for worker 3 with an angle of 35.1. The most risky leg angle is for worker 3 with an angle of 40˚ and the most risky upper arm angle is for worker 9 with an angle of 84.6˚.
c. Moving the frying pan
   In the activity of moving the frying pan, the riskiest back angle is for worker 3 with an angle of 72.3˚. The riskiest neck angle is for worker 3 with an angle of 34.1˚. The riskiest leg angle is for worker 3 with an angle of 23.4˚ and the riskiest upper arm angle is for worker 2 with an angle of 80.6˚.
d. Place the lid on the mould
   In the activity of closing the pan, the most risky back angle is found for worker 9 with an angle of 71.5. The most risky neck angle is found for worker 8 with an angle of 55.2. The most risky leg angle is found for worker 4 with an angle of 58.8˚ and the most risky upper arm angle is found for worker 9 with an angle of 86.3˚.

From From the results of the angle obtained, it can be seen that the worker is in a hunched position. The normal position of the spine should be kyphosis in the thorax and lordosis in the lumbar spine, and not tilted to the left or right. The hunched posture should not be more than 20 degrees, as the tissues in the back are normally loose in a neutral upright posture. Any posture that is not neutral will cause discomfort if done for a long time [17].

There is also a high-risk angle in the neck that causes workers to lean forward. According to Salsabila's research, a forward-leaning head posture can cause chronic pain, numbness in the arms and palms, improper breathing and pinched nerves [14]. In the legs, workers work in a standing position, using one or two feet for support. In the case of workers standing for long periods of time (static standing with minimal movement), it can result in work injuries, even standing for long periods of time causes physiological discomfort, muscle fatigue, pain and can also contribute to the development of serious health hazards such as Musculoskeletal Disorders (MSDs) with a particular focus on areas such as the back, legs and soles of the operator's feet [18].

On the other hand, according to Anggrianti, prolonged standing causes muscle contractions that block smooth blood circulation and cause blood reflux (blood pooling and static in the swollen vessels). Workers at the printing station stand for 8 hours and are constantly exposed to static loads. The upper arm develops a large shoulder angle, which increases the risk of injury [19].

Based on the identification of motion waste and the REBA score analysis, it can be seen that the motion waste at the printing workstation is caused by the height of the workstation, which does not comply with ergonomic standards. This condition forces workers to adopt a posture with excessive angles in the body, neck, legs and upper arms. As a result, the REBA score increases because workers have to bend over, the neck is too low, the upper arms are too open and the leg posture is not well supported, all of which increase the risk of fatigue, discomfort and injury to workers.

3.6 Statistical Test

Three statistical tests are used to test the data, namely the normality test, the linearity test and the Pearson correlation test. The results are explained as follows.

1. The Normality Test
   The normality test aims to determine whether or not the data used are normally distributed. In this case, the normality test was carried out using SPSS software and the Kolmogorov-Smirnov method. Based on the results of the normality test, the significance value is known to be 0.200. Since 0.200> 0.05, it can be concluded that the REBA score and the heart rate data of the workers are normally distributed, so that the conditions for carrying out the Pearson correlation test are met.
2. The Linearity Test
   The linearity test aims to determine whether the relationship between two variables is linear. Linearity is an important prerequisite for conducting a Pearson correlation test, as Pearson correlation is only relevant for linear relationships. The linearity test was performed using SPSS software. From the results of the linearity test, the deviation from linearity sig. value is 0.706. As the deviation from linearity sig. > 0.05, it can be interpreted that there is a linear relationship between the REBA score data and the worker's heart rate, thus meeting the requirements for performing a Pearson correlation test. Calculations were also made by comparing the calculated F and the F table. If the calculated F is 0.467 and the F table is 2.65, because the calculated F < F table, then the relationship can be accepted as linear.
3. Uji Korelasi Pearson
   The Pearson correlation test is used to measure the strength and direction of the linear relationship between two variables. Before performing this test, it is necessary to ensure that the data are normally distributed and that the relationship between the variables is linear. In this case, the Pearson correlation test was carried out using SPSS software.
4. The hypothesis of this study is as follows:
   H0: There is no relationship between REBA values at the printing workstation and workers' heart rates.
   H1: There is a relationship between the REBA values at the printing workstation and the heart rate of the workers.
   It is known that the significance value is 0.002 and the alpha significance value is 0.01. The Pearson correlation value is 0.22 and the Pearson correlation table value is 0.138. Based on these values it can be seen that H0 is rejected, which means that there is a significant relationship between the REBA values and the heart rates of the workers. The Pearson correlation value of 0.22 indicates that the relationship is weakly positive. The coefficient of determination (R squared) is 0.049 (4.9%), indicating that the heart rate factor has a small contribution to REBA.

3.7 Analysis of the Relationship between Rapid Entire Body Assessment (REBA) Scores and Heart Rate (HR)

The relationship between Heart Rate (HR) and Rapid Entire Body Assessment (REBA) exists because both provide information about the physical demands placed on workers. HR measures the level of physical fatigue, while REBA assesses posture, the load lifted and the type of activity to identify ergonomic risks. Jobs with high REBA scores tend to involve uncomfortable postures or heavy physical loads, which can increase HR. For example, jobs that require bending or repeatedly lifting a 35 kg printer load can result in a high REBA score and increase HR because the body has to work harder to maintain the posture.

Combining HR and REBA data provides a comprehensive picture of fatigue and injury risk. In short, HR and REBA are related because they measure different aspects of the physical strain experienced by workers. Jobs with high ergonomic risk (high REBA scores) tend to increase HR, so a combined analysis of the two provides better insight into how to improve working conditions. Below is a comparison of the REBA data with the highest scores and workers' heart rates. This is consistent with the study by Yassierli et al. (2016), which also found a significant relationship between work fatigue, measured by heart rate, and ergonomic risk assessment using REBA in specific groups of workers. This study suggests that the results of ergonomic risk assessments can be used as a basis for implementing ergonomic interventions to reduce the fatigue experienced by workers. Recommendations for good working postures can also reduce muscle strain, which contributes to fatigue in workers.

4. CONCLUSION

Based on the research that has been conducted, the following conclusions can be drawn:

a. The factor causing waste of motion at the frying pan printing workstation at IKM NN Aluminum is the height of the printing workstation which does not comply with ergonomic standards..

b. Un-ergonomic postures, such as excessive bending, too deep a lowering of the head, and improper body movements during the moulding process can cause fatigue and risk of physical injury to workers. In addition, the Lean Ergonomics analysis identified wasteful movements in the process that can affect worker productivity and health. Heart rate monitoring showed that workers had an average heart rate of 126,52 bpm, indicating a high physical workload due to un-ergonomic working postures. According to Seravalle & Grassi, a normal heart rate is 60–80 beats/minute with the exception of no history of disease, in healthy and trained subjects it is less than 50 beats/minute while in inactive subjects it is greater than 85 beats/minute [20].The Pearson correlation test confirmed a positive relationship between REBA scores and heart rate, indicating that the worse the posture, the greater the physical fatigue experienced by the workers.

5. ACKNOWLEDGEMENT

I would like to thank all parties who have helped the smooth running of this research, starting from licensing to writing the paper. especially to LPPM UAD which has provided funding support and IKM NN Alumunium which has given researchers the opportunity to apply their knowledge.

6. REFERENCES

[1] Sofani, I. S., Tanjung, Y. W. T., Kurnia, H. K., Ningrum, I. P. N., & Saputro, R. N. S., "Tinjauan Sistematik Pada Perancangan Sistem Kerja Di Industri Manufaktur Indonesia. Journal of Industrial and Engineering System," *3*(2), 179-186,2012.

[2] Wahyudi, W., Semmaila, B., & Arifin, Z., "Influences of work discipline, motivation and Working Environment Non physical on Civil apparatus Performance," Point Of View Research Management, 1(3), halaman 1-8, 2020.

[3] Toyota Production System – Toyota Motor Manufacturing Indonesia, https://www.toyota.co.id/industrial/tps, diakses pada tanggal 28 mei 2024.

[4] Lestari, K., & Susandi, D., "Penerapan Lean Manufacturing untuk mengidentifikasi waste pada proses produksi kain knitting di lantai produksi PT. XYZ," In Prosiding Industrial Research Workshop and National Seminar (Vol. 10, No. 1, pp. 567-575), 2019.

[5] Wardani, N. P., Septiani, W., & Safitri, D. M., "Lean Ergonomics Untuk Perbaikan Proses Assembly Core Bracket Trunion," Jurnal Ilmiah Teknik Industri, *10*(3), 245- 253, 2022.

[6] Brito, M. F., Ramos, A. L., Carneiro, P., & Gonçalves, M. A., "A continuous improvement assessment tool, considering lean, safety and ergonomics," International Journal of Lean Six Sigma, 11(5), 893–916, 2020.

[7] Kusuma, I. F., Hartanti, R. I., & Hasan, M., " Pengaruh posisi kerja terhadap kejadian low back pain pada pekerja di Kampung Sepatu, Kelurahan Miji, Kecamatan Prajurit Kulon, Kota Mojokerto," Jurnal Ilmu Kesehatan Masyarakat, *10*(1), 2014.

[8] Nurmutia, S., Ruspendi, Rusmalah, "Ergonomi Industri. Tanggerang Selatan," Unpam Press, 2022.

[9] Middlesworth, M., MS, ATC/L, CEES. "A Guide REBA: Rapid Entire Body Assessment". http://ergoplus.com/wp-content/uploads/REBA-A-Step-by-Step-Guide.pdf.

[10] Yassierli, Yassierli, Dwina Oktoviona, and Inayati Ulin Naâ., "Hubungan antara Indikator Pengukuran Kelelahan Kerja dan Metode Cepat Penilaian Risiko Ergonomi," Ergonomi dan K3 1.1, 2016.

[11] Afriza, F., Dipoatmodjo, T. S., & Ruma, Z., "Pengaruh Kompetensi Karyawan Terhadap Kinerja pada PT. Bank Negara Indonesia (Persero) Tbk. Kantor Cabang Bulukumba," Southeast Asia Journal of Business, Accounting, and Entrepreneurship, *2*(2), 8-16, 2024.

[12] Usmadi, U., "Pengujian Persyaratan Analisis (Uji Homogenitas Dan Uji Normalitas). Inovasi Pendidikan," 7(1), 50–62, 2020, https://doi.org/10.31869/ip.v7i1.2281.

[13] Astrand, P., & Rodahl, K., "Textbook of work physiology: Physiological based of exercise," McGraw Hill, New York, 1986.

[14] Artayasa, I. N., "Ergonomic Stairs Reduces Fatigue of Coconut Transporter Women in Bali," American Journal of Engineering and Technology Management 2021, 6(6), 117-125, 2021.

[15] Akbar, M., "The Infuence of Leadership and Work Environment on Employee Performance: A Case Study of Private University in Jakarta," European Journal of Research and Reflection in Educational Sciences, 5(1), 85–95, 2017.

[16] Yohanes, R., Al-Muqaffa, F. W., Kusnadi, "Analisis Postur Kerja Menggunakan Metode REBA dan Kuesioner NBM Pada Operator Mesin Sizing SA-80 N1 di Industri Otomotif," *INDUSTRIKA*. E-ISSN: 2579-5732. P. 164-174, 2025.
[17] Salsabila, N. R. N., "Perbaikan Sistem Kerja Menggunakan Pendekatan Lean Ergonomic Pada Proses Leveling Damper (Studi Kasus di PT. Yamaha Indonesia)". 2018.
[18] Noor, S. N. A. M., Ahmad, I. N., Wahab, N. A., Ma'arof, M. I. N., "Review of Studies Concerning Prolonged Standing Working Posture," Advanced Engineering Forum. Published by Trans Tech Publications Ltd, Switzerland. ISSN: 2234-991X, Vol. 10, pp 131-136, 2018, doi:104028/ www.scientific.net/EF.10.131.
[19] Anggrianti, S. M., Kurniawan, B., & Widjasena, B., "Hubungan antara postur kerja berdiri dengan keluhan nyeri kaki pada pekerja aktivitas mekanik section welding di PT. X.," Jurnal Kesehatan Masyarakat, *5*(5), 369-377, 2017.
[20] Seravalle, G., & Grassi, G., "Heart rate as cardiovascular risk factor," In Postgraduate Medicine (Vol. 132, Issue 4, pp. 358–367), 2017, Taylor and Francis Inc. https://doi.org/10.1080/00325481.2020.1738142

LOGIC
Journal of Engineering Design and Technology
Vol. 25 No.1 March 2025 ; p. 45-53

p-ISSN : 1412-114X
e-ISSN : 2580-5649
http://ojs2.pnb.ac.id/index.php/LOGIC

DETERMINATION THE COOLING CAPACITY OF THE FAN COIL UNIT (FCU) IN A HOTEL ROOM BASED ON HEAT TRANSFER ANALYSIS

Luh Putu Ike Midiani[1)], I Wayan Adi Subagia[1)], I Made Angga Antara[2)]

1) Mechanical Engineering Department, Politeknik Negeri Bali, Badung, Indonesia
2) Utilities Engineering Technology Study Programme, Mechanical Engineering Department, Politeknik Negeri Bali, Badung, Indonesia

Correponding email [1)] : putuikemidiani@pnb.ac.id

Abstract. Fan Coil Unit (FCU) with the appropriate cooling capacity is needed to obtain room thermal comfort. FCU installed based on the cooling load of the room. Cooling load is affected by room volume, material of : wall, floor, roof, equipment in a room, ventilation, infiltration, windows, outdoor air temperature and humidity, indoor air temperature and humidity. Appropriate and correct FCU installation will have an impact on the energy use of a building. Energy saving efforts are made when determining FCU capacity by calculating cooling load by analyzing heat transfer. This paper investigates and analyzes the amount of room cooling load using the CoolPack application. Calculation of cooling capacity using the CoolPack application is carried out after determining the thermal conductivity and material thickness, thermal resistance of the inner surface and outer surface of the wall, roof, floor, and heat transfer coefficient. Based on the results of calculations and analysis, it was concluded that the total cooling load was 3.58 kW. Furthermore, the FCU capacity to be installed must match the FCU capacity available on the market and be greater than the total cooling load in order to achieve the expected comfort. Proper and correct installation of FCUs will have an impact on energy use in a building is an effort to implement energy saving.

Keywords : Cooling capacity, cooling load, Fan Coil Unit, heat transfer analysis, thermal comfort

1. INTRODUCTION

Thermal comfort in the hospitality industry is urgently needed. to obtain thermal comfort and good environmental air quality, air conditioning equipment is needed. Air conditioning equipment is a system that can provide ventilation, reduce air infiltration, and maintain pressure relationships between spaces [1][2].

One of the air conditioning equipment that are widely used in hotels is Central Air Conditioning, where this system provides a large cooling capacity. The system operates with two types of refrigerants, which are differentiated into primary refrigerants and secondary refirgerants. The primary refrigerant circulated on the vapor compression system and the secondary refrigerant cool the supply air. The main components of this system are: chiller, Air Handling Unit (AHU) or Fan coil Unit (FCU) and cooling tower [3][4].

The chiller is the main cooling equipment in the central air conditioning (AC) system. In the chiller occurs the process of dissipating the heat of the working medium and subsequently distributing it throughout the room. FCU is a device consisting of a fan and cooling coil. The cooling coil dissipates air heat through heat transfer. The cooling tower is a heat exchanger with the working principle of releasing and transferring the heat of cooling water to the air [5][6][7].

In hotel buildings, FCU is one of the room air distribution equipment used for intensive and long operating hours. The FCU structure can be vertical or horizontal (airflow path) and open or recessed (stand), and can optionally use hydronic or direct expansion to perform filtration cycle and room temperature control of indoor air. In FCU, hot environmental air is passed on the cooling coil. The cooling coil gets cold water from the chiller will dissipate the heat of the air through the heat transfer process. FCU can be controlled by thermostat or remote [8].

To obtain room thermal comfort, a FCU with the appropriate cooling capacity is needed. FCU is installed based on the cooling load of the room. Cooling load is the heat or heat load released and absorbed by the

evaporator. Cooling load is affected by various factors, namely: room volume, material of : wall, floor, roof, equipment in a room, ventilation, infiltration, windows, outdoor air temperature and humidity, indoor air temperature and humidity [9]. Appropriate and correct FCU installation will have an impact on the energy use of a building. Based on research that has been done, energy consumption for air conditioning systems represents about 60% of all consumption of a building [10][11][12]. Thus building energy savings are the objective in installing FCU. Efforts to improve the energy efficiency of air conditioning equipment in commercial buildings have been widely carried out such as the application of energy-saving control methods for FCU carried out with fuzzy models, intelligent control methods with Stepless Variable Speed Drive Technology, optimizing fan coils by using high supply cold water temperature, using ice slurry as coolant in standard terminal fan coil units [13][14][15]. Energy saving efforts are made when determining FCU capacity by calculating cooling load by analyzing heat and mass transfer as done by Ma [16]. Based on the descriptions of these preliminary studies, this article investigates and analyses the amount of space cooling load by analysing heat and mass transfer using the new CoolPack application.

2. METHODS

Calculation of cooling capacity based on heat transfer analysis is carried out based on the steps as shown in Figure 1 and the room that will be calculated for cooling load is shown in Figure 2.

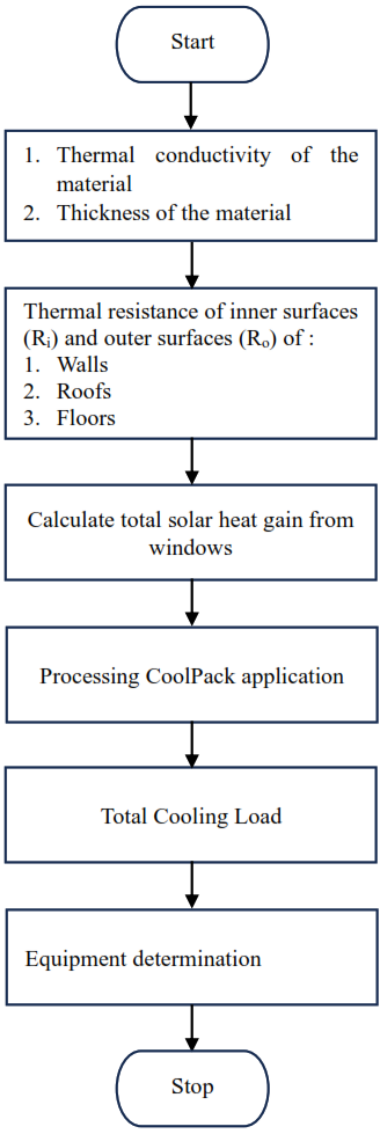

Figure 1 Flowchart of cooling capacity calculation

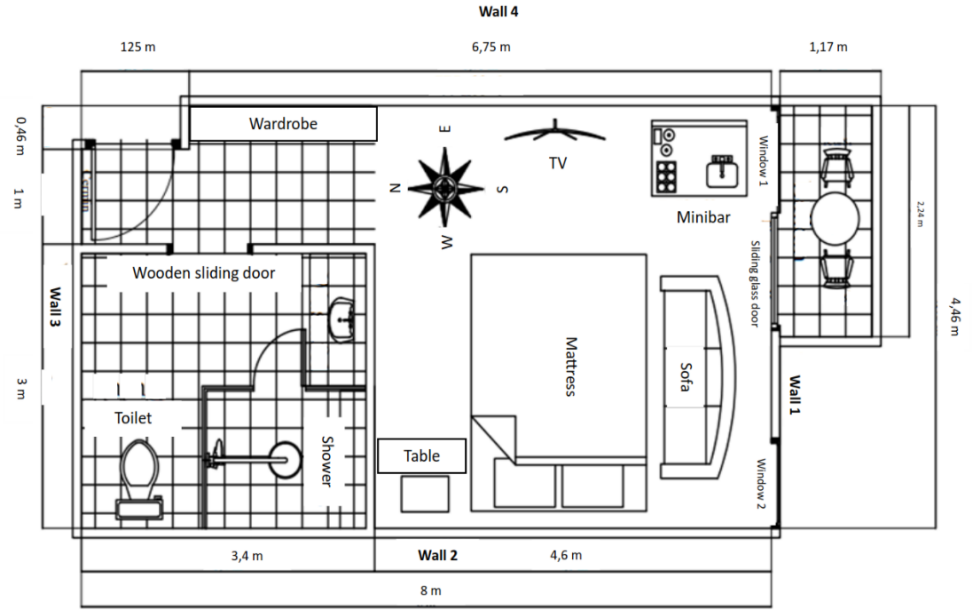

Figure 2. Room area

2.1. Thermal Conductivity and Thickness of The Material

Thermal conductivity is a value that indicates how fast heat will flow in a particular material [17]. Thermal conductivity has units of W/m.˚C, where thermal conductivity is affected by the thickness of the material (m), temperature (˚C) and heat flow rate (W).

2.2. Thermal Resistance of Inner (R_i) and Outer (R_o) Surfaces of Walls, Roofs and Floors

Thermal resistance is the resistance of a material to heat. The thermal resistance of a material depends on the geometry and thermal properties of the material [18]. Resistance to heat flow is represented by the letter R. Thermal resistance is indicated by determining several directions of heat flow, namely upward (roof), sideways (wall), and downward (floor), as shown in Table 1.

Table 1. Thermal Resistance of Inner and Outer Surfaces of Walls, Roofs and Floors

Surface Resistance ($m^2.K/W$)	Directions of heat flow		
	Upwards	Sideways	Down
R_i	0,10	0,13	0,17
R_o	0,04	0,04	0,04

2.3. Calculating the heat transfer coefficient of the walls, roof and floor [17]

$$U_{value} = \frac{1}{R_{total}} = \frac{1}{R_i + \frac{x_1}{k_1} + R_o} \quad (1)$$

where:
U_{value} = Coefficient of heat transfer from walls, roofs, and floors ($W/m^2.K$)
R_{total} = Total thermal resistance of wall, roof and floor ($m^2.K/W$)
R_i = Thermal Resistance of inner surfaces of wall, roof and floor ($m^2.K/W$)
R_o = Thermal Resistance of outer surfaces of wall, roof and floor ($m^2.K/W$)
x_1 = Thickness of wall, roof, and floor materials (m)
k_1 = Thermal conductivity of wall, roof, and floor materials (W/m. K)

If there are windows, doors, etc. on the walls, the overall heat transfer coefficient, obtained using the values of individual U_{value} and surface area respectively as follows [17]:

$$U_{mean} = \frac{(U_{wall} x A_{wall} + U_{door} x A_{door} + U_{window} x A_{window}}{A_{total}} \quad (2)$$

where:
U_{mean} = Average heat transfer coefficient (W/m^2. K)
U_{wall} = Wall heat transfer coefficient (W/m^2. K)
A_{wall} = Total wall area (m^2)
U_{door} = Door heat transfer coefficient (W/m^2. K)
A_{door} = Total width of doors (m^2)
U_{window} =Window heat transfer coefficient (W/m^2. K)
A_{window} = Total window area (m^2)

2.4. Calculating total solar heat gain window

To determining the total solar heat gain of glass windows used the formula (3) and the results of the calculation are shown in Table 2 [1]:

$$q_{win} = SC \; x \; SCL \quad (3)$$

where:
q_{win} = Solar heat gain (W/m^2)
SC = Solar radiation factor through glass
SCL = Solar cooling load factor (W/m^2)

Table 2. Solar Heat Gain

Glass Window Position	Solar Radition Factor Through Glass (SC)	Solar Cooling Load Factor / SCL (W/ m^2)	Solar Heat Gain Factor (SHGF) Building Envelope
North	0,48	43,24	1,04
Northeast	0,13	96,14	1,34
East	0,11	144,58	1,45
Southeast	0,14	131,50	1,45
South	0,22	79,38	1,16
Southwest	0,52	131,57	1,45
West	0,52	144,58	1,45
Northwest	0,47	96,14	1,34

2.5. Enter the data obtained into the CoolPack application

The final step to get the room cooling load is to enter the load calculation data of each floor, door and window into the CoolPack application.

3. RESULTS AND DISCUSSION

3.1 Room Size

V = P x L x T
= 4,46 x 8 x 2,5
= 89,2 m^3

3.2 Determining Wall, Roof, and Floor Specifications

3.2.1 Wall 1

Total wall area 1 ($A_{wall\ tot}$) = P x L = 4,46 x 2,5 = 11,15 m^2

a. Glass door

- Total glass door area (A_{tot1})
  = P x L = 1,24 x 2,04 = 2,52 m^2
- Glass door area (A_1)
  = P x L = 0,97 x 1,72 = 1,66 m^2
- Wooden frame area of glass doors (A_2)
  = total glass door area – glass door area = 2,52 – 1,66 = 0,86 m^2
- Thermal conductivity of glass (k_1) = 5,1 W/m.K , Thick (x_1) = 0,01 m

- Thermal conductivity of wooden frame (k_2) = 0,18 W/m.K , Thick (x_2) = 0,15 m

b. Window 1

- Total Window Area 1 (A_{tot2}) = P x L = 1,13 x 2,04 = 2,3 m^2
- Window glass area 1 (A1) = P x L = 1,1 x 1,92 = 2,11 m^2
- Wooden window frame area 1 (A_2) = total windows frame area 1 – windows glass area = 2,30 – 2,11 = 0,19 m^2
- Thermal conductivity of glass (k_1) = 5,1 W/m.K , Thick (x_1) = 0,01 m
- Thermal conductivity of wooden frame (k_2) = 0,18 W/m.K , Thick (x_2) = 0,15 m

c. Window 2

- Total Window Area 2 (A_{tot3}) = P x L = 0,95 x 1,64 = 1,55 m^2
- Window glass area 2 (A_1) = P x L = 0,75 x 1,44 = 1,08 m^2
- Wooden window frame area 2 (A_2) = total windows area 2 – window glass area 2 = 1,55 m^2 – 1,08 m^2 = 0,47 m^2
- Thermal conductivity of glass (k_1) = 5,1 W/m.K , thick (x_1) = 0,01 m
- Thermal conductivity of wooden frame (k_2) = 0,18 W/m.K , thick (x_2) = 0,15 m

d. GRC + Glasswool Carpet (A_{tot4})

= total wall area 1 – total glass doors area – total window area 2
= 11,15 – 2,52 – 2,3 – 1,55 = 4,78 m^2

- Thermal conductivity of GRC (k_1) = 0,9 W/m. K, thick (x_1) = 0,009 m
- Thermal conductivity of glasswool carpets (k_2) = 0,03 W/m. K, thick (x_2) = 0,002 m
- In direct contact with outside air = 32 ℃

3.2.2 Wall 2

a. Total wall area 2 ($A_{wall\ tot}$)

= P x L = 8 m x 2,5 m = 20 m^2

- GRC area + Glasswool carpet (A_{tot1}) = P x L = 4,6 x 2,5 = 11,5 m^2
- Thermal conductivity of GRC (k_1) = 0,9 W/m. K, thick (x_1) = 0,009 m
- Thermal conductivity of glasswool carpets (k_2) = 0,03 W/m. K, thick (x_2) = 0,002 m

b. Plastering 1 + concrete brick + plastering 2 + ceramic

= Total wall area 2 – GRC area + glasswool carpets (A_{tot2}) = 20 – 11,5 = 8,5 m^2

- Thermal conductivity of plastering 1 (k_1) = 0,94 W/m. K, thick (x_1) = 0,01 m
- Thermal conductivity of concrete brick (k_2) = 0,77 W/m. K, thick (x_2) = 0,1 m
- Thermal conductivity of plastering 2 (k_3) = 0,88 W/m. K, thick (x_3) = 0,01 m
- Thermal conductivity of ceramics k_4 = 1,3 W/m.K , thick (x_4) = 0,01 m
- In direct contact with outside air = 22 ℃

3.2.3 Wall 3 ($A_{wall\ tot}$)

a. Total wall area 3

= P x L = 4,46 x 2,5 = 11,15 m^2

b. Plastering 1 + concrete brick + plastering 2 + glass

A_{tot1} = P x L = 1 x 2,5 = 2,5 m^2

- Thermal conductivity of plastering 1 (k_1) = 0,94 W/m . K , thick (x_1) = 0,01 m
- Thermal conductivity of concrete brick (k_2) = 0,77 W/m . K, thick (x_2) = 0,1 m
- Thermal conductivity of plastering 2 (k_3) = 0,88 W/m . K , thick (x_3) = 0,01 m
- Thermal conductivity of glass (k_4) = 5,1 W/m . K , thick (x_4) = 0,01 m
- Thermal conductivity of concrete brick (k_5) = 0,77 W/m . K, thick (x_5) = 0,1 m
- Thermal conductivity of plastering 2 (k_6) = 0,88 W/m . K, thick (x_6) = 0,01 m
- Thermal conductivity of glass (k_7) = 5,1 W/m . K , thick (x_7) = 0,01 m

c. Plastering 1 + concrete brick + plastering 2 + ceramic

A_{tot2} = P x L = 3 x 2,5 = 7,5 m^2

- Thermal conductivity of GRC (k_1) = 0,9 W/m . K, thick (x_1) = 0,009 m
- Thermal conductivity of glasswool carpets (k_2) = 0,03 W/m . K, thick (x_2) = 0,002 m

d. GRC + glasswool carpets

= 11,15 – 2,5 – 7,5 = 1,15 m^2

- Thermal conductivity of GRC (k_1) = 0,9 W/m . K, thick (x_1) = 0,009 m

- Thermal conductivity of glasswool carpets (k_2) = 0,03 W/m . K, thick (x_2) = 0,002 m
- In direct contact with outside air = 26 ºC

3.2.4 Wall 4

a. Total wall area 4 ($A_{wall\ tot}$)

= P x L = 8 x 2,5 = 20 m^2

b. GRC + glasswool carpet (A_{tot1})

= 6,75 x 2,5 = 16,875 m^2

- Thermal conductivity of GRC (k_1) = 0,9 W/m . K, thick (x_1) = 0,009 m
- Thermal conductivity of glasswool carpets (k_2) = 0,03 W/m . K, thick (x_2) = 0,002 m

c. Wooden Door

- Wooden door area (A_{tot2}) = Total wall area 4 – GRC area + glasswool carpets = 20 – 16,875 = 3,125 m^2
- Thermal conductivity of wooden doors (k_1) = 0,18 W/m . K, thick (x_1) = 0,05 m
- In direct contact with outside air = 22 ºC

3.2.5 Ceiling

a. Total roof area ($A_{roof\ tot}$)

= P x L = 4,46 x 8 = 35,68 m^2

b. Gypsum + rooftile

- Thermal conductivity of Gypsum (k_1) = 0,18 W/m . K, thick (x_1) = 0,009 m
- Thermal conductivity of rooftile (k_2) = 1 W/m . K, thick (x_2) = 0,01 m
- In direct contact with outside air = 32 ºC

3.2.6 Floor

a. **Total wall area ($A_{floor\ tot}$)**

= P x L = 4,46 x 8 = 35,68 m^2

b. Concrete + Wood

- Concrete Area + wood (A_{tot1}) = P x L = 4,46 x 4,6 = 20,516 m^2
- Thermal conductivity of concrete (k_1) = 1,13 W/m . K, thick (x_1) = 0,2 m
- Thermal conductivity of wood (k_2) = 0,13 W/m . K, thick (x_2) = 0,003 m

c. Concrete + plastering + ceramic

- Concrete Area + plastering + ceramic (A_{tot2}) = 35,68 - 20,516 = 15,16 m^2
- Thermal conductivity of concrete (k_1) = 1,13 W/m . K, thick (x_1) = 0,2 m
- Thermal conductivity of plastering (k_2) = 0,88 W/m . K, thick (x_2) = 0,01 m
- Thermal conductivity of ceramic (k_3) = 1,3 W/m . K, thick (k_3) = 0,01 m
- In direct contact with outside air = 22 ºC

3.3 Calculating U value

The results of the calculation of U value using formula 2 are shown in Table 3:

Table 3. U Value Calculation

Wall 1	
Glassdoor (U_1)	5,84 W/m^2. K
Wooden frame of the door (U_2)	1 W/m^2. K
U average (U_{rtot})	4,18 W/m^2. K
Wall 2	
GRC + glasswool carpet (U_1)	4,16 W/m^2. K
Plastering 1 + concrete brick + plastering 2 + ceramic (U_2)	3,14 W/m^2. K
U average (U_{rtot})	3,72 W/m^2. K
Wall 3	
Plastering 1 + concrete brick + plastering 2 + glass (U_1)	3,2 W/m^2. K
Plastering 1 + concrete brick + plastering 2 + ceramic (U_2)	3,14 W/m^2. K
GRC + glasswool carpet (U_3)	4,16 W/m^2. K
U average (U_{rtot})	3,25 W/m^2. K
Wall 4	
GRC + glasswool carpet (U_1)	4,16 W/m^2. K
Plastering 1 + concrete brick + plastering 2 + ceramic (U_2)	2,27 W/m^2. K
U average (U_{rtot})	3,86 W/m^2. K
Roof	
Gypsum + rooftile (U_1)	5 W/m^2. K
Floor	
Concrete + wood (U_1)	2,47 W/m^2. K
Concrete + plastering + ceramic (U_2)	2,47 W/m^2. K
U average (U_{rtot})	2,45 W/m^2. K

There are 2 windows on the wall and the wall faces south, so that the total solar heat gain:
1. Window area 1 = 2,3 m^2
2. Window area 2 = 1,55 m^2
3. Total area = 3,85 m^2

The estimated for equipment and occupant loads:
1. Occupant = 4 orang
2. Lamp = 13 × 5 Watt = 65 Watt
3. TV 150 Watt = 1 piece
4. Fan blower FCU = 107 Watt
5. Minibar 37,4 Watt = 1 piece
6. Activities = light

The infiltration load is differentiated as follows:
1. Infiltration air temperature = 32 ℃
2. Infiltration air humidity = 80 %

Air Change = 0,5 AC/Hr = 12 ACF (Air Change Factor), because only 1 wall includes an exterior wall, namely wall 1, and the rest is an interior wall.

Other parameters that must be considered are:
1. Room Air Temperature = 22 ^{o}C
2. Room Air Humidity = 50 %

Next, the data obtained above is entered into the CoolPackprogram, as shown in Figure 3.

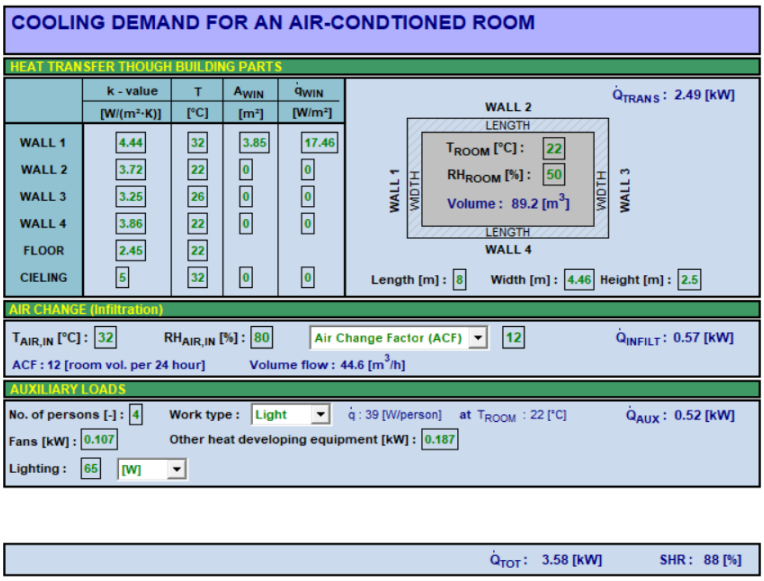

Figure 3. Results of Total Cooling Load using the CoolPack Application

Based on the CoolPack application calculation, the total cooling load is:

Q_{TOT} = 3,58 kW. It is known that 1 kW = 3.412 Btu/h, so

Q_{TOT} = 3,58 kW x 3.412 Btu/h

= 12.214,96 Btu/h

The total cooling load in the room is 3.58 kW, so the capacity of the FCU to be installed should be equal to or slightly greater than the total cooling load. If the FCU capacity is smaller than the cooling load, the FCU performance will be heavier and less efficient. However, if the FCU capacity is too large, there will be a waste of energy. FCU selection must consider the appropriate airflow so that the air can circulate properly. Airflow is expressed in CFM (Cubic Feet per Minute) or m³/h (cubic metres per hour). The installation location of the FCU will affect efficiency and power consumption. Therefore, FCUs with high energy efficiency and low power consumption are selected. Energy saving efforts are made when determining FCU capacity by calculating cooling load by analyzing heat and mass transfer as done by Ma [16]. Where the large air flow rate is the main factor that causes high energy consumption. Therefore, calculations using the CoolPack application help the data processing process to get the correct total cooling load.

4. CONCLUSIONS

Calculation of cooling capacity using the CoolPack application is carried out after determining the thermal conductivity and material thickness, thermal resistance of the inner surface and outer surface of the wall, roof, floor, and heat transfer coefficient. The result of the cooling capacity is 3.58 kW. Furthermore, the FCU capacity installed must be in accordance with the FCU capacity available on the market. If no suitable capacity is found, an FCU capacity that is slightly larger than the total cooling load can be installed in order to achieve the expected comfort. An FCU with too large a capacity will cause large energy usage and cause energy waste. Furthermore, for the future, the use of the CoolPack application provides precise and accurate results.

5. REFERENCES

[1] S. K. Wang, "Handbook Of Air Conditioning And Refrigeration," New York: Mc Graw Hill, 2001.
[2] K. Noh, J. Jang, And M. O. Ã, “Thermal Comfort And Indoor Air Quality In The Lecture Room With 4-Way Cassette Air-Conditioner And Mixing Ventilation System,” Vol. 42, Pp. 689–698, 2007, Doi: 10.1016/J.Buildenv.2005.10.033.
[3] S. Nicklas, G. Strehlow, S. W. Duda, And P. Simmonds, "Ashrae-Handbook-2016-Hvac-Systems-And-Equipment," No. 28, 2016.
[4] L. S. Peris, “Performance Evaluation Of A Hvac System In A Pharmaceutical Plant,” No February, 2019.
[5] J. C. Hensley, “Cooling Tower Fundamentals,” 2009.
[6] A. A. R. Hakim And E. A. Kosasih, “Analysis Of Heat And Mass Transfer On Cooling Tower Fill,” No. December, 2020, Doi: 10.17146/Jfn.2020.14.1.5812.
[7] L. P. I. Midiani, I. W. Temaja, I. P. M. Adnyana, I. K. Dwiana, I. Made, And P. Yoga, “Analisa Kinerja Cooling Tower Tipe Counter Flow Induced Draft,” Vol. 2, Pp. 72–77, 2021.

[8] H. Chuang, J. Chi, K. Chang, And C. Lee, “Study On A Fan Coil Unit And Chiller By An Intelligent Control Method With A Stepless Variable Speed Driving Technology,” Vol. 132, No. January, Pp. 137–146, 2018.
[9] S. I., "Ashrae Handbook Fundamentals," Vol. 30329, No. 404, 2009.
[10] A. D. Althouse And H. Cari, “Modern And Refrigeration And Air Conditioning,” 2004.
[11] V. Vakiloroaya, B. Samali, A. Fakhar, And K. Pishghadam, “A Review Of Different Strategies For Hvac Energy Saving,” Vol. 77, Pp. 738–754, 2014.
[12] M. Kameni *Et Al.*, “A Review On Energy Consumption In The Residential And Commercial Buildings Located In Tropical Regions Of Indian Ocean : A Case Of Madagascar Island,” Vol. 24, No. April, 2019, Doi: 10.1016/J.Est.2019.04.022.
[13] X. Li, T. Zhao, And J. Zhang, “Development Of Network Control Platform For Energy Saving Of Fan Coil Units, A Computationally Efficient Method For Fault Diagnosis Of Fan-Coil Unit Terminals In Building Heating Ventilation And Air Conditioning Systems,” *J. Build. Eng.*, 2017.
[14] M. Bai, F. Wang, J. Liu, And Z. Wang, “Experimental And Numerical Studies Of Heat And Mass Transfer Performance And Design Optimization Of Fan-Coil With High Supply Chilled Water Temperature In Air-Conditioning System,” *Sustain. Energy Technol. Assessments*, Vol. 45, No. March, P. 101209, 2021, Doi: 10.1016/J.Seta.2021.101209.
[15] F. J. Uhı And J. A. Dopazo, “Experimental Analysis On Pressure Drop And Heat Transfer Of A Terminal Fan-Coil Unit With Ice Slurry As Cooling Medium,” Vol. 3, 2010, Doi: 10.1016/J.Ijrefrig.2010.04.013.
[16] Z. Ma, X. Liu, And T. Zhang, “Measurement And Optimization On The Energy Consumption Of Fans In Semiconductor Cleanrooms,” *Build. Environ.*, Vol. 197, No. December 2020, P. 107842, 2021, Doi: 10.1016/J.Buildenv.2021.107842.
[17] J. P. Holman, "*Heat Transfer," 10th Edition*, 2010.
[18] Y. A. Cengel, "*Heat And Mass Transfer A Practical Approach," 3rd Edition*. 2005.

LOGIC
Journal of Engineering Design and Technology
Vol. 25 No.1 March 2025 ; p. 54 - 60

p-ISSN : 1412-114X
e-ISSN : 2580-5649
http://ojs2.pnb.ac.id/index.php/LOGIC

MOLD DESIGN FOR INJECTION MOLDING MACHINE USING RECYCLED ALUMINUM

Amadeus Renaldy [1)], Risa Nurin Baiti [1)*], I Putu Gede Sopan Rahtika [1)], Komang Widhi Widantha [1)]

1) Mechanical Engineering Department, Politeknik Negeri Bali

Correponding email [1)] : nurinbaiti@pnb.ac.id

Abstract. The use of aluminum is widely spread from beverage cans, car parts, airplanes, trains, and household furniture. This is due to its lightweight and good corrosion resistance. However, as a metal aluminum waste is difficult to be decomposed naturally. Aluminum metal takes 80 to 100 years to decompose. So the accumulation of untreated scrap aluminum can pollute the environment. One of the solutions is to recycle aluminum by melting and re-casting it into a new shape: a mold for polymer processing. The waste of beverage cans was cleaned from any dirt and adhesive. Then, they were turned into small parts by a crusher. The melting process was done at 650ºC. The molten aluminum was poured into a sand mold in the shape of mold of a tensile testing specimen. The recycled product can be used to prepare tensile testing samples of polymer or polymer-based composite with injection molding technique. To evaluate the quality of recycled aluminum, a hardness test was done with a value of 69.31 $\pm$ 3.02 HB. This value is lower than first-use aluminum. This is due to a combination of microstructural changes due to repeated heating, the presence of additives and impurities, and the effects of heat treatment and open cooling. Metallographic testing was carried out to evaluate the microstructure of the material resulting from the smelting of scrap aluminum using sand molds. In this test, the etching solution used consisted of 100 ml of water and 20 g of sodium hydroxide. The results of the metallographic images on the recycled aluminum material show the presence of a stand-alone silicon (Si) element and an aluminum-copper alloy ($CuAl_2$).

Keywords : aluminum, mold, injection molding, design, and recycling.

1. INTRODUCTION

The use of aluminum as a base material continues to increase due to its widespread availability and diverse applications in industries such as automotive, aerospace, railways, and household furniture [1]. This increase has led to an increase in the amount of aluminum waste that is no longer used, such as alloy wheels, household appliances, soft drink cans, and engine blocks. As a result, new problems with the accumulation of aluminum waste have emerged [2]. Aluminum waste is solid waste and is difficult for the environment to decompose. Aluminum metal takes 80 to 100 years to decompose [3], so the accumulation of untreated scrap aluminum can pollute the environment. This happens because metals take a long time to dissolve in water and decompose in the soil [2]. Pollutants can come from waste that has been buried for a long time without being processed. The rain will wet the garbage pile and will make the situation worse. On the other hand, the production of aseptic packaging in Indonesia reaches 4 billion items per year, or around 333 million items per month, which makes it one of the largest contributors to waste. Most people burn aseptic packaging waste to dispose of it, but this method is considered ineffective because aluminum foil and CO2 gas are left behind to pollute the air and pollute the environment [4]. If no effort is made to overcome environmental pollution caused by waste, this problem will become worse over time.

Recycling is the best way to eliminate aluminum waste [4]. Aluminum can be recycled through the casting

process [2]. One of the most commonly used types of aluminum casting is by sand casting technique. Sand casting has the advantages of low production costs, reusable, heat resistance, easy operation, and good casting product results. Sand casting method is environmentally friendly and efficient for industrial practices. The sand casting process requires special attention to several key aspects to ensure optimal results. The channel system, as shown in the first study, has a vital role in facilitating the flow of molten metal into the sand mold. Various channel models, such as split channels, split channels with additives, and direct channels, affect tensile strength and possible shrinkage defects in cast results [5]. Furthermore, the second study highlights the importance of sand mold variations in recycled aluminum casting. Variations such as red sand mold, dumpling sand mold, and mixed sand mold affect the percentage of shrinkage and hardness of cast products. Another significant aspect in the casting process is the selection of molding materials, where the use of RCS (Resin Coated Sand) waste as a substitute for silica sand can provide positive benefits to the environment and the economy. Overall, a deep understanding of the channel system, mold variation, and mold material selection is key to improving quality and efficiency in the sand casting process.

In addition to its high recyclability, which significantly reduces the carbon footprint, aluminum also has the mechanical strength and durability required for the injection molding process [5]. The integration of sand casting in aluminum recycling not only minimizes environmental impact but also enhances efficiency in industrial production. Utilizing recycled aluminum in the manufacturing of injection molding molds presents a significant opportunity to improve sustainability while simultaneously reducing waste. This research aims to promote the application of recycled aluminum in support of plastic recycling efforts, thereby addressing both environmental and industrial challenges through a sustainable and innovative approach.

2. METHODS

Figure 1 shows the intended final shape of recycled aluminum, which is the mold for injection molding equipment. Usually, the mold for injection molding technic is made out from metal block. Then, it is shaped by machining process such as frais and bor that results in many unused metal chips.

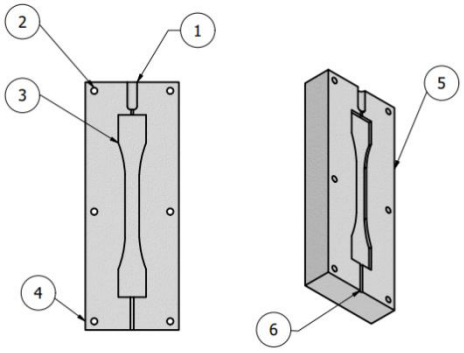

Figure 1. Designed shape of recycled aluminum

Image Legend:
1. Nozzle
2. Bolts
3. ASTM D638 tensile test sample specimen mold
4. Bottom mold
5. Top mold
6. Vent

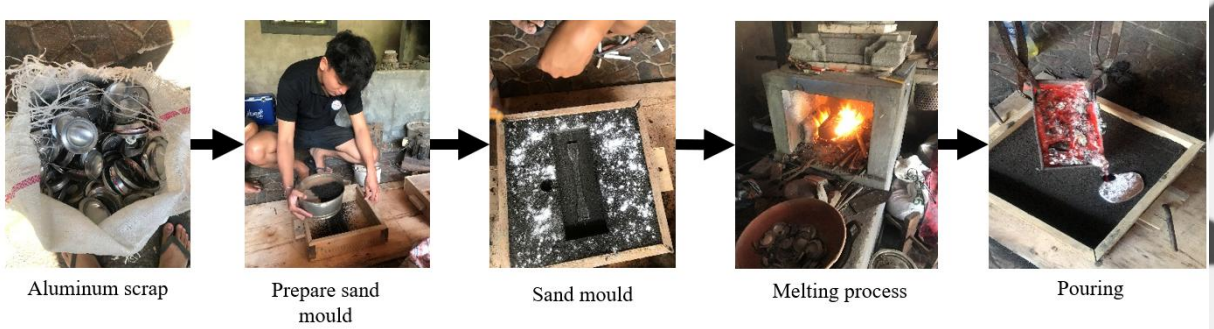

Figure 2. Aluminum recycling process

The process of aluminum recycling process is shown in Figure 2. The sand mold was prepared using uniformly sized silica sand mixed with a bentonite binder to improve cohesion and mold integrity. The sand mixture was

then compacted to ensure uniform density and reduce defects in the final cast product. The melting process was done in a crucible pot at 650ºC. To improve the quality of the molten aluminum, flux was added to remove oxides and other impurities, and a degassing process was performed to eliminate trapped gases, reducing porosity in the final cast. The purified molten metal was then carefully poured into the cavity of the sand mold. The bottom and top molds were separately prepared in dedicated sand molds to facilitate assembly.

The mechanical properties of the recycled aluminum were evaluated through Brinell Hardness testing and metallography, both conducted at the Material Testing Laboratory, Bali State Polytechnic. The Brinell Hardness test was performed using a 10 mm diameter hardened steel ball indenter under a 500 kgf load, following ASTM E10 standards. Each test was conducted for 10 to 15 seconds to allow proper indentation. The diameter of the indentation left by the steel ball was measured using a precision microscope, and the Brinell Hardness Number (BHN) was calculated. Multiple readings were taken at different locations on the sample to ensure accuracy and uniformity in hardness distribution. Metallography testing was carried out to analyze the microstructure of the cast aluminum and identify key structural characteristics such as dendritic formations, grain boundaries, and porosity levels. The samples were carefully sectioned using a precision cutting machine, followed by sequential grinding with silicon carbide abrasive papers (ranging from 240 to 2000 grit) and polishing with alumina suspension to achieve a mirror-like surface. Observations were made using an optical metallurgical microscope at magnifications ranging from 100x to 500x, enabling a detailed examination of grain structure, defects, and phase distribution.

The final stage involved evaluating the functionality and efficiency of the recycled aluminum mold in an injection molding machine. The mold was securely installed in the machine, and HDPE (*High-Density Polyethylene*) plastic was used as the test material. Key parameters, including mold filling behavior, cooling efficiency, and ejection performance, were monitored throughout the process. After molding, the plastic specimens were inspected for defects such as warping, incomplete filling, sink marks, and surface roughness. Dimensional accuracy was assessed using a digital caliper, while visual inspection under proper lighting conditions helped identify surface imperfections. The results were analyzed to determine the effectiveness of the recycled aluminum mold in producing high-quality plastic components, ensuring its suitability for injection molding applications.

3. RESULTS AND DISCUSSION

3.1 Sand Casting

Sand Casting requires sand as a printing medium, and the quality of sand greatly affects the quality of the products produced. Mountain sand, beach sand, river sand, and silica sand are the most commonly used types of printed sand [6]. Molding sand should have the following properties: formable, permeable, large grain distribution, resistance to the temperature of the metal being poured, proper composition, durable, and inexpensive [7]. The selection of the main materials in the form of river sand and bentonite is based on the characteristics of each material that the needs of the metal casting process using sand molds. River sand was chosen because it is easy to obtain, has a uniform grain size, and has a relatively low cost. Experimental grain size analysis revealed an average particle size of 200 µm, indicating a suitable balance between permeability and strength. In addition, river sand has good refractory properties, being able to withstand high temperatures without experiencing significant deformation. Bentonite, a type of clay with high binding ability, was chosen to be mixed with river sand. The binding properties of bentonite help in improving the strength and stability of sand molds. Many studies have shown that bentonite, the most commonly used binder material, is an ideal binder for sand molds. However, the price of bentonite is quite expensive in the market when compared to other types of binders. The CaO (clay) content in bentonite is higher than in coal-burning waste ash [8].

The selection of the 4:1 ratio between river sand and bentonite is based on several theoretical and empirical considerations. Too much bentonite in the mixture will make the mold too rigid and difficult to form, while too little bentonite will reduce the binding strength, causing the mold to be easily damaged during the casting process. By using clay or bentonite soil as a binder, cast sand exhibits a variety of different properties according to the moisture content. If the clay content is made constant and the moisture content is added, the strength gradually increases until it reaches its peak, then decreases. A similar situation occurs if the moisture content is made constant and the clay content is added. As the excess water clay fills the space between the grains of sand, its strength and permeability will decrease [8]. The 4:1 ratio is considered ideal because it provides the right balance between flexibility and mold strength. This composition results in a mold that is strong enough to withstand the pressure of molten metal and flexible enough to disassemble without damaging the shape of the mold.

The metal raw materials, the type of furnace used, and the amount of material to be melted must be appropriate [9]. The aluminum smelting process is carried out using a melting furnace assisted by *Blower* to ensure strong and constant airflow, and improve the efficiency of burning coconut charcoal as fuel. Coconut charcoal was chosen because of its abundant availability and ability to produce high temperatures sufficient to melt aluminum. The blower is used to maintain the required high temperature during the smelting process, ensuring that the aluminum melts perfectly before being poured into the sand mold.

3.2 Hardness Test

The test results showed that the average hardness of the material was 69.31 HB±3.02. This value reflects the consistency and homogeneity of the material quite well, which indicates that the smelting and casting process has been carried out correctly. This test was carried out with 10 data retrievals.

Table 1. Comparison of aluminum hardness

No.	Cast materials	Hardness (HB)	Reference
1	Pure Aluminum	101.26	[10]
2	Aluminum cans	124.44	[11]
3	Used motorcycle rim + Si	42	[12]
4	Aluminum cans	69.31	author

The use of aluminum recycled materials can lead to a decrease in mechanical properties, in particular its hardness value (see Table 1). This is due to several factors related to the repeated forming and heating process experienced by recycled aluminum, as well as a decrease in its purity level due to the mixing of additives and impurities because during the smelting process, the quality of aluminum should not be mixed with dirt or other foreign objects which can reduce the quality of the melted aluminum to get good casting results [9]. Recycled aluminum has often undergone various previous heating and forming processes, which can lead to changes in the material's microstructure, such as excessive grain growth or the formation of unwanted phases. And the material becomes softer due to the larger grain limit due to the longer cooling time. Excessive grain growth reduces the hardness of the material because larger grains have fewer grain limits per unit volume, thus lowering the resistance to plastic deformation.

This is in line with research conducted by [12] which shows that the hardness of the cast brinnel has the highest hardness value at 670°C, with an average hardness value of 42 HB. The hardness value decreases in general as the pouring temperature increases. In the context of microstructures, this condition indicates that large microstructures have a high hardness value, while small-sized microstructures have a low hardness value [12]. In addition, if the pouring temperature is higher than 650°C, the hardness value of the casting will decrease as shown in Figure 3 [13]. And recycled aluminum usually contains additives and impurities that enter during the recycling cycle, which can lead to the formation of unwanted inclusions and phases in the aluminum microstructure, weaken the bonds between atoms, and reduce hardness and other mechanical properties.

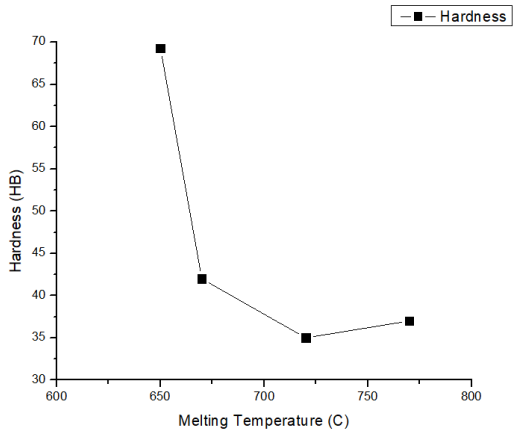

Figure 3. Effect of melting temperature in recycled aluminum hardness value.

During the finishing process, recycled materials are often subjected to additional heat treatments such as *annealing* or *normalizing*. Heating temperature, the time required to maintain the temperature (*holding time*), cooling rate, and environment are some of the variables that affect heat treatment. Heat treatment is the combination of the process of heating or cooling a metal and combining it in a solid state to achieve the desired properties. Temperature limits and cooling speeds are essential to achieve this. For example, normalization is a heat treatment process in which a heating temperature is reached and then cooled slowly using an air conditioning medium. It is the cooling process that greatly affects the mechanical properties of the material. Materials with higher strength and hardness mechanical properties if cooling is done quickly, while if cooling is done slowly, the opposite will happen.

It was concluded that the longer the specimen was subjected to normalized heat treatment, the lower the hardness value. The long heat treatment also causes changes in the microstructure of the specimen [14]. Thus, the decrease in hardness in aluminum recycled materials is due to a combination of microstructure changes due to repeated heating, decreased purity due to additives and impurities, as well as the effects of heat treatment and open cooling

which leads to the formation of unwanted microstructures and thermal tension. The pouring temperature affects the microstructure and hardness of recycled Al-Si.

3.3 Metallography

In this test, the etching solution used consisted of 100 ml of water and 20 g of sodium hydroxide, in accordance with aluminum metallurgical guidelines [15]. This test is important because the microstructure of a material can determine the mechanical properties and performance of a material in a given application. The results of the metallographic images on recycled aluminum materials, shown in Figure 4, give the presence of a stand-alone silicon (Si) element and an aluminum-copper alloy ($CuAl_2$). The microstructural examination showed relatively coarse grains, indicating a slow cooling rate during solidification, which promotes grain growth and reduces hardness. The Si phase was evenly dispersed within the aluminum matrix, while $CuAl_2$ appeared along grain boundaries, contributing to strength but also increasing brittleness. Additionally, some defects such as porosity and microcracks were observed, likely caused by gas entrapment or impurities introduced during the recycling and remelting processes. These defects can negatively impact mechanical properties by reducing overall strength and fatigue resistance. The presence of these phases and structural imperfections helps explain the hardness reduction and mechanical performance of recycled aluminum, emphasizing the effects of grain growth, impurity segregation, and casting defects.

Based on the guidelines on beverage containers 3104-H19, it is known that the compound content in the aluminum material includes Si elements of 0.61%, Fe 0.8%, and Cu in the range of 0.05%-0.25%. This microstructure reflects the original composition of the 3104-H19 aluminum beverage container material, where the presence of elements such as Si and Cu corresponds to the specifications of the alloy.

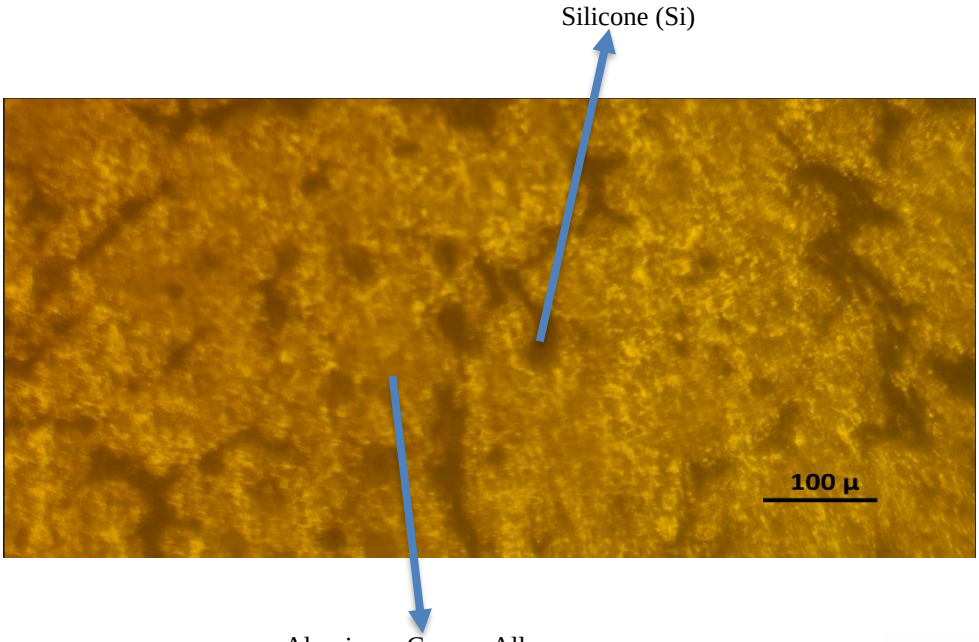

Figure 4. Microstructure of recycled aluminum

3.4 Mold testing in injection molding equipment

The results of the HDPE (*High-Density Polyethylene*) test were carried out using *injection molding*. This test is focused on the use of melted gallon caps using *injection molding* molds that will be the form of the tensile test sample. Testing is carried out with several variations in process parameters, namely mold temperature, melting temperature, and melting time.

This test was performed with variations in mold temperature at 200°C and 250°C, while melting temperatures varied at 200°C, 230°C, and 250°C. The melting time also varies, namely 3 minutes, 4 minutes, and 5 minutes. The results of these tests provide an overview of how these parameters affect the quality of the final product, such as material homogeneity, product density, and shape stability.

Figure 5. Recycled plastic product

The optimal combination of parameters was found at a mold temperature of 250°C with a melting time of 4 minutes, producing a well-formed product with a fully filled mold. However, slight defects were still present, primarily due to air or gas entrapment during the injection process and rapid cooling of the melt inside the mold. This premature cooling restricted proper flow, preventing full cavity filling and resulting in minor imperfections. To further assess product quality, the plastic specimens were examined for defects such as warping, incomplete filling, sink marks, and surface roughness. Dimensional accuracy was measured using a digital caliper, while visual inspections under proper lighting conditions helped identify surface imperfections. Warping was observed in some samples due to uneven cooling rates within the mold, causing differential shrinkage between sections. Incomplete filling was noted in certain areas where premature solidification hindered the melt from spreading evenly. Sink marks appeared on thicker sections as a result of internal shrinkage during solidification, with the outer layers cooling faster than the inner material. Surface roughness was attributed to an uneven mold surface or inadequate injection pressure. Slight variations in dimensional accuracy were detected, mainly due to mold contraction and thermal shrinkage during cooling, but most specimens remained within acceptable tolerance limits. Overall, the analysis confirmed that the recycled aluminum mold is capable of producing high-quality plastic components, making it a viable option for injection molding applications.

4. CONCLUSION

This study shows that the manufacture of injection molding molds, with dimensions of 18322.179 mm^3 and using aluminum material from used beverage cans with a specific gravity of 2.7 g/cm^3, has an important role in the recycling process, especially in converting aluminum waste into new products with useful value. The sand casting method used in this process has proven to be effective in aluminum recycling. The process involves melting using a melting furnace and a blower to keep the heat constant, pouring the melt at 659°C into the sand mold, dismantling the mold, and finishing by hand grinding to achieve precise results. As a result, aluminum waste is successfully converted into new products with high quality. With the right control of process variables, this technology not only reduces waste but also produces products that meet standards, playing an important role in the development of more efficient and environmentally friendly recycling.

In addition, this study aims to find out how the type of aluminum waste affects the hardness value of the product resulting from the casting process, as well as to develop injection molding as a new way to recycle aluminum. This study found that the material has a hardness value of 69.31 HB at a pouring temperature of 659°C. The microstructures formed show small dendrites, which affect the material's ability to withstand loads so that in the end the hardness value of the material decreases. These findings make an important contribution to the development of aluminum recycling techniques and show great potential in improving the efficiency and sustainability of recycling processes.

5. REFERENCES

[1] N. A. Sinaga, “Pemanfaatan Limbah Alumunium Sebagai Bahan Baku Aksesoris,” *Art Des.*, vol. 3, no. 2, pp. 269–279, 2016.

[2] F. Fasya and N. Iskandar, “Melt Loss dan Porositas pada Aluminium Hasil Daur Ulang,” *J. Tek. Mesin S-1*, vol. 3, no. 1, pp. 44–50, 2015, [Online]. Available: https://ejournal3.undip.ac.id/index.php/jtm/article/view/8694%0Ahttps://ejournal3.undip.ac.id/index.php/jtm/article/download/8694/8457

[3] S. Prakoso, M. Burhannudinnur, G. Yasmaniar, S. Rahmawan, and S. Irham, “A systematic effect of clay volume on porosity - P-wave velocity relationship,” *J. Phys. Conf. Ser.*, vol. 1402, no. 4, 2019, doi: 10.1088/1742-6596/1402/4/044096.

[4] L. Anggraeni, E. Yenie, and S. Elystia, "Daur Ulang Sampah Aluminium Foil Kemasan Aseptik menjadi Tawas," *Jom FTEKNIK*, vol. 4, no. 1, p. 2017, 2017.
[5] H. Hendaryati and M. I. Mamungkas, "Pengaruh Tipe Saluran Pengecoran Terhadap Sifat Mekanik Dan Struktur Mikro Aluminium Al 6061 Dengan Metode Sand Casting," *Rotor*, vol. 14, no. 2, p. 43, 2021, doi: 10.19184/rotor.v14i2.22086.
[6] P. Sihite, D. Masnur, M. Badri, and P. Nawangsari, "Studi Potensi Pasir Sungai Di Provinsi Riau Sebagai Pasir Cetak Pada Pengecoran Logam," *Jurnal Sains dan Teknologi*, pp. 63–69, 2014.
[7] S. E. Susilowati and S. Permana, "Pengaruh Bentuk Sprue Well Pada Gatting System Terhadap Aliran Fluida Logam Dan Nilai Kekerasan Pada Pengecoran Aluminium Daur Ulang Menggunakan Sand Casting," *JKTM*, vol. 5, no. 2, pp. 104–115, Sep. 2020, doi: 10.52447/jktm.v5i2.4186.
[8] W. Y. Persatika, "Modifikasi Pasir Lampung Sebagai Raw-Material Pasir Cetak Pada Proses Peleburan Scrap Aluminium," Universitas Lampung, Bandar Lampung, 2018.
[9] M. Wahyudi, "Analisis Kemampuan Material Tungku Dalam Menahan Panas Pada Tungku Lebur Aluminium Dengan Bahan Bakar Gas," Universitas Medan Area, Medan, 2014.
[10] B. Widodo and A. Subardi, "Pengujian Sifat Mekanik dan Struktur Mikro Aluminium Matrix Composite (Amc) Berpenguat Partikel Silikon Karbida (SiC) dan Alumina (AL2O3)," p. 9, Feb. 2019.
[11] D. Dwi Putra, F. Haqqoni, M. Nurhilal, and U. Ulikaryani, "Pengaruh Jenis Limbah Aluminium Pada Proses Pengecoran Menggunakan Tungku Krusibel Terhadap Nilai Kekerasannya," *infotekmesin*, vol. 14, no. 2, pp. 413–417, Jul. 2023, doi: 10.35970/infotekmesin.v14i2.1948.
[12] B. Hidayanto, A. Wardoyo, M. Wahyu Darojad, and Wijoyo*, "Pengaruh Variasi Temperatur Tuang Pada Pengecoran Daur Ulang Al-Si Terhadap Struktur Mikro Dan Kekerasan Dengan Pola Lost Foam," *Flywheel: Jurnal Teknik Mesin Untirta*, vol. 4, no. 1, pp. 45–48, 2018.
[13] R. Siswanto, "Analisis Pengaruh Temperatur Tuang Terhadap Kekerasan Dan Kekuatan Tarik Dari Paduan Al-19,6Si-2,5Cu,2,3Zn (Daur Ulang) Hasil Pengecoran Evaporative," 2017.
[14] V. B. Sardi, S. Jokosisworo, and H. Yudo, "Pengaruh Normalizing dengan Variasi Waktu Penahanan Panas (Holding Time) Baja ST 46 terhadap Uji Kekerasan, Uji Tarik, dan Uji Mikrografi," *Jurnal Teknik Perkapalan*, vol. 6, no. 1, 2018.
[15] X. Jiang, "Metallographic Preparation Of Aluminum And Aluminum Alloys," *Struers*, 2017.

LOGIC
Journal of Engineering Design and Technology
Vol. 25 No.1 March 2025 ; p. 61 - 71

p-ISSN : 1412-114X
e-ISSN : 2580-5649
http://ojs2.pnb.ac.id/index.php/LOGIC

THE ROLE OF ALUMINIUM NITRIDE AS REINFORCEMENT MATERIAL FOR PHASE CHANGE MATERIALS (PCMs)

A Review on Synthesis, Characterization and Applications in Thermal Energy Storage

I Kadek Ervan Hadi Wiryanta [1,4], Tjokorda Gde Tirta Nindhia [2], Wayan Nata Septiadi [2], I Made Joni [3]

1) Study Program of Doctor Engineering Science, Faculty of Engineering, Udayana University
2) Mechanical Engineering Study Program, Faculty of Engineering, Udayana University
3) Department of Physics, Padjadjaran University, Jl Raya Bandung Sumedang KM 21, Jatinangor, Jawa Barat, Indonesia
4) Mechanical Engineering Department, Politeknik Negeri Bali, Badung, Bali, Indonesia

Corresponding email [1] : ervanhw@pnb.ac.id

Abstract. The improvement of thermal energy storage and management has become a significant focus in various industrial applications, including EV battery thermal management, solar energy storage, and high-power electronics. Phase Change Materials (PCM) are widely used for thermal energy storage due to their capacity to absorb and release latent heat. However, organic-based PCMs like paraffin have limited heat conductivity (~0.2 W/mK), limiting their efficiency. This research investigates the potential of Aluminum Nitride (AlN) as a reinforcing material to improve the thermal conductivity and stability of PCM composites. AlN has strong thermal conductivity (~300 W/mK), chemical stability, and oxidation resistance, making it a promising material for increasing PCM thermal performance. Several synthesis methods, including Carbothermal Reduction Nitridation (CRN), sol-gel, hydrothermal, and thermal plasma procedures, have been investigated to produce AlN nanoparticles with appropriate characteristics for integrating into PCM matrices. Furthermore, multiple dispersion strategies, including ultrasonication, surface functionalization, and surfactant-assisted dispersion, are studied to ensure uniform distribution and prevent sedimentation. The use of surfactants like Sodium Dodecyl Sulfate (SDS) and Sodium Stearoyl Lactylate (SSL) further improves dispersion and stability, preventing phase separation and maintaining long-term efficiency. In applications such as EV battery thermal management, AlN-enhanced PCMs demonstrate superior heat dissipation, reducing battery peak temperatures by 19.4% compared to conventional air-cooled systems. Further research is recommended to explore hybrid nanocomposites, optimize AlN particle size and morphology, and develop advanced dispersion techniques to maximize the efficiency of PCM-AlN composites.

Keywords : PCM, Aluminium Nitride, Synthesis, Characterization, Thermal Energy Storage.

1. INTRODUCTION

Improving the efficiency of thermal energy storage and management is becoming a major focus in various industrial applications, including battery thermal management systems for electric vehicles (EV), solar energy storage, HVAC systems, and high-power electronic equipment that require optimal heat management [1]. Phase change material (PCM) is a thermal energy storage mechanism that utilizes materials that can store and release energy through a phase change process. PCM is part of the energy storage method, where in general, there are three (3) types of thermal energy storage systems, namely latent heat, latent sensible, and thermochemical. Latent heat energy storage using PCM is the most widely developed, due to its advantages in terms of ease of operation, and has a similar energy storage density [2]. When a material changes from a solid to a liquid, or from a liquid to a gas, or vice versa, latent heat storage occurs as a result of heat absorption or release. [3]. The following equation expresses the storage capacity of the latent heat system with PCM:

$$Q = \int_{T_i}^{T_m} mCp\ dT + ma_m \Delta h_m + \int_{T_m}^{T_f} mCp\ dT \quad (1)$$

$$Q = m[C_{sp}(T_m - T_i) + a_m \Delta h_m + C_{lp}(T_f - T_m)] \quad (2)$$

Where: Q denotes the amount of energy stored in joules (J). Ti, Tm, and Tf are the initial, melting, and final temperatures (in °C). The specific heat (Cp), average specific heat between Ti and Tm (Csp), and average specific heat between Tm and Tf (Clp) are all expressed in kJ/kg.K, m is the mass of the heat storage media (kg), a_m and Δh_m both are the liquid fraction and heat of fusion per unit mass (J/kg). However, a major challenge in the use of organic-based PCM, such as paraffin, is their low thermal conductivity (~0.2 W/mK), which limits the heat transfer rate and overall performance of the thermal energy storage system [4]. Furthermore, PCMs' long-term thermal degradation and mechanical stability must be considered in practical applications [4].

A common method to improve the performance of PCM is to add reinforcing materials, including carbon-based materials (CNTs, graphene), boron nitride (BN), and metal oxides [5]. Aluminium Nitride (AlN) is a popular reinforcing material due to its exceptional thermal conductivity (~300 W/mK), thermal stability, compatibility with organic PCMs, and great electrical insulation qualities [6]. AlN has an advantage over other materials because of its resistance to oxidation at high temperatures and ability to maintain PCM stability in long-term applications. The addition of AlN nanoparticles to organic PCM can significantly increase its thermal conductivity, and a small concentration of AlN nanoparticles can also help maintain the PCM composite's latent heat value [7].

Although several studies have explored the performance improvement of PCMs with AlN addition, there are still gaps in the understanding of its dispersion method, the effect of the addition ratio on thermal performance, and its application in electric vehicle battery cooling systems [8]. Another challenge that needs to be considered is the processing method of AlN so that it can be homogeneously dispersed in PCM and how variations in AlN particle size can affect the improvement of heat transfer [9]. Therefore, this review aims to analyze the role of aluminum nitride as a reinforcement material in PCM, i.e., the structure and thermal properties of AlN, the synthesis and dispersion method of AlN into PCM, the effect of AlN addition on improving thermal performances of PCM, and its prime potential in the thermal management system of battery electric vehicles (EV).

2. METHODS

The method used in this review includes collecting literature from reputable articles and analyzing and determining research gaps that can be used in the development of further research. The paper used in this literature review focusing on the use of AlN as reinforcement material for PCMs, includes the scope of material science, thermal energy storage, and renewable energy. The selected paper is from a highly reputable journal with an impact factor of more than 0.1 and a publication date of about 10 years, used as primary literature. The research gap for further research is conducted from the gap research about the synthesizing process of nano AlN, the mixing method of nanomaterials into composite PCMs, and the application of PCMs in thermal energy storage.

2.1 Aluminium Nitride: Synthesis and characterization methods

AlN is a promising material with a broad energy bandgap that can be used in high-temperature and high-power electrical and optoelectronic devices. With a binding energy of 4.2 eV, which is higher than the C-C binding energy in diamond (3.8 eV), AlN is ionic and also has extremely strong bonds. At high temperatures (2792 K), AlN starts to break down. The typical deposition temperatures for AlN thin films are 700°C to 1080°C [10]. The challenge of using aluminum nitride nanomaterial is its limited availability and relatively high price. This has led to numerous studies on the synthesis of aluminum nitride using different materials and techniques. Research on the materials and processes used in the synthesis of aluminum nitride is given in Table 1.

Table 1. Synthesis and characterization of AlN

Methods	Materials	Characterization	Results and Highlights	Reference
Gas-reduction–nitridation	$Al(OH)_3$, NH_3, C_3H_8	XRD, TGA, FTIR, SEM	AlN conversion of over 70% at temperatures above 1200°C	[11]
Direct nitridation (with and without additives)	Aluminum Powder, N_2	XRD, SEM, Raman Spectroscopy	Additives enhance the nitridation rate of Al to AlN, accelerating the formation of pure phases	[12]

CRN	Sodium Aluminate ($NaAlO_2$), Carbon Black	XRD, SEM, BET	AlN with an average particle size of 0.50 ± 0.18 µm at 1400°C	[13]
CRN	Al_2O_3, NH_3,, glucose, SF	XRD, SEM, FTIR, BET	Smaller AlN particles, better distribution, no agglomeration	[14]
CRN in-situ nitridation	Al_2O_3 and carbon	XRD, Raman, SEM	AlN nanopowder with good size distribution	[15]
CRN – sol-gel	Al_2O_3/Phenol Resin	XRD, SEM, FTIR, BET	AlN synthesis with more uniform grain size and better particle distribution	[16]
CRN - slurries	$Al(OH)_3$, Carbon Black, PVB	XRD, SEM, TEM, FTIR	PVB improves mixing homogeneity and nitridation efficiency	[17]
CRN - hydrothermal precursor	Al_2O_3, NH_3,, glucose, PEG	XRD, SEM, TEM, FTIR	AlN nanofibers with diameters of 90-110 nm at 1400°	[18]
Hydrothermal synthesis	Aluminum-based precursor	XRD, TEM, FTIR, UV-Vis	Particle size is controlled by hydrothermal pressure and temperature	[19]
Electrical Explosion of Wire (EEW)	Aluminum Wire	XRD, TEM, EDS	Al/AlN nanoparticles with controlled size through explosion parameters	[20]
Thermal Plasma Reactor (TPR) synthesis	Aluminum 1100 discs	XRD, SEM, TEM, EDS	High-purity nanocrystalline AlN with a thin carbon layer, enhancing oxidation resistance	[21]
RF Induction Thermal Plasma synthesis	Aluminum powder, N_2	XRD, SEM, TEM, FTIR, BET	AlN nanoparticles (20–60 nm) with high purity, controlled via plasma power and gas flow rate	[22]

2.2 Method of Aluminum Nitride Dispersion in PCMs

The thermal conductivity of organic PCM can be enhanced by adding the nanomaterial AlN, but integrating nanomaterials with PCM leads to challenges due to density differences that cause a propensity for agglomeration and sedimentation. To prevent this phenomenon, a variety of methods of PCM mixing with various nanomaterials are employed to produce uniform and even PCM composites. Table 2 shows several mixing methods of nanomaterial addition into PCM.

Table 2. Methods of nanomaterial addition

PCM Material	Dispersion Method	Added Nanomaterial	Results and Highlight	Reference
Paraffin	Mixing with Sodium Stearoyl Lactylate (SSL) surfactant	Nano-Al_2O_3	Thermal conductivity increased by 31% (solid phase) and 13% (liquid phase); melting rate improved by 27%.	[23]

PCM Material	Dispersion Method	Added Nanomaterial	Results and Highlight	Reference
Bio-based PCM (PureTemp PCM)	Addition of surfactants SDS, SDBS, and SSL	Graphene nanoplatelets (GnPs)	Thermal conductivity increased up to 1.03 W/mK.	[24]
Nano-emulsion water-based PCM	Phase Inversion Temperature (PIT) method using dual surfactants	n-Hexadecane, Brij L4, Tween 60	High stability for 120 days and 300 thermal cycles with droplet size below 80 nm.	[25]
PCM with carbon additives	Direct mixing with stabilizer (PVP)	Carbon nanotubes, Graphite, Graphene	Heat transfer rate increased up to 3.35 times at 5.0 vol% Graphite.	[26]
PCM A70	Dispersion of graphene nanoplatelets with surfactant	Graphene nanoplatelets with SDBS surfactant	Thermal conductivity increased by 122.26% compared to conventional PCM.	[27]
PCM PT-58	Dispersion with copper foam	Graphene nanoplatelets (GNPs), Magnesium oxide (MgO)	Maximum temperature reduced by 16% with 0.02 wt.% GNPs addition.	[28]
Stable-form composite PCM	Adsorption of aluminum nitride into the matrix	Aluminum nitride (AlN)	Thermal conductivity increased by 2903% compared to pure PCM.	[29]
Aluminum nitride-based PCM	Vacuum adsorption and nano-encapsulation	Aluminum nitride (AlN), nano-encapsulated PCM	Thermal conductivity increased up to 3.5 W/mK, approximately 17.5 times higher than pure PCM.	[30]
Nanocomposite PCM	Blending, encapsulation, and impregnation	Al, Cu, Al_2O_3, TiO_2, Fe_2O_3, CNT, Graphene nanoplatelets	Improved energy storage efficiency and thermal conductivity depending on the method used.	[31]
Paraffin wax	Dispersion of various nanoparticles	Fe_3O_4, Al_2O_3, CNT	Enhanced PCM stability with carbon-based and metal oxide additives.	[32]
Paraffin-based PCM	Mechanical dispersion (stirring & sonication)	Al_2O_3, BN, CNTs	Improved thermal conductivity and stability over multiple heating cycles.	[33]
PEG-based PCM	Functionalization with acid treatment	MWCNTs	Enhanced dispersion stability and increased heat transfer performance.	[34]
Organic PCM	Microencapsulation via spray drying	Nano-SiO_2, Graphene oxide	Improved leakage prevention and long-term stability.	[35]

3. RESULTS AND DISCUSSION

3.1 Aluminum Nitride: Structure, Properties, and Potential as Reinforcement Material

Aluminum Nitride (AlN) is a ceramic material with remarkable thermal conductivity, high electric insulation, and chemical stability. Its crystal structure is classified under the wurtzite phase, which explains its high thermal conductivity at about 300 W/mK. Due to its high thermal conductivity and chemical stability, AlN is an ideal reinforcement material for PCM in use for energy storage.

Aluminium Nitride (AlN) has a limitation in terms of availability and very high prices. This has led to research in synthesizing aluminium nitride using various methods and materials. In recent years, the methods used in synthesizing AlN are: Direct Nitridation, Carbothermal Reduction Nitridation (CRN), Sol-Gel, Thermal Plasma, and hydrothermal, as shown in Table 1. The results in particle size and phase purity from Table 1 are shown in Figure 1:

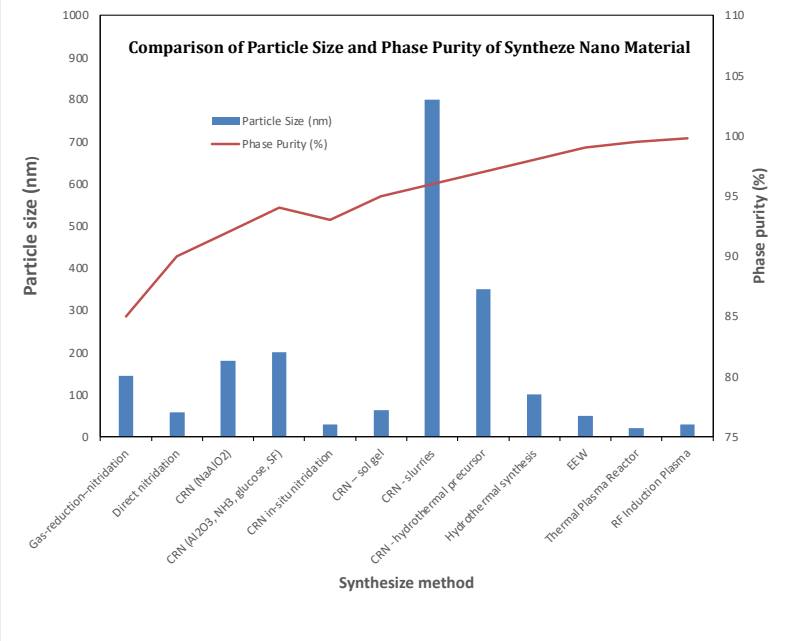

Figure 1. Particle size and phase purity of AlN from different methods of synthesizing

The most common methods used in synthesizing nano-AlN were direct nitridation of aluminium and the use of carbon as a reduction agent (CRN methods). CRN-based AlN synthesis using carbon precursors leads to improved thermal conductivity due to better phase purity and controlled particle size distribution; this caused the CRN methods to become major methods used in synthesizing AlN [13], [14], [15], [16], [17]. From Figure 1 it can be known that the gas-reduction nitridation and direct nitridation methods produce aluminium nitride in lower phase purity (80% and 90%) compared to the other methods. The CRN method, which has an advantage in simpler processes than the plasma methods, became a major method that is used on an industrial scale to produce nano AlN. In addition, AlN synthesis through plasma-based techniques exhibits finer grain structures and enhanced dispersion properties, making them more effective for integration into PCM matrices, but this process requires a high operating temperature in the reactor [21], [22]. The smaller particle size of AlN nanoparticles can improve the thermal conductivity of PCM because it can be homogeneously mixed in the composite matrix because it is well distributed and prevents agglomeration.

To confirm the structure and properties of synthesized AlN, several characterization techniques are employed:

a. Fourier Transform Infrared Spectroscopy (FTIR): Identifies chemical bonds within the material. Peaks at ~600 cm^{-1} indicate Al-N stretching vibrations, confirming AlN formation.
b. Scanning Electron Microscopy (SEM) & Transmission Electron Microscopy (TEM**)**: Provide insights into the morphology, grain size, and distribution of synthesized AlN. Nanoparticles with uniform size and minimal agglomeration exhibit better dispersibility in PCM.
c. X-Ray Diffraction (XRD): Used to determine the crystallinity and phase purity of AlN. The presence of sharp diffraction peaks corresponding to the wurtzite AlN phase confirms successful synthesis.
d. UV-Vis Spectroscopy & Photoluminescence (PL)**:** Used to measure the optical properties and bandgap energy. A bandgap around 6.1 eV is typically observed for high-purity AlN.
e. Thermogravimetric Analysis (TGA)**:** Evaluates the thermal stability and weight loss behavior of AlN.
f. Raman Spectroscopy**:** Used to detect vibrational modes and assess the structural integrity of AlN. Raman peaks corresponding to E2(high) and A1(LO) modes indicate high crystallinity and phase purity. The presence of additional peaks or shifts can signal structural defects, impurities, or stress in the lattice.
g. Particle Size Analysis (PSA): Determines the size distribution of AlN nanoparticles, which significantly affects their dispersion and performance in PCM. A uniform and narrow particle size distribution enhances the stability and thermal conductivity of the composite material.

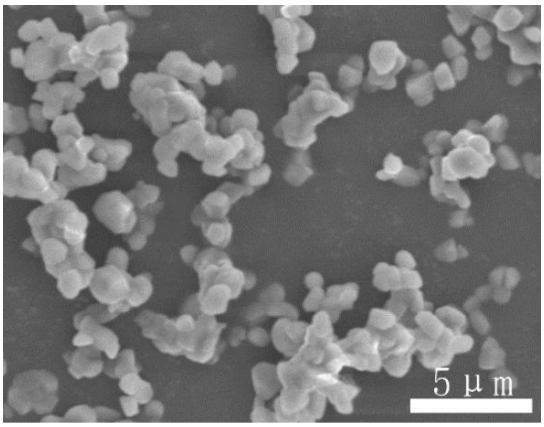

Figure 2. SEM morphology of AlN synthesized using CRN-slurries method [17]

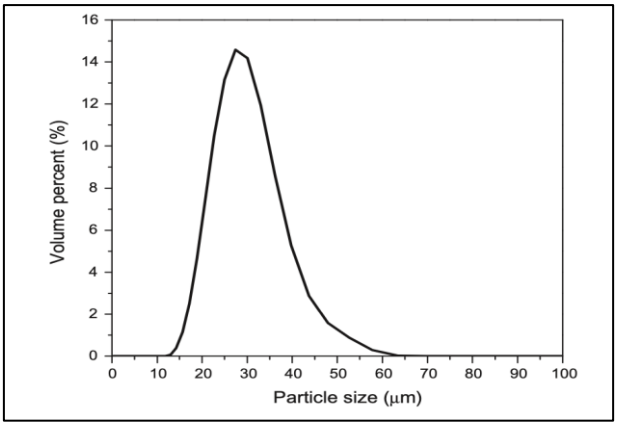

Figure 3. The particle size of AlN using PSA analysis [36]

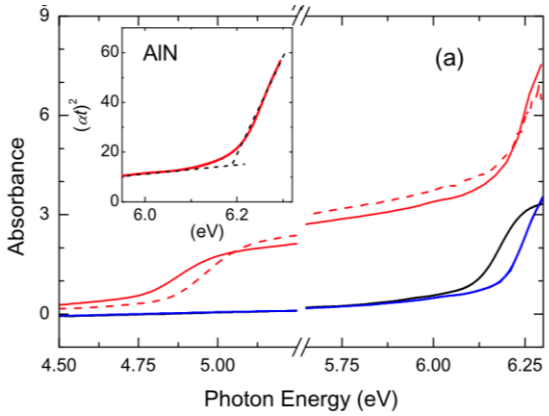

Figure 4 Photon energy of AlN using UV-vis diagram analysis [37]

Figure 2 shows the SEM image of aluminum nitride at 5 um scale. The AlN was synthesized using the CRN-slurries method. The results show that the AlN particles have a granular morphology with a non-uniform size distribution. Particles with non-uniform morphology can have a larger specific surface area, which could potentially improve the thermal contact between PCM and AlN. To ensure homogeneous distribution in PCMs, it is necessary to modify the particle morphology or use better dispersion methods to avoid aggregation and sedimentation in PCM-based heat storage systems.

Figure 3 shows the particle size analysis of AlN using PSA, with an average size of about 30 µm. AlN particle sizes in the 30-40 µm range can still increase the thermal conductivity of PCM but are less effective than nanoparticles. For PCM-based thermal energy storage applications, it is more advisable to use AlN on a nanoscale (<100 nm) so that the increase in thermal conductivity is more optimal and the dispersion stability in PCM is better.

From the UV-vis spectrograph in Figure 4 known that aluminium nitride has a wide band gap (6.0 – 6.2 eV) and photon energy of about 6.0 eV. With a wide band gap (6.0 - 6.2 eV), AlN has excellent thermal resistance, which prevents degradation of the material structure when used in repeated heating-cooling cycles in PCMs. The high energy absorption of AlN enables more uniform heat distribution in the PCM, reducing the risk of hot spots and improving thermal management efficiency in thermal energy storage applications.

3.2. Thermal Conductivity Enhancement and PCM-AlN Efficiency

The addition of AlN into PCM improves both thermal conductivity and heat storage efficiency. The dispersion method is the most important in determining AlN's efficiency as a reinforcing agent. From Table 2, there were several methods used in the dispersion of nanomaterials into PCM, including vacuum adsorption and nano-encapsulation technologies, which resulted in excellent integration, enhancing the thermal performance of PCM-AlN composites [30], [35]. The thermal conductivity of pure PCM is around 0.2-0.3 W/mK. AlN-reinforced PCM can reach values of up to 3.5 W/mK, marking a nearly 17.5-times improvement compared to conventional PCM. This improvement ensures faster heat transfer rates during phase transitions, reducing the risk of overheating and improving overall energy efficiency. In addition, the nanoencapsulation of AlN in the PCM matrix minimizes phase separation issues and ensures stable cycle performance over long operational periods.

The use of surfactants in the dispersion of nanomaterials into PCM also plays an important role. The study of addition surfactants such as sodium dodecyl sulfate (SDS), sodium dodecyl benzene sulfonate (SDBS), and sodium stearoyl lactylate (SSL) shows results that using SDS surfactant in PCM composites leads to maximum thermal conductivity across all PCM mass fraction variations. The addition of 3% SDS increases the thermal capacity of PCM composites while adding SSL increases the PCM enthalpy value [24]. Another result using SSL as a surfactant in dispersing nano-Al_2O_3 into paraffin has a similar finding where the effective thermal conductivity of paraffin increased from 0.20 to about 0.28 and 0.29 W/mK (enhancement of more than 43%) [23].

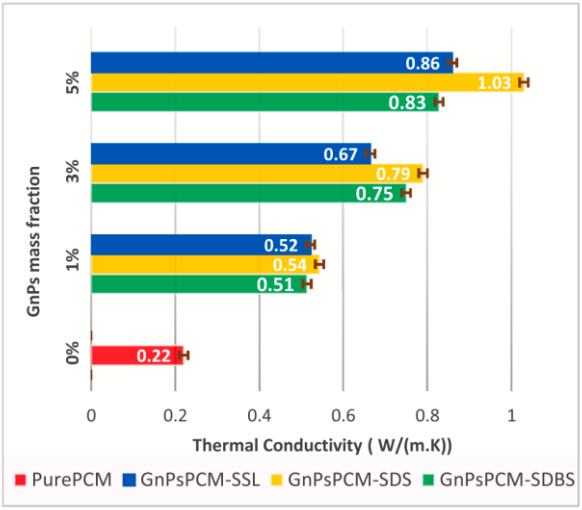

Figure 5. Thermal conductivity of nanocomposite PCM- Graphene Nanoplatelets and surfactants [24]

From Figure 5 we can see clearly that the addition of surfactant (SDS, SSL, SDBS) into nano-enhanced PCM-GnP significantly increases the thermal conductivity compared to pure PCM. According to the study of literature, it is known that a combination of ultrasonication, surface functionalization, and surfactant-assisted dispersion yields the highest enhancement in thermal conductivity of PCM. This is because the combination methods can ensure that AlN remains well-distributed within PCM without excessive sedimentation or aggregation. The optimization of these dispersion methods is crucial for maintaining the long-term stability and effectiveness of PCM-AlN composites.

3.3 Application of PCM-AlN for Thermal Energy Storage

The addition of nanomaterial AlN to PCM can significantly increase the thermal conductivity and stability of composite PCM. This makes the nanocomposite PCM/AlN a promising application in the thermal management system of battery electric vehicles (EV). Efficient heat dissipation is crucial for maintaining battery temperature within an optimal range, preventing thermal runaway, and extending battery lifespan.

The integration of nano-AlN into paraffin increased the thermal conductivity, mechanical strength, and volume resistivity, of which the addition of 20 wt% AlN is the most effective. The result in the battery module shows better heat dissipation and temperature uniformity compared to an air-cooled battery module, leading to a

19.4% decrease in the maximum temperature and a less than 1°C temperature difference at a high discharge rate of 3C. This indicated that the AlN-enhanced composite PCM thermal management system has significant temperature control and balancing capability for the battery module. [38]. Similar research in the addition of AlN in organic PCM polyethylene glycol (PEG) was also done, and the result shows that increasing AlN nanopowder into composite PCM polyethylene glycol (PEG) will increase the thermal conductivity of composite PCM, and the latent heat of composite PCM will decrease. [39]

Another research is also done to improve the solar panel output by adding composite PCM (NePCM) for passive cooling in surface solar panels. Solar panel efficiency has increased from 10.11% to 13.19%. The maximum power produced was 46.22 W when the PV working temperature reached 52.62°C. It has been demonstrated that using the NePCM system improves simple PCM's capacity to absorb heat [40].

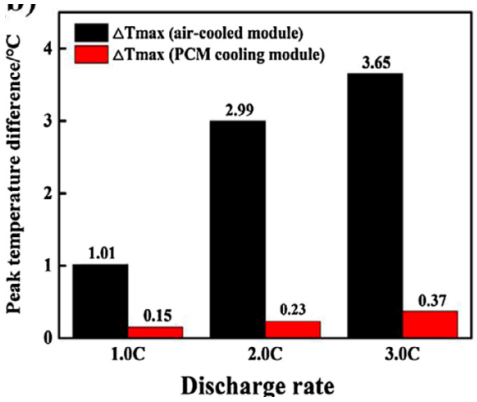

Figure 5. Temperature of battery module using air-cooled and nanocomposite PCM [38]

3.4 Potential Research and Development: Sustainability and Recyclability Aspects

While significant advancements have been made in PCM-AlN composites, several areas still require further research and development to optimize their performance, sustainability, and recyclability, ensuring long-term viability in thermal management and energy storage systems:

a. Optimization of AlN nanoparticle size and morphology:
Research into the impact of nanoparticle size on PCM performance can lead to enhanced thermal stability, efficiency, and durability. Smaller, well-dispersed AlN nanoparticles improve thermal conductivity while minimizing sedimentation and phase separation in PCM composites. From a sustainability perspective, optimizing particle size can reduce material waste, improve heat cycle stability, and extend the lifespan of thermal storage systems, decreasing environmental impact.

b. Hybrid nanocomposite approaches**:**
Research of the effects of combining AlN with various materials, i.e graphene nanoplatelets (GnPs), expanded graphite (EG), and carbon nanotubes (CNTs) could enhance thermal performance, mechanical strength, and stability of PCM-AlN composites. This hybrid approach can lead to more durable and high-performance thermal storage materials, reducing material degradation over multiple heating cycles.

c. Dispersion methods for enhanced stability and recyclability:
Research on efficient dispersion techniques—such as functionalization, surfactant-assisted methods, and ultrasonic dispersion—can improve nano-PCM stability and reusability. Ensuring long-term dispersion stability is essential for achieving recyclable and sustainable PCM-AlN composites, allowing for multiple thermal cycles without loss of performance.

By integrating sustainable synthesis techniques, optimized dispersion strategies, and recyclable hybrid nanocomposite materials, future research can significantly contribute to green energy solutions in thermal management applications for battery electric vehicles (EVs), buildings, and renewable energy storage.

4. CONCLUSION

From the result of this study, it can be concluded that aluminum nitride (AlN) in the form of nanometers has great potential as a reinforcement material for PCM. Its high thermal conductivity, chemical stability, and high oxidation resistance can increase the thermal performance of PCM, which is suitable for application in energy storage and thermal management systems of battery EVs. The method of dispersing AlN into PCMs plays a major role in the optimal performance of composite PCMs. This is because the differences in density between AlN and PCM can lead to agglomeration and sedimentation, which can reduce the characteristics of AlN in PCM. According to this conclusion, more studies may be conducted by optimizing the size and morphology of nano-AlN, hybrids, or

combinations of nano-AlN and other materials to optimize the thermal performance and also optimize the methods of dispersion of AlN into PCM.

5. ACKNOWLEDGEMENT

This study is a part of the Doctoral Program of Program Studi Doktor Ilmu Teknik, Universitas Udayana.

6. REFERENCES

[1] M. Ghalambaz *et al.*, "Latent heat thermal storage of nano-enhanced phase change material filled by copper foam with linear porosity variation in vertical direction," *Energies (Basel)*, vol. 14, no. 5, Mar. 2021, doi: 10.3390/en14051508.

[2] N. Radouane, "A Comprehensive Review of Composite Phase Change Materials (cPCMs) for Thermal Management Applications, Including Manufacturing Processes, Performance, and Applications," Nov. 01, 2022, *MDPI*. doi: 10.3390/en15218271.

[3] A. Sharma, V. V. Tyagi, C. R. Chen, and D. Buddhi, "Review on thermal energy storage with phase change materials and applications," Feb. 2009. doi: 10.1016/j.rser.2007.10.005.

[4] W. Cui *et al.*, "Heat transfer analysis of phase change material composited with metal foam-fin hybrid structure in inclination container by numerical simulation and artificial neural network," *Energy Reports*, vol. 8, pp. 10203–10218, Nov. 2022, doi: 10.1016/j.egyr.2022.07.178.

[5] B. Zhao *et al.*, "Thermal conductivity enhancement and shape stabilization of phase change thermal storage material reinforced by combustion synthesized porous Al2O3," *J Energy Storage*, vol. 42, Oct. 2021, doi: 10.1016/j.est.2021.103028.

[6] L. Zhang *et al.*, "Thermal conductivity enhancement of phase change materials with 3D porous diamond foam for thermal energy storage," *Appl Energy*, vol. 233–234, pp. 208–219, Jan. 2019, doi: 10.1016/j.apenergy.2018.10.036.

[7] Q. Huang, J. Deng, X. Li, G. Zhang, and F. Xu, "Experimental investigation on thermally induced aluminum nitride based flexible composite phase change material for battery thermal management," *J Energy Storage*, vol. 32, Dec. 2020, doi: 10.1016/j.est.2020.101755.

[8] Y. Zhang *et al.*, "Effects of expanded graphite and nano-AlNon the thermal conductivity and specific heat capacity of phase change materials". *Energy Proceedings*, vol. 27, 2022, doi: 10.46855/energy-proceedings-10214

[9] X. Li, H. Li, X. Kong, and H. Yang, "Characterization and experimental investigation of composite phase change materials based on aluminum nitride/expanded graphite," *J Energy Storage*, vol. 35, Mar. 2021, doi: 10.1016/j.est.2021.102326.

[10] H. M. Wu and Y. W. Peng, "Investigation of the growth and properties of single-crystalline aluminum nitride nanowires," *Ceram Int*, vol. 41, no. 3, pp. 4847–4851, Apr. 2015, doi: 10.1016/j.ceramint.2014.12.042.

[11] T. Yamakawa, J. Tatami, K. Komeya, and T. Meguro, "Synthesis of AlN powder from Al(OH)3 by reduction-nitridation in a mixture of NH3-C3H8 gas," *J Eur Ceram Soc*, vol. 26, no. 12, pp. 2413–2418, 2006, doi: 10.1016/j.jeurceramsoc.2005.04.030.

[12] S. Angappan, R. A. Jeneafer, A. Visuvasam, and L. J. Berchmans, "AlN süntees lisandainete juuresolekul ja ilma nendeta," *Estonian Journal of Engineering*, vol. 19, no. 3, pp. 239–249, 2013, doi: 10.3176/eng.2013.3.05.

[13] G. Li, B. Li, B. Ren, H. Chen, B. Zhu, and J. Chen, "Synthesis of Aluminum Nitride Using Sodium Aluminate as Aluminum Source," *Processes*, vol. 11, no. 4, Apr. 2023, doi: 10.3390/pr11041034.

[14] H. Wu *et al.*, "AlN powder synthesis by sodium fluoride-assisted carbothermal combustion," *Ceram Int*, vol. 40, no. 9 PART A, pp. 14447–14452, 2014, doi: 10.1016/j.ceramint.2014.07.014.

[15] "Synthesis of Aluminum Nitride Nanopowders by Carbothermal Reduction of Aluminum Oxide and Subsequent In-situ Nitridization," *Journal of Korean Powder Metallurgy Institute*, vol. 13, no. 6, pp. 432–438, Dec. 2006, doi: 10.4150/kpmi.2006.13.6.432.

[16] D. T. Mylinh, D. H. Yoon, and C. Y. Kim, "Aluminum nitride formation from aluminum oxide/phenol resin solid-gel mixture by carbothermal reduction nitridation method," *Archives of Metallurgy and Materials*, vol. 60, no. 2, pp. 1551–1555, 2015, doi: 10.1515/amm-2015-0171.

[17] Q. Wen *et al.*, "Carbothermal reduction synthesis of aluminum nitride from al(Oh)3/c/pvb slurries prepared by three-roll mixing," *Materials*, vol. 14, no. 6, Mar. 2021, doi: 10.3390/ma14061386.

[18] Q. Yang, H. Wang, R. S. Lei, and S. Xu, "Low temperature formation of AlN nanofibers by carbothermal reduction nitridation of hydrothermal precursor fibers," *Journal of Asian Ceramic Societies*, vol. 5, no. 1, pp. 13–17, Mar. 2017, doi: 10.1016/j.jascer.2016.12.001.
[19] O. Schäf, H. Ghobarkar, and P. Knauth, "HYDROTHERMAL SYNTHESIS OF NANO-MATERIALS."
[20] M. I. Lerner *et al.*, "Synthesis of Al nanoparticles and Al/AlN composite nanoparticles by electrical explosion of aluminum wires in argon and nitrogen," *Powder Technol*, vol. 295, pp. 307–314, Jul. 2016, doi: 10.1016/j.powtec.2016.04.005.
[21] N. Labrador, D. Gutiérre-Campos, O. Rapaud, H. Ageorges, and A. Maitre, "Synthesis of AlN nanopowder coated with a thin layer of C, using a thermal plasma reactor," *Ceram Int*, vol. 45, no. 9, pp. 11677–11685, Jun. 2019, doi: 10.1016/j.ceramint.2019.03.042.
[22] K. I. Kim, S. C. Choi, J. H. Kim, W. S. Cho, K. T. Hwang, and K. S. Han, "Synthesis and characterization of high-purity aluminum nitride nanopowder by RF induction thermal plasma," *Ceram Int*, vol. 40, no. 6, pp. 8117–8123, 2014, doi: 10.1016/j.ceramint.2014.01.006.
[23] M. Nourani, N. Hamdami, J. Keramat, A. Moheb, and M. Shahedi, "Thermal behavior of paraffin-nano-Al2O3 stabilized by sodium stearoyl lactylate as a stable phase change material with high thermal conductivity," *Renew Energy*, vol. 88, pp. 474–482, Apr. 2016, doi: 10.1016/j.renene.2015.11.043.
[24] Y. Sheikh, M. F. Orhan, M. Umair, E. Mehaisi, and A. Azmeer, "Variation in cooling performance of a bio-based phase change material by adding graphene nanoplatelets with surfactants," *International Journal of Thermofluids*, vol. 16, Nov. 2022, doi: 10.1016/j.ijft.2022.100201.
[25] L. Liu, J. Niu, and J. Y. Wu, "Formulation of highly stable PCM nano-emulsions with reduced supercooling for thermal energy storage using surfactant mixtures," *Solar Energy Materials and Solar Cells*, vol. 223, May 2021, doi: 10.1016/j.solmat.2021.110983.
[26] D. H. Choi, J. Lee, H. Hong, and Y. T. Kang, "Thermal conductivity and heat transfer performance enhancement of phase change materials (PCM) containing carbon additives for heat storage application," *International Journal of Refrigeration*, vol. 42, pp. 112–120, 2014, doi: 10.1016/j.ijrefrig.2014.02.004.
[27] M. A. Fikri *et al.*, "Enhanced Thermal Properties of Phase Change Materials through Surfactant-Functionalized Graphene Nanoplatelets for Sustainable Energy Storage," *Energies (Basel)*, vol. 16, no. 22, Nov. 2023, doi: 10.3390/en16227668.
[28] F. Hassan, A. Hussain, F. Jamil, A. Arshad, and H. M. Ali, "Passive Cooling Analysis of an Electronic Chipset Using Nanoparticles and Metal-Foam Composite PCM: An Experimental Study," *Energies (Basel)*, vol. 15, no. 22, Nov. 2022, doi: 10.3390/en15228746.
[29] X. Qiao, X. Kong, and L. Wang, "Thermal performance analysis of a thermal enhanced form-stable composite phase change material with aluminum nitride," *Appl Therm Eng*, vol. 187, Mar. 2021, doi: 10.1016/j.applthermaleng.2021.116581.
[30] L. Wang, X. Kong, J. Ren, M. Fan, and H. Li, "Novel hybrid composite phase change materials with high thermal performance based on aluminium nitride and nanocapsules," *Energy*, vol. 238, Jan. 2022, doi: 10.1016/j.energy.2021.121775.
[31] T. Amberkar and P. Mahanwar, "Phase Change Material Nanocomposites for Thermal Energy Storage Applications," MDPI AG, Jul. 2022, p. 8. doi: 10.3390/materproc2022009008.
[32] V. Saydam and X. Duan, "Dispersing different nanoparticles in paraffin wax as enhanced phase change materials: A study on the stability issue," *J Therm Anal Calorim*, vol. 135, no. 2, pp. 1135–1144, Jan. 2019, doi: 10.1007/s10973-018-7484-4.
[33] J. D. Williams and G. P. Peterson, "A review of thermal property enhancements of low-temperature Nano-enhanced phase change materials," *Nanomaterials*, vol. 11, no. 10, Oct. 2021, doi: 10.3390/nano11102578.
[34] S. Zhang, J. Y. Wu, C. T. Tse, and J. Niu, "Effective dispersion of multi-wall carbon nano-tubes in hexadecane through physiochemical modification and decrease of supercooling," *Solar Energy Materials and Solar Cells*, vol. 96, no. 1, pp. 124–130, Jan. 2012, doi: 10.1016/j.solmat.2011.09.032.
[35] J. Pereira, A. Moita, and A. Moreira, "An Overview of the Nano-Enhanced Phase Change Materials for Energy Harvesting and Conversion," Aug. 01, 2023, *Multidisciplinary Digital Publishing Institute (MDPI)*. doi: 10.3390/molecules28155763.
[36] K. T. Lai, C. H. Shih, C. Te Wu, M. Y. Yang, and C. S. Hsi, "Preparation of aluminum nitride granules by a two-step heat treatment method," *Advanced Powder Technology*, vol. 29, no. 4, pp. 849–854, Apr. 2018, doi: 10.1016/j.apt.2018.01.001.

[37] S. Sohal, W. Feng, M. Pandikunta, V. V. Kuryatkov, S. A. Nikishin, and M. Holtz, "Influence of phonons on the temperature dependence of the band gap of AlN and AlxGa1-xN alloys with high AlN mole fraction," *J Appl Phys*, vol. 113, no. 4, Jan. 2013, doi: 10.1063/1.4784170.

[38] J. Zhang *et al.*, "Characterization and experimental investigation of aluminum nitride-based composite phase change materials for battery thermal management," *Energy Convers Manag*, vol. 204, Jan. 2020, doi: 10.1016/j.enconman.2019.112319.

[39] W. Wang, X. Yang, Y. Fang, J. Ding, and J. Yan, "Enhanced thermal conductivity and thermal performance of form-stable composite phase change materials by using β-Aluminum nitride," *Appl Energy*, vol. 86, no. 7–8, pp. 1196–1200, 2009, doi: 10.1016/j.apenergy.2008.10.020.

[40] B. Hussain, H. W. Malik, F. U. Hasnain, and M. Irfan, "Phase Change Material for the Cooling of Solar Panels—An Experimental Study †," *Engineering Proceedings*, vol. 45, no. 1, 2023, doi: 10.3390/engproc2023045043.

LOGIC
Journal of Engineering Design and Technology
Vol. 25 No.1 March 2025 ; p. 72 - 77

p-ISSN : 1412-114X
e-ISSN : 2580-5649
http://ojs2.pnb.ac.id/index.php/LOGIC

APPLICATION OF ANTHROPOMETRIC DATA ON REDESIGN OF LIGHTWEIGHT BRICK-CUTTING TOOLS TO REDUCE WORKERS' MUSCULOSKELETAL COMPLAINTS

I Gede Bawa Susana[1)], I Made Suartika[2)], Gilang Ade Putra[3)]

1) Mechanical Engineering Study Program, Faculty of Engineering, University of Mataram, Jl. Majapahit No. 62 Mataram-Nusa Tenggara Barat 83125 Indonesia
2) Industrial Engineering Study Program, Faculty of Engineering, University of Mataram, Jl. Majapahit No. 62 Mataram-Nusa Tenggara Barat 83125 Indonesia
3) Mechanical Engineering Study Program Students, Faculty of Engineering, University of Mataram, Jl. Majapahit No. 62 Mataram-Nusa Tenggara Barat 83125 Indonesia

Correponding email [1)] : gedebawa@unram.ac.id

Abstract. The work of cutting lightweight bricks manually with the help of cutting tools still leaves problems. Unnatural working postures are a form of problems faced by workers. This causes musculoskeletal complaints that have an impact on comfort at work. To overcome this, a redesign of the lightweight brick-cutting tool was carried out using worker anthropometric data. The redesign was carried out on the pedal switch and work chair because this caused complaints from workers. The results of the redesign reduced the musculoskeletal complaints of workers who did lightweight brick-cutting work by an average of 49.36%. This figure was obtained from measurements after working on the old and new tools. The decrease occurred from an average of 62.8 when using the old tool to 31.8 after the intervention. The study results can be used as a guideline for workers doing manual work to create a comfortable and sustainable working atmosphere.

Keywords : Anthropometry, Musculoskeletal complaints, Redesign, Ergonomics.

1. INTRODUCTION

Musculoskeletal complaints are often experienced by workers who work manually. This is the impact of unnatural work postures due to the lack of compatibility between workers and their work and the work tools used. Unnatural and unusual work postures cause musculoskeletal complaints, and exposure increases the risk of work injuries [1, 2]. Applying anthropometric data to manual work, such as in lightweight brick-cutting workers, can produce a natural work posture. Existing work tools are redesigned with data on the body dimensions of workers as users to reduce the occurrence of musculoskeletal complaints. This is part of ergonomic measures to prevent sources of disease through engineering.

By redesigning work tools based on workers' anthropometric data, engineering is needed as an ergonomic intervention step so that work postures become more natural. The decrease in musculoskeletal disorders (MSDs) is currently widely the impact of ergonomic interventions [3]. Complaints in the musculoskeletal system are complaints in the skeletal muscle felt by a person, ranging from very mild to very painful. Complaints that result in permanent injuries are usually called musculoskeletal disorders (MSDs) or injuries to the musculoskeletal system. Creating an effective, comfortable, safe, healthy, and efficient work atmosphere resulted from anthropometric data in creating a match between users and the tools used [4]. Anthropometric data is measured based on measurements of important body dimension parts according to the work tool to be designed. This is to determine the workers' interaction with their work equipment so that it is ergonomic and in accordance with the workers' body dimensions. Decreased levels of pain, risk of work posture, and increased productivity as a result of improvements in workstations [5]. Musculoskeletal disorders during manual handling, such as activities that

produce vibrations, lifting, lowering, pushing, and pulling, indicate that workers have high ergonomic issues that can be helped through ergonomic equipment categorization to select specific task risk analysis and posture analysis [6]. Manual work carried out by workers using tools that are not to the worker's posture is common. Some factors that cause musculoskeletal complaints include excessive muscle stretching, for example, pushing or pulling; repetitive activities, for example, hoeing; unnatural work postures, for example, squatting, bending, out of reach; and combinations, for example, working under exposure to the hot sun. This is due to workers' low knowledge regarding ergonomic work postures, experience, and carelessness. In addition, workers pay less attention to the comfort and sustainability of the work being done. The production process carried out manually or manual handling, if done incorrectly, causes disorders of the nervous system, tendons, bones, and muscles, which are referred to as musculoskeletal disorders [7]. Manual material handling that occurs in small and medium industries causes musculoskeletal disorders experienced by workers [8]. Lower and upper back pain, hands, shoulders, neck, wrists, ankles, knees, and elbows as symptoms of musculoskeletal disorders and can be reduced by training workers in ergonomics and alternating work postures [9, 10]. Work, as shown in Figure 1, is classified as manual with the help of work tools that are not yet ergonomic. This can be seen from the worker's less natural posture, especially in the feet and hands, which affects the sitting position.

Figure 1. Workers and lightweight brick-cutting tools

Based on Figure 1, the pedal switch is located quite far from the reach of the feet, so workers experience complaints such as sore left legs after working. In addition, the sitting work position causes complaints in the waist because the seat used is not by the worker's working posture. Based on preliminary data collection using the Nordic Body Maps (NBM) questionnaire, the average level of musculoskeletal complaints was found to be above 60 points. According to Tarwaka [11], a score of 50-70 is in the moderate risk category, and corrective action is needed. Repairs were made to work tools that caused musculoskeletal complaints to workers. Measurement of the level of musculoskeletal complaints is part of the application of ergonomic principles. A production process like this requires ergonomic handling to reduce complaints due to unnatural working postures. The ergonomic approach, through the application of anthropometric data on rice threshing machines, can reduce operator musculoskeletal complaints from 60 to 12 [12]. The application of ergonomics with worker anthropometric data in the design of work tools for small farmers, such as mangosteen harvesters, solar hybrid dryers, drying chambers, and metal liquid pouring tools, can reduce musculoskeletal complaints and increase productivity [13, 14, 15, 16]. Redesigning work tools is needed through collaboration between the ergonomics and mechanical engineering fields, which is called ergo-mechanical. Work problems related to work tools, ergonomics, and occupational health and safety can be overcome by implementing ergo-mechanical [17]. Modifying work equipment with ergonomic interventions in the production process has an impact on reducing unnecessary movements, physical demands, workers' compensation costs, and injury rates [18]. The application of Ergo-mechanical to redesign or design work tools is a system of implementing integrated ergonomic and mechanical principles to create ergonomic work tools, namely technical standards such as service requirements, products, and materials, as well as comfortable use by workers [19]. In the study, work tools and seats were redesigned according to the posture of workers cutting lightweight bricks. Redesign based on input from workers to create comfortable, safe work and easy-to-operate work tools.

2. METHODS

The study used tools and materials such as lightweight brick cutting tools, lightweight bricks, workers as samples, Nordic body maps questionnaires, anthropometers or meters, anthropometric tables, and percentile tables. It was conducted through a case study in one of the industries that produces lightweight bricks in Batunyala, Central

Praya, Central Lombok Regency-Lombok. The application of anthropometry is measuring the dimensions of the worker's body according to the needs of the redesigned work tools and worker seats.

The worker anthropometric data was measured for a sitting position because the work was done with a sitting posture. In this study, a redesign of the lightweight brick-cutting tool was carried out, especially on the pedal switching, worker seat, and the addition of a footrest. The location of the pedal switching, as in Figure 1, is far from the reach of the worker's feet, causing complaints such as pain in the left leg. The pedal switching was redesigned by changing the position and dimensions. A footrest was added to support the workers' feet so they would not fall into the existing channel. The worker's seat was redesigned by changing the dimensions and adding armrests and foam. Worker anthropometric data was used in redesigning the work tool by measuring important or needed body dimensions in the redesign, determining the user population, in this case, workers who cut lightweight bricks, calculating percentile values, and applications in the redesign of the tool. Anthropometric data and percentile values used include popliteal height and 5th and 95th percentile values; popliteal buttock distance with 50th percentile value; shoulder width with 50th percentile value; hip width with 95th percentile value; shoulder height with 50th percentile value; elbow height with 5th and 95th percentile values; arm width with 95th percentile value; arm length with 50th percentile value; foot length using 95th percentile value; foot width using 50th percentile value. The number of samples based on workers working in the lightweight brick-cutting section is 5 men. The calculation of the 5th, 50th, and 95th percentile values is as presented in Equations 1-3 sequentially.

$$\text{Percentile } 5 = \bar{x} - (1{,}65 \text{ x SD}) \quad (1)$$

$$\text{Percentile } 50 = \bar{x} \quad (2)$$

$$\text{Percentile } 95 = \bar{x} + (1{,}65 \text{ x SD}) \quad (3)$$

with $\bar{x}$ the mean and SD is the standard deviation, as shown in Equation 4.

$$\text{SD} = \sqrt{\frac{\sum(x_i - \bar{x})^2}{n-1}} \quad (4)$$

x_i is the measurement data, $\bar{x}$ is the average of the measurement data, and n is the number of measurement data.

3. RESULTS AND DISCUSSION

Table 1 presents the results of measuring workers' body dimension data or anthropometry. Measurements are made based on static anthropometric measurements of workers in a sitting position. Body dimension data are measured based on workers who do lightweight brick-cutting work. Age and length of service are 26-33 years and 3-4 years, respectively.

Table 1. Body Dimension Data for Lightweight Brick-Cutting Workers

No	Data Type	Sample (cm)						
		1	2	3	4	5	Mean	Standard Deviation
1.	Popliteal Height	39.7	39.2	44.5	38.9	41	40.6	2.2919
2.	Buttock-popliteal Distance	41.3	42.7	46.1	39.8	43.2	42.62	2.3531
3.	Shoulder Width	42.1	42.9	46.2	40.4	44.6	43.24	2.2412
4.	Hip Width	37.7	37.6	42.9	41.5	41	40.14	2.3776
5.	Shoulder Height	50.1	49.9	56	49.3	51.9	51.44	2.7273
6.	Elbow Height	18	18.5	20.2	17.9	19.7	18.86	1.0359
7.	Arm Width	8.2	8.1	8.4	7.3	8	8	0.4183
8.	Arm Length	27.9	28.1	29.1	25.5	28.3	27.78	1.3535
9.	Length of the Sole of the Foot	23.5	24.1	25.3	23.1	25.4	24.28	1.0402
10.	Foot Width	9.4	9.3	10	9.2	9.7	9.52	0.3271

From the data in Table 1, the percentile value calculation is carried out to obtain the dimensions applied to redesign the work tool. The results of the calculation of the 5th percentile (P5), 50th percentile (P50), and 95th percentile (P95) values are presented in Table 2. The redesign uses data from Table 2 and as the dimensions of the new work tool. The results of the redesign are as presented in Figure 2. For the chair height, the design will add 10 cm to the height according to the footrest height.

Table 2. Data for calculating the percentile value of lightweight brick-cutting worker

No	Data Type	P5 (cm)	P50 (cm)	P95 (cm)	Application
1	Popliteal Height	38.8	-	42.54	Chair Height
2	Buttock-popliteal Distance	-	42.62	-	Chair Length
3	Shoulder Width	-	43.24	-	Backrest Width
4	Hip Width	-	-	42.1	Seat Width
5	Shoulder Height	-	51.44	-	Backrest Height
6	Elbow Height	18	-	19.72	Armrest Height
7	Arm Width	-	-	8.33	Armrest Width
8	Sleeve Length	-	27.78	-	Armrest Length
9	Length of the Sole of the Foot	-	-	25.14	Footrest Width
10	Width of the Sole of the Foot	-	9.52	-	Width of Pedal Switching

(a)

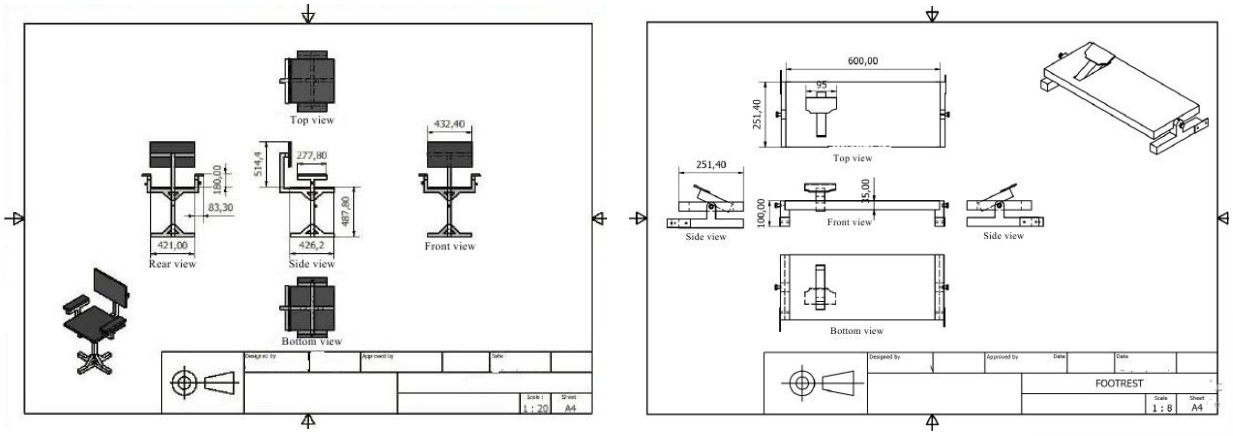

(b) (c)

Figure 2. a) Results of work tool redesign, b) and c) technical drawing (millimeter)

Figure 2 is the result of the redesign of Figure 1 using anthropometric data of male workers working in lightweight brick cutting. From Figure 2, it can be seen that the results of the redesign include changes in the position of the pedal switch on and improvements to the work chair. This redesign provides changes in the level of musculoskeletal complaints in workers. The results of tests conducted on the level of musculoskeletal complaints of workers using the Nordic body maps questionnaire showed a decrease in the level of complaints from using the new redesigned tool compared to using the old tool. This is shown in Figure 3.

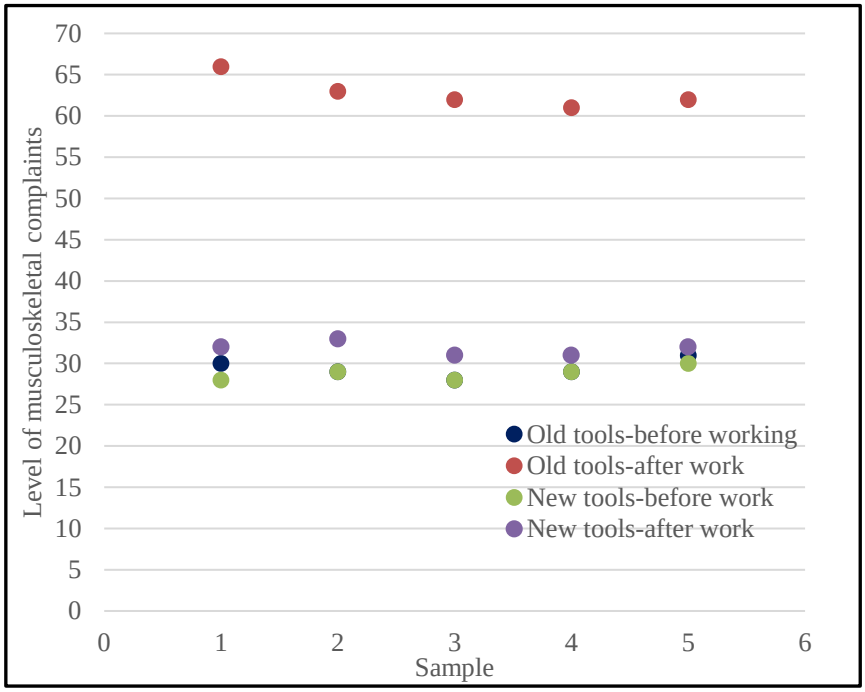

Figure 3. Comparison of levels of musculoskeletal complaints among workers

The decrease in musculoskeletal complaints in workers based on the condition of completion or after work was an average of 49.36%. When workers finish or work using old tools, the level of musculoskeletal complaints reaches an average of 62.8, with a range of 61-66. While using new tools gave a level of musculoskeletal complaints of an average of 31.8 with a range of 31-33. The level of musculoskeletal complaints with a total individual score of 50-70 has a moderate risk level and requires corrective action [11]. This shows that workers experience a moderate risk level and require corrective action on the tools used. The measurements before working on the old and new tools showed an average level of musculoskeletal complaints of workers of 29.4 with a range of 28-31 and 28.8 with a range of 28-30, respectively. This shows workers do not experience musculoskeletal complaints before working on the old or new redesigned tools. The level of musculoskeletal complaints with a total individual score of 28-49 has a low risk level [11]. Redesigning work tools based on workers' anthropometric data has been shown to have an impact on reducing workers' musculoskeletal complaints, in this case, in lightweight brick-cutting work. Workers do their work with a natural posture. This study is on the results of [20], which states that to minimize musculoskeletal injuries through natural work postures. In addition, the use of workers' anthropometric data creates an effective, comfortable, safe, healthy, and efficient work atmosphere [4]. The emergence of a natural work posture due to the application of ergonomics through measuring workers' anthropometric data, so that the level of musculoskeletal complaints can be reduced. This is in line with Olowogbon et al., that musculoskeletal disorders arise due to poor working posture in manual handling [9].

Harmony between work tools and workers is created by training workers in ergonomics. Based on the International Ergonomics Association, it is explained that ergonomics is a science related to the relationship between humans and other elements of a system and a profession that applies methods, data, theories, and principles to design in order to optimize the overall results of the system and human welfare [21]. The application of ergonomic principles to design work tools provides a sustainable, effective, comfortable, safe, healthy, and efficient way of working, and does not cause new problems after the tool is applied in a production process. Reducing musculoskeletal complaints can affect the level of productivity and quality of life of workers.This is in accordance with productivity calculated physiologically, namely the level of productivity influenced by production results compared to the level of musculoskeletal complaints. If the level of musculoskeletal complaints can be kept low, then the level of productivity will also be maintained optimally.

4. CONCLUSION

The application of anthropometric data to the redesign of lightweight brick-cutting tools resulted in a decrease in the level of musculoskeletal complaints in workers. The redesign was carried out only on the pedal switch and work chair because this was what caused complaints from workers. The changes made were able to reduce the level of musculoskeletal complaints in workers by 49.36%. Measurements using the Nordic body maps questionnaire showed that before working on the old and new tools, workers did not experience musculoskeletal complaints and were at a low-risk level. The average level of musculoskeletal complaints was 29.4 and 28.8,

respectively. Workers using the tool before the intervention had an average level of musculoskeletal complaints of 62.8. Corrective action was needed regarding the tools used in the work. The improvements made to the pedal switch on the cutting tool and work chair were able to have an impact on the level of musculoskeletal complaints at a low risk level reaching an average of 31.8. This condition provides a comfortable working situation and a natural working posture. The results of the work tool redesign in this study can be applied in other places provided that the work tool conditions are similar and the workers are male. A wider sampling is needed with variations in male and female workers.

5. REFERENCES

[1] R.S. Bridger, *Introduction to the Ergonomics, Second Edition*. New York: Taylor & Francis, 2003.
[2] OSHA, *Ergonomics*, Available online: https://www.osha.gov/ergonomics (Accessed 9 November 2024).
[3] L. Benos, D. Tsaopoulos, and D. Bochtis, "A Review on ergonomics in agriculture. Part I: manual operations," *Applied Sciences*, vol. 10, no. 6, pp. 1905, 2020.
[4] T.N. Sari, R. Fil'aini, and D. Cahyani, "Analisis desain gagang cangkul berdasarkan antropometri petani pria dan beban kerja penggunanya pada lahan sawah di Kecamatan Wedung, Demak, Jawa Tengah," *Jurnal Optimasi Teknik Industri*, vol. 2, no. 2, pp. 66-71, 2020.
[5] D.M.N.D. Anggara, I G.N. Priambadi, and A.A.I.A.S. Komaladewi, "Perbaikan stasiun kerja sebagai Upaya mengurangi keluhan muskuloskeletal guna meningkatkan produktivitas perajin di Sutama Gamelan," *Jurnal Mettek*, vol. 9, no. 1, pp. 45-53, 2023.
[6] M. Rajendran, A. Sajeev, and R. Shanmugavel, "Ergonomic evaluation of workers during manual material handling," *Materialstoday: Proceedings*, vol. 46, no. 17, pp. 7770-7776, 2021.
[7] N. Evadarianto and E. Dwiyanti, "Postur kerja dengan keluhan musculoskeletal disorders pada pekerja manual handling bagiang rolling mill," *The Indonesian Journal of Occupational Safety and Health*, vol. 6, no. 1, pp. 97-106, 2017.
[8] L. Lady and S.F. Nuraeni, "Preventing musculoskeletal disorders due to manual material handling in the production process of clean water," *Journal Industrial Servicess*, vol. 10, no. 1, pp. 125-132, 2024.
[9] T.S. Olowogbon, R.O. Babatunde, E. Asiedu, and A.M. Yoder, "Prevalence and exposure to ergonomic risk factors among crop farmers in Nigeria," *Applied Sciences*, vol. 11, pp. 11989, 2021.
[10] M. Barneo-Alcántara, M. Díaz-Pérez, M. Gómez-Galán, A. Carreño-Ortega, and A.J. Callejón-Ferre, "Musculoskeletal disorders in agriculture: a review from web of science core collection," *Agronomy*, vol. 11, pp. 2017, 2021.
[11] Tarwaka, *Ergonomi Industri: Dasar-dasar Pengetahuan Ergonomi dan Aplikasi di Tempat Kerja, Edisi 2 dengan revisi*, Surakarta: Harapan Press, 2019.
[12] A. Kristanto, S.C. Widodo, "Perancangan ulang alat perontok padi yang ergonomis untuk meningkatkan produktivitas dan kualitas kebersihan padi," *Jurnal Ilmiah Teknik Industri*, vol. 14, no. 1, pp. 78-85, 2015.
[13] S. Fiana, W.K. Sugandi, A. Thoriq, A. Yusuf, "Analisis antropometri petani dan aplikasinya pada desain alat pemanen manggis," *Jurnal Ergonomi Indonesia*, vol. 5, no. 1, pp. 25-31, 2019.
[14] I G. Santosa, I N. Sutarna, "Use of solar energy hybrid dryer with techno-ergonomic application to increase productivity of dodol wokers in Buleleng, Bali", *IOP Conf. Series: Journal of Physics: Conf. Series*, vol. 953, no. 1, pp. 012087, 2018.
[15] I G. Bawa Susana, "Rancangan ruang pengering berbasis ergonomi menurunkan keluhan muskuloskeletal perajin ikan," *Dinamika Teknik Mesin*, vol. 6, no. 1, pp. 15-21, 2016.
[16] L.K. Wilogo, T.I. Oesman, J. Susetyo, "Perbaikan alat penuang cairan logam berdasarkan pendekatan ergonomis mengurangi resiko cedera fisik pada karyawan di PT. Aneka Adhilogam Karya Klaten," *Prosiding SENDI_U*, pp. 625-632, 2019.
[17] I W.G. Suarjana, M.F. Pomalingo, and B.R. Parhusip, "Penerapan ergo-mechanical design sebagai upaya peningkatan kualitas Kesehatan pekerja CV. Victoria," *Jurnal Abdimas Jatibara*, vol. 1, no. 1, pp. 73-83, 2022.
[18] Occupational Safety and Health Administration, *Ergonomics: solutions to control hazards*, Available online: https://www.osha.gov/ergonomics/control-hazards (Accessed 1 August 2024).
[19] I G. Bawa Susana, I K.P. Putra, and I G.A.K. Chatur Adhi Wirya Aryadi, "Aplikasi alat bantu ergonomis pada kerja manual berdasarkan kajian ergo-mechanical untuk petani kecil," *Energy, Materials and Product Design*, vol. 3, no. 1, pp. 176-183, 2024.
[20] I. Pratiwi, Purnomo, R. Dharmastiti, and L. Setyowati, "Evaluasi resiko postur kerja di UMKM gerabah menggunakan metode quick exposure checklis," *Seminar Nasional IENACO*, pp. 132-138, 2015.
[21] International Ergonomics Association (IEA), *What is Ergonomics*, Available online: https://iea.cc/what-is-ergonomics/ (Accessed 8 October 2024).